MANUFACTURING OF LAB-ON-A-CHIP DEVICES:
CHARACTERIZING SEALS FOR ON-BOARD REAGENT DELIVERY

BY

TEJAS SATISH INAMDAR
B.TECH. MECHANICAL ENGINEERING (2011)
COLLEGE OF ENGINEERING, PUNE, INDIA

SUBMITTED TO THE DEPARTMENT OF MECHANICAL ENGINEERING
IN PARTIAL FULFILLMENT OF THE REQUIREMENTS FOR THE DEGREE OF
MASTER OF ENGINEERING IN MANUFACTURING
AT THE
MASSACHUSETTS INSTITUTE OF TECHNOLOGY
FEBRUARY 2013

SIGNATURE OF AUTHOR.....
DEPARTMENT OF MECHANICAL ENGINEERING
DECEMBER 21, 2012

CERTIFIED BY.....
DR. BRIAN W. ANTHONY
LECTURER, DEPARTMENT OF MECHANICAL ENGINEERING
THESIS SUPERVISOR

ACCEPTED BY.....
PROF. DAVID E. HARDT
CHAIRMAN, COMMITTEE ON GRADUATE STUDENTS

MANUFACTURING OF LAB-ON-A-CHIP DEVICES:
CHARACTERIZING SEALS FOR ON-BOARD REAGENT DELIVERY

BY

TEJAS SATISH INAMDAR

B.TECH. MECHANICAL ENGINEERING (2011)

COLLEGE OF ENGINEERING, PUNE, INDIA

SUBMITTED TO THE DEPARTMENT OF MECHANICAL ENGINEERING
IN PARTIAL FULFILLMENT OF THE REQUIREMENTS FOR THE DEGREE OF
MASTER OF ENGINEERING IN MANUFACTURING

ABSTRACT

DECEMBER 21, 2012

The reagent delivery mechanism in a point-of-care, HIV diagnostic, microfluidic device is studied. Reagents held in an aluminum pack are released on the opening of a fluidic seal. Fluidic seals, controlling the flow of reagents, are characterized to reduce anomalies in the desired flow pattern. The nature of the current seal was investigated. Four seal patterns – line hemisphere, line flat, chevron hemisphere and chevron flat were created and tested for reagent delivery using a flow sensor and a force gauge. Preliminary experiments suggested that one of the patterns – "line-flat" – resulted in fewer flow anomalies. A parameter scoping exercise involving sealing process parameters (temperature, time, gap and distance) was performed for the line flat seal.

The findings of this research can be divided into three categories – 1) bonding phenomenon in current seals, 2) influence of seal pattern on flow and rupture mechanics and 3) process parameters which result in the least flow anomalies. The current seal is found to be a bond between the exposed aluminum on the lid film and the heat seal coating on the dome film. The two chevron patterns result in large amounts of flow anomalies, the line hemisphere pattern also resulted in some instances of flow anomalies. The line-flat pattern creates a seal with the least flow anomalies. A specific set of temperature, time, gap and distance which minimizes flow anomalies was found. The flow performance of the reservoir improved and delamination decreased as the distance of the seal from the reservoir was reduced.

The thesis also develops a model to better understand the deformation of the reagent carrying dome and flow dynamics prior to and following the opening of the seal. The dome deformation model provides a framework for relating volume, delamination and flow rate to the geometry and material properties of the reservoir pack.

Advisor: Dr. Brian Anthony
Title: Lecturer

Dedicated to my beloved grandma (ajji),
who sadly passed away during the writing of this thesis.

Acknowledgements

A big thank you to everyone at Daktari – Bill, whose humility, leadership and dedication are truly inspiring, Aaron who continually amazes me for the breadth of his knowledge and expertise, Amy, who was ever helpful for any of my questions and my never ending need for reservoir packs and Betsy, for charming up every day. Rob has been one of the best mentors I have had. His ideas, depth of knowledge and passion carried me through this research. I am incredibly gratified by his advice, support and encouragement. Watching Daktari grow from 6 people in January to over 12 in August has been very exciting and I would like to wish the very best in all their future plans.

Thanks to my thesis supervisor Dr. Brian Anthony and Dr. David Hardt for their support and ideas. I am grateful to them and everybody at MIT who provided me with the opportunity to explore and learn through the Master of Engineering program. A special mention for Jennifer Craig for her guidance and encouragement throughout my thesis.

I had an incredible group of friends to work with. I can't imagine working without my teammates – Aabed, Ben and Nikhil. Their ideas and hard work helped me carry this project no doubt, but it was so much more - Video chatting from across the room with Nikhil, blasting music for those late night hours with Ben and hitching rides in Aabed's Challenger. Each one of them made this experience a very special one.

Finally, and most importantly I would like to thank my family and friends for their belief, patience and guidance. Thanks do not even begin to describe my gratitude to my parents for their unconditional love, endless support and encouragement.

Contents

TABLE OF FIGURES

Chapter 1: Introduction

This thesis describes research on seal design and manufacturing in the context of microfluidic devices used to monitor global health needs specifically to Daktari Diagnostic Inc.'s point of care HIV diagnostic device.

1.1 Motivation

Cluster of Differentiation 4 (CD4) cells are white blood cells acting as the barometer for an individual's ability to combat diseases. Human Immunodeficiency Virus (HIV) attacks these cells resulting in a drop in the CD4 count leading to reduced immunity. Healthy individuals have a CD4 count of 500 - 1200 cells/mm^3 of blood [1] A CD4 count lower than 200 cells/mm^3 qualifies as an AIDS diagnosis which leads to an increased risk of opportunistic infections. [2] The ability to measure the immune system strength is crucial in order to schedule treatment and monitor the effectiveness of HIV treatment.

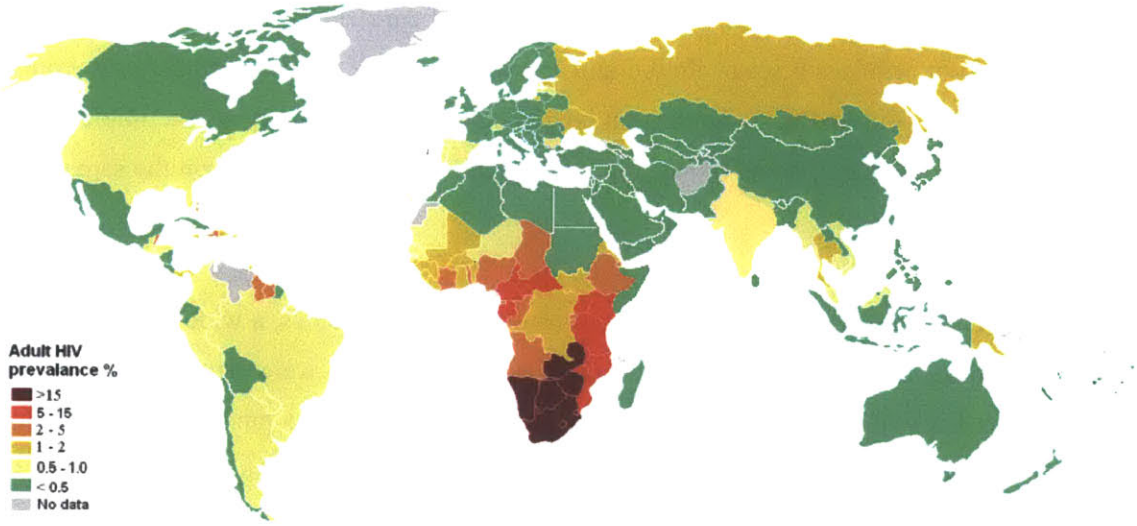

Figure 1: HIV in Developing Countries [3]

Since 1981, over 30 million people have died from AIDS. In 2010 alone, it is estimated that 1.8 million died from AIDS and 2.7 million have been infected by HIV. Today, there are more than 35 million people living with HIV and AIDS worldwide, and ever increasing. [4] Although Africa is home to about 14.5% of the world's population, it is estimated to be home to 69% of all people living with HIV and to 72% of all AIDS deaths in 2009 (Figure 1). [3] Timely diagnosis through CD4 counts will greatly reduce fatalities caused by HIV – AIDS.

Typically, CD4 analysis is performed via a process called flow cytometry. However, this process requires run time of between 18-24 hours on a stationary, expensive, and complex lab machine under the guidance of a trained technician. A flow cytometer unit can range from $30,000 - 150,000 limiting their use to major cities. A single CD4 test result can take 2 weeks considering the logistics involved. These challenges result in significant limitations in access to the targeted developing world populations.

Seventy percent of the HIV-infected population worldwide does not have access to proper diagnostics, preventing them from receiving necessary treatment. The complexity of current CD4 counting equipment requires trained lab technicians. The lack of laboratory infrastructure, reliable power and environmental controlled packaging are also severe constraints in CD4 diagnostics. [5] These limitations make a compelling argument in favor of the importance of an affordable, practical, quick and accurate means for CD4 counting. [5] [6]

Microfluidic devices show great potential to address the challenges associated with CD4 cell counting in resource-limited settings, ideally revolutionizing the point-of-care (POC) diagnostics industry. [7] A microfluidic platform provides a set of fluidic unit operations, which are designed for easy combination within a well-defined (and low cost) fabrication technology. The platform allows the implementation of different application specific systems (assays) in an easy and flexible way, based on the same fabrication technology. [8][9]

Following early efforts in dispensing nano and sub-nano liter fluid volumes, a wide array of microfluidic components such as micro pumps, valves, mixers and other types were developed. An integrated approach on the lines of the microelectronics industry led to the development of more complicated combined systems, commonly referred to as Lab-on-a-chip microfluidic devices.

Microfluidic systems can be designed to obtain and process measurements from small volumes of complex fluids with efficiency and speed, and without the need for an expert operator; this unique set of capabilities is precisely what is needed to create portable point of-care (POC) medical diagnostic systems. [9] [10] In fact, microfluidic instrumentation has been applied to several of the four most common centralized laboratory techniques — blood chemistries, immunoassays, nucleic-acid amplification tests and flow cytometry. [11] Despite the rising popularity of microfluidic devices, the transition from laboratory research to engineering product development is often challenging given the constraints of large scale production and the need for low cost for adoption in developing countries, where Daktari's POC HIV diagnostic will be most beneficial.

1.2 The Masters of Engineering in Manufacturing Capstone Project

This document serves as partial fulfillment of the graduation requirements for the Masters of Engineering in manufacturing program at the Massachusetts Institute of Technology. A team of 4 students co-advised by Lecturer Dr. Brian Anthony and Professor David Hardt conducted research and laboratory experiments at Daktari Diagnostics Inc. (Cambridge, MA). The author of this thesis, Tejas Inamdar, worked with reservoir packs focusing on seal design, process characterization and extended work on modeling flow delivery. Aabed Saber characterized the effect of bonding process parameters on bonding strength of the reservoir packs. [12] Nikhil Jain worked on reducing variability in electrode production [13] and Benjamin Judge developed a process for bonding electrodes to the backbone to create microfluidic channels. [14]

1.3 Problem Statement

Daktari Diagnostics uses on-board reagents stored in hermetically sealed reservoir packs. A seal opens under the action of a plunger to release reagents driving blood through the fluidic channels and to cause cell lysis which is measured as the CD4 count. Seals provide hermetic sealing and quick reagent delivery but flow from the reservoir pack after the exit seal ruptures has anomalies such as flow overshoot (Anomaly 1) or flow delay (Anomaly 2) along with dome delamination which pose challenges in flow control. Characterizing the seal (its shape, its sealing parameters and its rupture mechanics) is a key step in improving flow performance. However, to fully understand the import of this research the next chapter briefly discusses microfluidics and describes Daktari's CD4 product.

This page is intentionally left blank

Chapter 2: Microfluidics

This chapter provides a brief overview of Micro-Electro-Mechanical Systems, Microfluidics and their combination to create Lab-on-a-Chip devices which can perform laboratory like analysis at low volumes, low cost and less time.

2.1 MEMS

Micromachining and micro-electromechanical system (MEMS) technologies can be used to produce complex structures, devices and systems on the scale of micrometers. A wide variety of transduction mechanisms allow the conversion of real world signals from one form of energy into another thereby enabling many micro-sensors, micro-actuators, and microsystems. [15] The scaling of microsystems dramatically changes material and mechanical properties, performance and cost of production of these systems.

All MEMS devices exploit one of the following advantages offered by micro-scale behavior –

1. Advantageous scaling properties – Some phenomenon perform better / efficient on a micrometer scale.
2. Batch Fabrication – Lithographic processes and batch fabrication work better with economies of scale reducing manufacturing costs.
3. Circuit Integration – Tremendous value is derived by integrating circuits with MEMS devices. [15]

2.2 Microfluidics

Microfluidics is an extension of the MEMS technology. It is the science and technology of systems that process or manipulate small (10^{-9} to 10^{-18} liters) amounts of fluids, using channels with proportional dimensions of tens to hundreds of micrometers. [16] In micro-scale fluidic systems, surface tension, energy dissipation and fluidic resistance significantly contribute to flow dynamics. In particular, the Reynolds number, which compares the effect of the fluid momentum to the effect of its viscosity, can become very low, resulting in a highly laminar flow systems in which fluids do not regularly mix. [17]

Some of the main advantages of microfluidic devices can be outlined as follows:

1. Efficient use of reagents helps minimize costs.
2. Modular design allows flexibility.
3. Faster results (potential for real time analysis)
4. Precise control over small fluid volumes.
5. Low cost of production.

2.3 Lab-on-a-Chip Technology

With the recent development of technology in microfluidics, small systems capable of performing laboratory functions on small chips using microliters of fluid began to be developed and were coined "Lab-on-a-Chip" devices. Areas of application are constantly expanding. Currently technology exists in chemical analysis, environmental monitoring, colonics, and medical diagnostics as is seen at Daktari. However, these benefits come with new challenges as well. Microscopic systems are far more susceptible to physical anomalies, tight tolerances and considerations to phenomenon such as capillary action must be factored in design.

Daktari is capitalizing on the advantages provided by microfluidics to develop a point of care CD4 device which is reliable, cost effective and easy to use. The next chapter provides a brief description of Daktari's product and their specific use of microfluidic and sensing technology.

Chapter 3: Daktari CD4

Daktari Diagnostics Inc. is a medical devices company in Cambridge, MA. Daktari CD4 is the company's flagship product developed to monitor HIV patients by providing low cost, easy to use, point of care diagnostic care. Using microfluidics and electrochemical sensing methods eliminates complex sample preparation and fragile, expensive optical sensors.

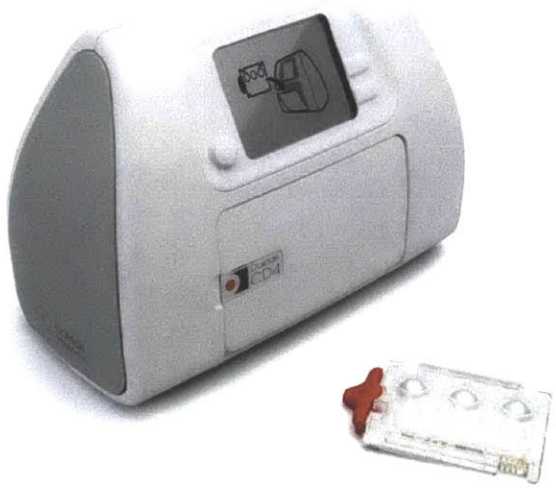

Figure 2: Daktari CD4 Instrument with Cartridge

3.1 Daktari CD4: Microfluidics

The Daktari system (Figure 2) includes an array of channels on its disposable cartridge which serve to control the flow of blood and reagents to appropriate areas. Using actuators located in the instrument, metered quantities of fluid can be pushed from reagent filled reservoir packs and routed through microfluidic channels. These actuators then also determine the direction of flow by opening and closing valves. In Daktari's system, a fixed amount of blood is passed through the channels and the particular CD4 cell desired is separated using antibodies and counted through electrochemical sensing. The use of microfluidics allows for a small volume of liquid and high surface area to volume channels to make accurate diagnostic reports with minimal preparation and processing. All of this work can be completed within minutes in small portable systems, eliminating the need for large-scale laboratories with extremely high capital costs. The assay process has three main stages. The stages are: (A) the blood sample flows through the assay chamber and CD4 cells attach to the antibody; (B) other cells are washed out of the chamber. (C) CD4 cells' cell membranes are ruptured, or lysed by a high-impedance solution, and the difference in impedance is measured.

3.2 Daktari CD4: Assay

The Daktari system combines microfluidics and electrochemical sensing to achieve CD4 cell testing by using cell lysate impedance spectroscopy. Cell lysis involves the placement of antibody along the fluidic channel in which the targeted blood will flow. These antibodies are specifically selected to capture CD4 cells only. After reagents are flowed through the same channel to flush out all other cells and ions, the cells are lysed. More specifically, the environment around the cells is flooded with fluid with low salt concentration which then causes osmosis to occur. The cells ingest water in order to establish equal salt concentration inside and outside until they burst and release their ions (Figure 3). During this process, electrical impedance is measured and the change in impedance after lysing the cells can be linearly correlated to the cell count of the blood.

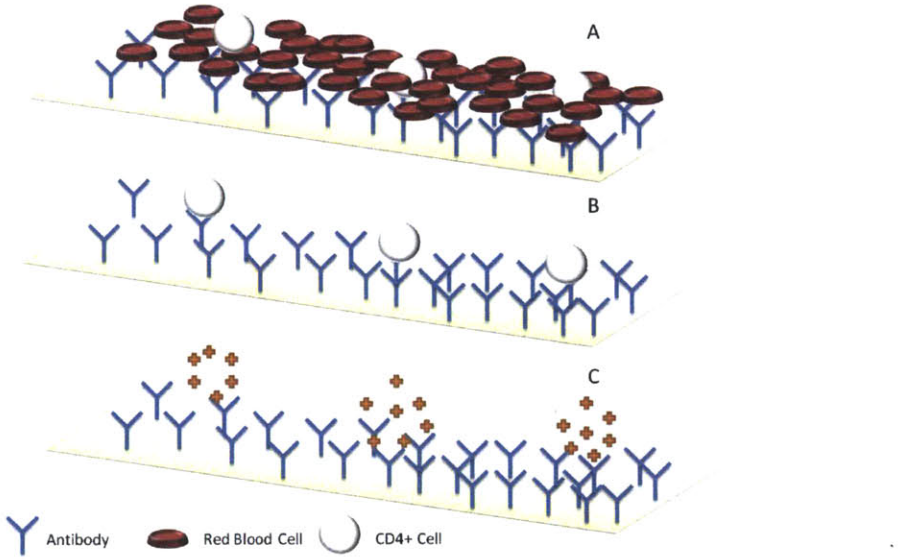

Figure 3: Assay Process Diagram [18]

3.3 Daktari CD4: Point of Care

This product would typically be used by a trained operator carrying the portable instrument and a supply of disposable cartridges to patients in remote locations. The device is to be used where a flow cytometer is not easily accessible. The operator pricks the patient's finger with a lancet and allows the blood to flow into the sample entry port of the card. Once a sufficient amount of blood has entered the card, the operator caps the card, which seals the cartridge, and helps the patient with a bandage to reduce the risk of exposure. The capped card then goes into the instrument, and the test begins. Servo actuated plungers in the instrument drive the fluid reagents, which are stored in reservoirs on the card, out of the reservoir in a controlled manner. Actuation of valves guides the sample through an assay chamber. Antibodies that were deposited to the electrode foil capture the CD4 cells. The captured cells' membranes are ruptured (lysed) by a high-impedance solution. The contents of the cells reduce the impedance of the

solution. This reduction of impedance is measured and is correlated to the concentration of CD4 cells in the blood sample; subsequently the concentration is displayed on the instrument's LCD display.

3.4 The Instrument

The battery-powered instrument is designed for the simplest possible user interaction and portability. The standalone instrument contains the actuators for driving the reagents and operating the valves (Figure 4). The instrument connects to the electrode in the cartridge to read the impedance measurements in the assay chamber. The measurements are used to determine the CD4 cell count in the sample, and the rest of the electronics needed to display the results and drive the actuators are contained in the instrument. Figure 4 shows how the disposable cartridge will go into the unit. Inserting the cartridge is similar to how a cassette goes into a cassette player. The assay is completed in less than 10 minutes with immediate results.

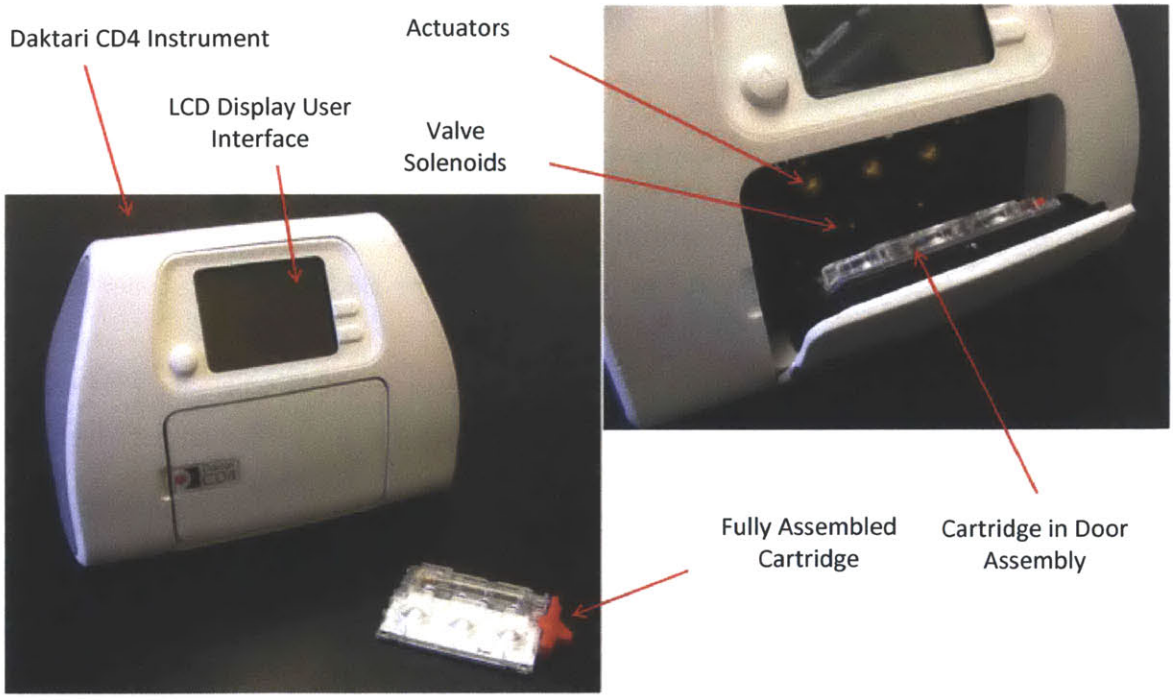

Figure 4: Daktari Instrument [19]

3.5 The Cartridge

Each test cartridge (Figure 5) is consumable for the test and is immediately disposed of after the assay. The cartridge is a microfluidic device with reagents and the sensing mechanism to measure the CD4 cell count in a sample of blood. Each cartridge contains the following 7 parts:

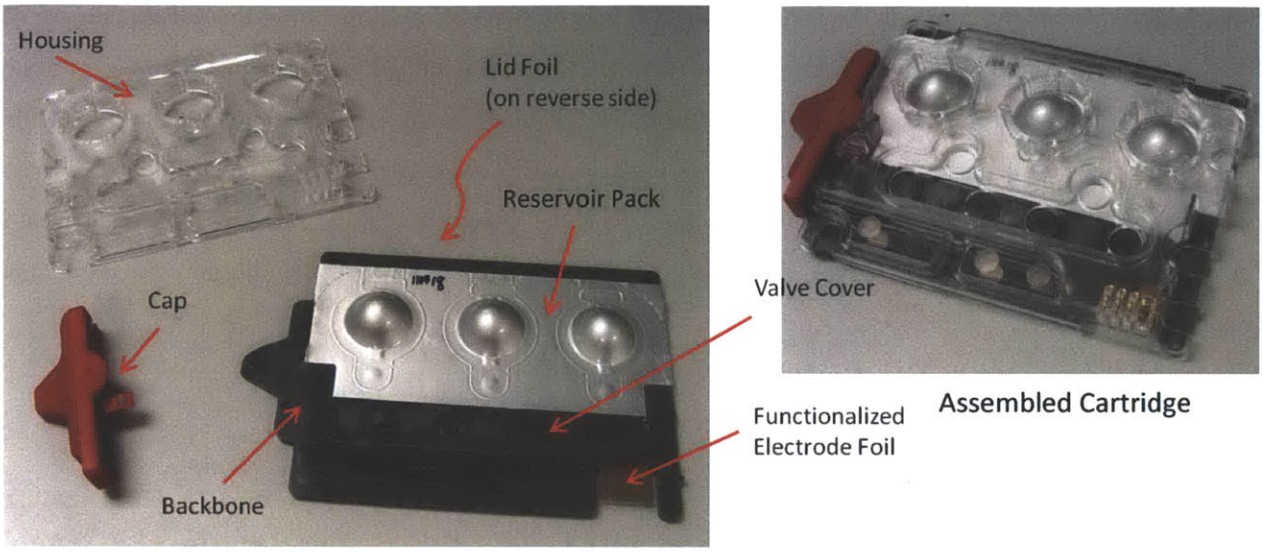

Figure 5: Daktari Cartridge [19]

1. Backbone - Injection molded PMMA (polymethyl methacrylate) card with microfluidic channels.
2. Lid film is a transparent PMMA sheet that is bonded to one side of the backbone to seal the microfluidic channels on the backbone.
3. Functionalized electrode foil – a PMMA foil that covers the 'assay chamber' where the CD4 cell count is performed. This foil has an electrode layer on it. It is then coated with antibody solution, which is used to trap the desired CD4 cells.
4. Reservoir pack is the three semispherical domes in Figure 5 containing the three liquid reagents that drive blood through the cuvette and cause CD4 cell lysis.
5. Valve cover is a layer of polymer used to create a seal on the valves that are used to direct flow through the system.
6. Housing is injection molded PMMA and protects the reservoir pack and functionalized foil.
7. Cap is a polymer component that seals the blood entry port after the blood is sampled and closes vents that are necessary to allow capillary flow of blood into the card.

The Daktari cartridge is the key focus of innovation. In order to explore the true nature of the seals and its influence on flow patterns it is necessary to first understand the reservoir pack.

Chapter 4: Reservoir Pack Research

Today's reagent handling in microfluidic systems rely on either time consuming manual pipetting or highly integrated but large and immobile pipetting robots. In the field of mobile analytical applications on-chip reagent storage systems are required. The encapsulation of liquids in glass tubes has been demonstrated. There have also been experiments at delivery through stick packages releasing reagents upon centrifugation. [20] Daktari uses an on board reagent carrying reservoir pack which releases liquids upon plunger actuation performed using servo motors in the instrument. This chapter describes Daktari's reservoir pack followed by challenges in reagent flow through reservoirs.

4.1 Reservoir Architecture

As discussed extensively in Sevlakumar's thesis [18], the reservoir pack is the reagent containment and delivery component of the Daktari CD4 microfluidic device. The on-board reservoir pack allows the cartridge to act as a stand-alone device without the need of external reagents. Reservoirs deform under the actuation of plungers (Figure 6). The seal opens and discharges the reagent through the reservoir via. Similar to packaging for drugs these reservoir packs are also made of two films bonded together.

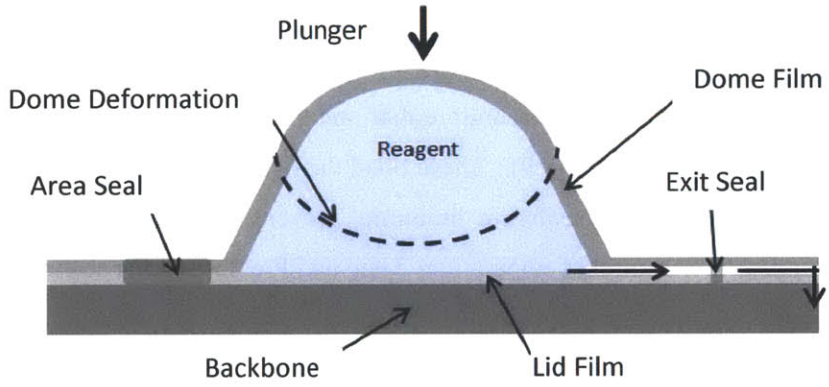

Figure 6: Reservoir Pack Side View

4.1.1 Reservoirs

There are three dome shaped reservoirs on the reservoir packs – B1, B2 and B3 each carrying a fixed volume of reagents. (Figure 7) Each reservoir performs a specific function in the assay. The three reagents R1, R2 and R3 are ionic solutions of varying degrees. The reservoirs are named in the order of their operation. B1 is popped, releasing R1 the most ionic solution which first drives blood through the cuvette and then clears the cuvette. B2 is popped later, releasing R2 which has slightly lesser ionic concentration and clears out the R1 solution. Finally B3 is popped releasing R3 the least ionic solution which drives out R2. Once R3 resides in the cuvette volume, the CD4 lysis begins and changes the impedance of the solution.

The reservoir dome has been carefully designed taking into consideration several aspects of flow which are discussed later. The dome deformation must result in a clean change in profile. Wrinkling of the dome film is undesirable since these wrinkles result in noise in the reagent flow.

This shape has also been extensively studied in Selvakumar's thesis in 2010 [18]. His research indicates that there is no significant change in flow rate as a result of imperfect application of plunger force either angular or axial. .

4.1.2 Dome Film

The reservoir domes are made of aluminum film. This layer is thicker than the flat lid film used to seal the reservoirs from the under-side. The aluminum film has several layers around it which facilitate bonding and improve environmental barrier properties

4.1.3 Lid Film

The reservoir Lid Film is a covering sheet for the underside of the reservoirs. This film is usually the push through sheet in conventional tablet based packs. This film also has additional layers around a thin layer of aluminum.

4.1.4 Area Seal

There are two main area seals – one is circumferential and the other is rectangular, which is introduced after reagents are filled. (Figure 8, Figure 9). These bond the two halves of the reservoir – the Dome Film and the Lid film - together. These seals are hermetic, preventing any leakage of reagents along the periphery. An optimal combination of Temperature, Time and Pressure of the sealing process is necessary to achieve this strength.

4.1.5 Exit Seal

The exit seal is the focal point of this thesis. The seal is a thin line bonding the dome film and the lid film across the exit channel (Figure 8, Figure 9). The plunger actuation leads to deformation of the reservoir dome to such a point that the reagents can no longer be held inside due to the incompressibility of liquids and results in opening of the seal. This opening of the exit seal is poorly understood and is the subject of this research. Once the seal opens, the reagents exit the reservoir pack and flow into the microfluidic channels in the backbone.

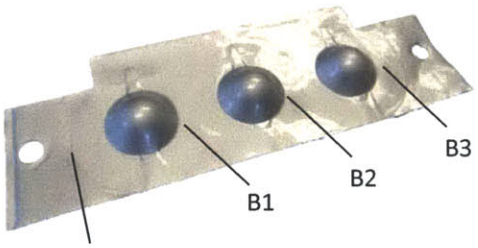

Figure 7: Reservoir Pack

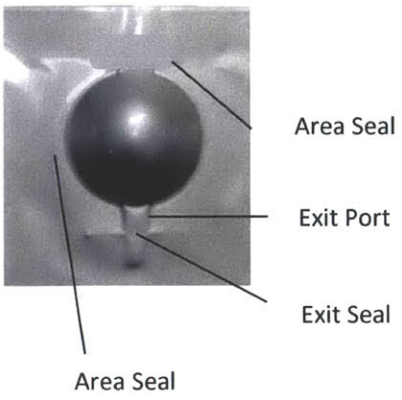

Figure 8: Reservoir Dome (Dome film)

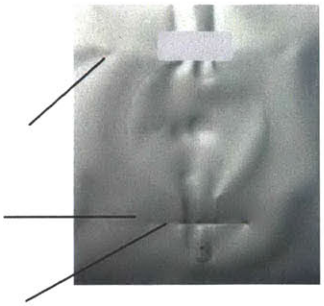

Figure 9: Reservoir Pack (Lid film)

4.2 Flow Dynamics

The flow pattern in this microfluidic structure is designed to ensure that the assay can be successfully performed. The flow must satisfy two key characteristics – the reagent flow rate must follow a predefined predictable pattern and it must not wash away the CD4 cells due to high flow rates. In an ideal situation the reservoir flow must follow a square wave pattern. The flow initiation must be instantaneous and be constant for a period of time followed by an instantaneous drop of flow rate. Flow is often redirected at its initiation as well as its conclusion to the waste channel (referred to as priming) to utilize a section of the flow in control. This is done through a set of valves designed into the backbone and is operated by servo motor actuation in the instrument. The flow exiting the reservoirs at a port called the reservoir via is measured using flow sensors. The experiments conducted so far indicate that there are two important anomalies observed in the actual flow rate patterns.

4.2.1 Anomaly 1

This flow anomaly is defined as the flow rate higher than the upper limit of the requested flow rate. Anomaly 1 is analogous to a signal overshoot in control theory. (Figure 10) This spike of flow maybe a result of the pressure build up just before the exit seal breaks open allowing reagents to flow through the reservoir via. This anomaly may have unknown consequences such as lack of knowledge about the amount of waste volume needed, washing away of the CD4 cells and the lack of repeatability. The Anomaly 1 anomaly is postulated to be associated with the reservoir pack and backbone bonding.

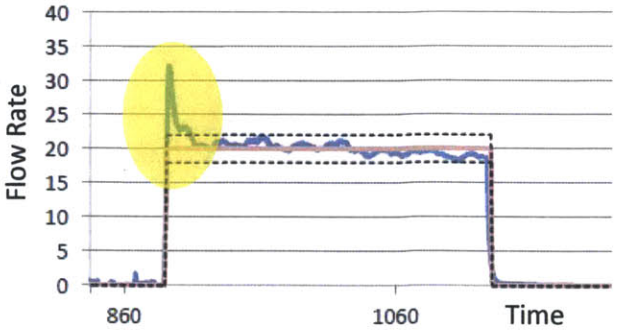

Figure 10: B2 Reservoir Anomaly 1 Case

4.2.2 Anomaly 2

The response time required to achieve requested flow rate is termed as Anomaly 2. (Figure 11) This could be shifting from zero flow rate to the desired flow rate and vice versa. This phenomenon can be thought of as the delay characteristics in a control theory or signal processing. The unpredictability in Anomaly 2 duration makes it challenging to program reservoir sequencing and priming operations. The Anomaly 2 may be associated with sealing.

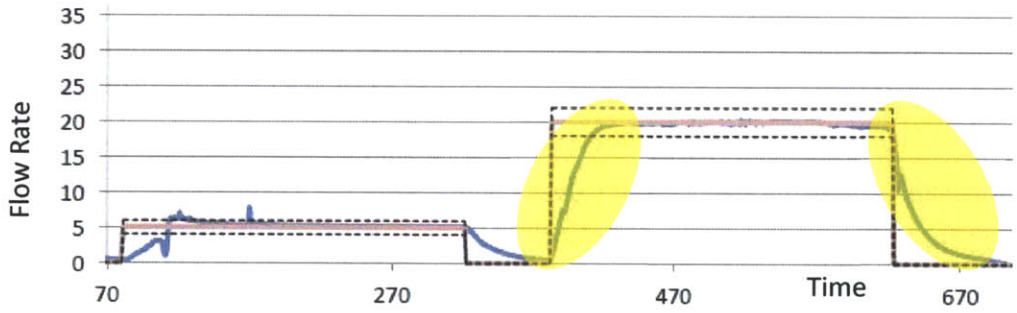

Figure 11: B1 Reservoir Anomaly 2 Case

4.2.3 Reservoir Dome Delamination

The bond held by the heat seal coating on the dome film as well as the lid film is of critical importance to ensure that the dome retains its boundary structure before and after the dome deformation. It has been observed previously that the boundary defining the reservoir domes often shows signs of delamination which is thought to contribute to flow anomalies resulting from a change in effective volume of the reservoir dome. This delamination could be a result of the strength of the peripheral seal or a result of the tolerances on the tool.

Changes in operating parameters of temperature, time and pressure have shown to result in changes in anomalies. The strength of the three seals seems to have an effect on the above mentioned flow anomalies. Thus, the exit seal could be one of the reasons for flow anomalies.

Chapter 5: Exit Seal

Rupturable seals have been in existence for a long time. Inventions related to the fields of these seals have been documented as patents since the 1950's. The author conducted an extensive survey of developments in the fields on breakable seals. Although these seals have been used for a variety of applications, there exists a common theme of mixing of different materials and an easily rupturable seal surrounded by barrier seals. The following discussion on related patents in the field helps to understand the possibilities that have been explored and build upon those seals to design experiments to create a seal with a predictable failure pattern. Daktari's current exit seal is investigated later in the chapter.

5.1 Rupturable Seal Separating Compartments

The invention of a compartmented bag and package [21] envisages a package having two adjacent compartments, separated by a rupturable sealing partition wall. (Figure 12) The two compartments contain solutions which must be stored separately and mixed just at the point of use. The seal is more readily ruptured than the outer barrier walls either by using a different thickness of material or by some other weakening means.

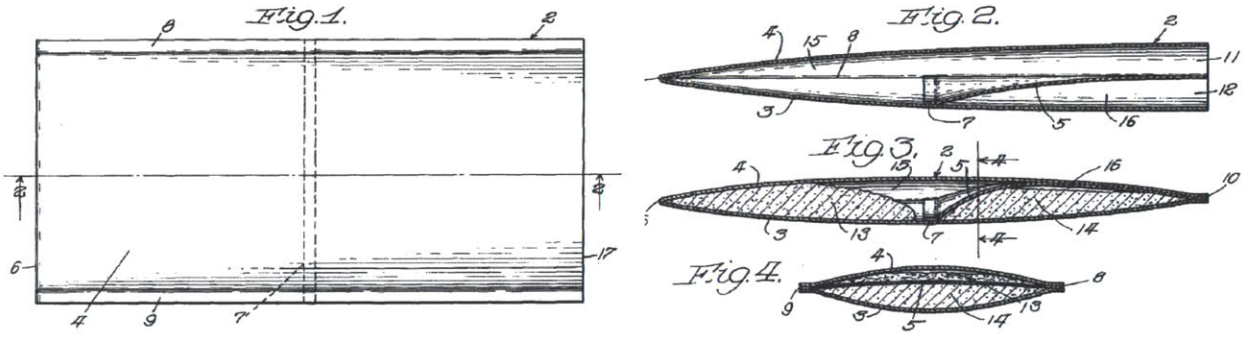

Figure 12: A rupturable seal separating two compartments containing dissimilar solutions. [21]

5.2 Breaker Strip

Another invention [22] proposes the use of an internal breaker strip to create an exit seal. (Figure 13) Any attempt to produce a differential heat seal by pressing two films directly together at temperatures or pressures lower than those required, providing a rupture resistant edge seal invariably results in a weak seal which cannot maintain the desired separation between the two compartments of the envelope. Temperature, Pressure and Time can be accurately controlled; however the normal variations in thickness of extruded film, surface irregularities, and other uncontrollable variations impede the formation of such internal seals on a commercially useful basis. The package is a hermetically closed envelope of thermoplastic polymer film enclosing a hollow breaker between the two film sections. The breaker strip

can be chemically similar, only necessitating a difference in the physical orientation. The breaker strip is made of a fibrous layer, which separates along an interior plane between the envelope and the surface of the breaker strip. The rupturing stress is incapable of breaking the outer barrier walls.

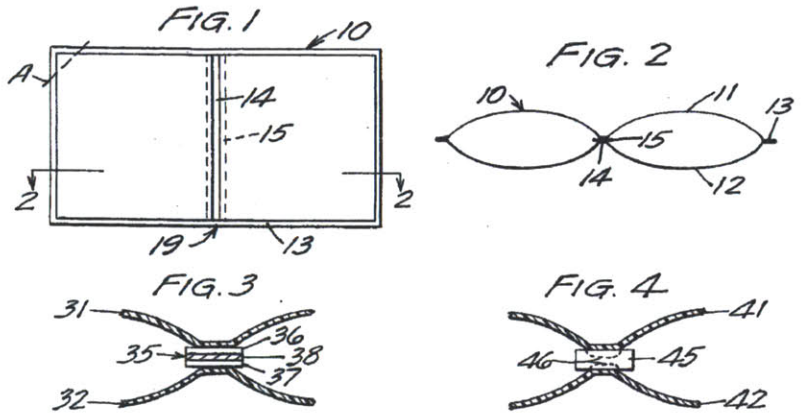

Figure 13: Seal ruptures along the envelope and the surface of the breaker strip [22]

5.3 Easy to peel Hermetic Seals

Yoshida et al [23] disclose an idea for a plastic container having an easy to peel seal forming compartments. The easy to peel open-ability of the resin mixture is obtained by melting and mixing resins of different miscibility and forming sheets whose surfaces are divided into minute areas having different heat seal-ability. The sealing temperatures must be so chosen that they are lower than the melting starting temperature of the resin. On the other hand the hermetically sealing property is obtained by ensuring mutual dissolution of the resins so that the bonding strength is close to the strength of the mixture. For good hermetic seals the sealing temperatures must be chosen so that they are higher than the melting temperatures for the resins. Excessive resin compatibility produces seals which are incompatible with the easy-to-peel requirement. Resins which are poorly compatible create a poor hermetic seal. Thus, balancing easy-to-peel with hermetic seal-ability is a tradeoff.

5.4 Masking Seams

Expressing the same concerns to predictable failure as those enumerated in the previous section, another Combination Package invention [24] proposes a seam seal having a predictable resistance to rupture which is less than the tear strength of the material. Reduced resistance to rupture is imparted to the seam by virtue of a masking means, creating uniformly dispersed islands seals separated by openings of non-joiner, reducing the total area of the seam (Figure 14). The concept proposes approximately 50 % through openings, separating the fused islands. The stress applied to the seam is supposed to be concentrated at the islands, permitting progressive rupture from island to island.

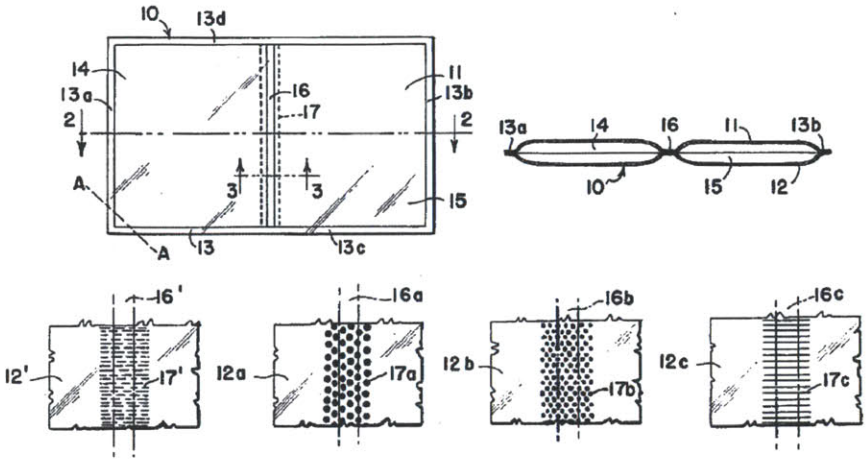

Figure 14: Patterned seals for variable bonding strength [24]

5.5 Sealing Interlayers

The inventors propose a rupturable seal comprising two films of polymer and a sealing interlayer. [25] The sealing interlayer has a melting temperature higher than the two polymer films and comprises of an array of microfibers ranging from 2.5 μm to 7 μm. Fusion bonding of the films to the two sides of the sealing interlayer creates a rupturable seal having a breakable interface. The application of force causes a gap separating the two polymer films.

5.6 Enclosure Configuration

The patent titled "Break seal before access dual chamber bag" [26] discloses an invention where two breakable seals separate an access port. The inner seal ruptures first allowing the solutions to mix followed by the second seal that opens the entrance to the access port. The enclosure housing the two compartments can have multiple configurations – stepped shape bottom, round bottom, triangular shaped bottom.

5.7 Radio Frequency Welding to form Breakable Seal

In an improved method of forming a burstable pouch, the inventor proposes a method to select a laminated polymeric film with an outer layer which is Radio Frequency responsive and an inner layer which is non-responsive, to a radio frequency winding field [27]. The inner layer is composed of bi-axially oriented polymeric material such that the cohesive strength in thickness is less than in directions along the film. The outer layer also has a higher melting temperature than the inner layer. This method uses RF welding in a unique way to fuse the inner layers to achieve highly consistent breakable pouches (Figure 15). This technique has the advantage of allowing wider manufacturing tolerances. Although this technique is not explored in depth as a part of this thesis, the author believes that this method should be explored further to optimize the seal manufacturing process.

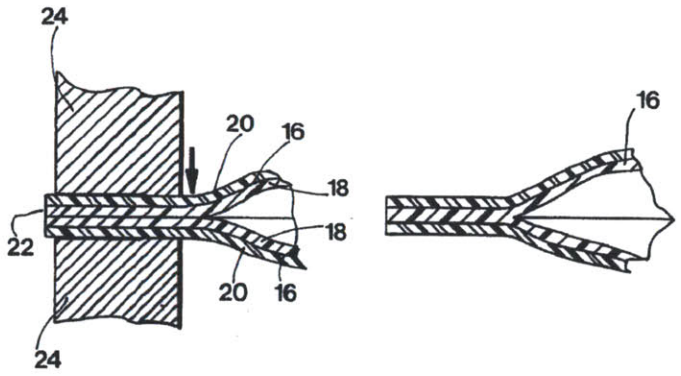

Figure 15: Exit seals using radio frequency welding allows wider manufacturing tolerances [27]

Based on the research into seal designs and methods of formation, it is evident that any alternative design must address some key considerations for liquid containment –

1. Predictable, Consistent rupture.
2. Hermetic Seal
3. Gradual vs. Rapid Seal Rupture
4. Easy to Peel
5. Leak-Proof

These considerations are thus an addition to the flow considerations – flow rate and flow anomalies specific to the Daktari Reservoir pack. The next section focuses on Daktari's exit seal investigating the nature of bonding and the resultant topography of the film.

5.8 Daktari Exit Seal Investigations

The seal ruptures when the plunger applies pressure on the reservoir domes. This pressure is a function of the strength of the bond forming the seal. The strength is again influenced by a number of parameters – materials, process parameters – time, temperature, seal pressure, seal profile, speed of plunger actuation etc. However, the rupture characteristics are highly unpredictable. The film has several layers and the repeatability of the failure boundary influences not just the pressure limit of the seal but also the pressure build up prior to flow initiation and the back pressure from the flow of reagents. It is important to know if the seal breaks along a central plane, top plane (dome film aluminum) or the bottom plane (lid film aluminum) of the bond. The author investigated the nature of Daktari's seal and is presented in this section.

The reservoir pack is a superimposition of several layers. The sealing is a simple process where a tool presses down on the lid film under a specific temperature and pressure for a pre-defined hold time. The tool embosses a thin line seal through the lid film, melting a coating on the lid film as well as the coating on the dome film. It is worth studying what happens at the locally melted pool of coating and the resultant topography of the lid film and dome film as a result of the pressing process.

5.8.1 Peel Process

Establishing the peel protocol is an important step in studying the exit seal structure. There are three phenomena occurring at the seal – effect on the two heat seal bonds – a) dome film and the heat seal coating, b) lid film and the heat seal coating and creation of a cohesive bond – c) the coatings on both films. Understanding where notch propagation occurs and proceeds is important to analyze the exit seal topography. Two different protocols were established to distinguish the structure resulting from the peel as opposed to the structure resulting from the exit seal rupture. The area adjoining the exit seal is peeled by pulling the lid film in one protocol while the dome film is peeled in the second protocol. The layer being pulled has an impact on which of the heat seal cohesive bonds are separated. The peeled sections were then closely observed for topography, material characteristics and geometry.

5.8.2 Observations and Inferences

Four approaches were adopted to study the exit seal area as follows –

1. Microscopy
2. Interferometry
3. Thermal
4. Chemical

5.8.2.1 Microscopy

The peeled areas adjoining the exit seal were observed at the microscopic level. The image (Figure 16) indicated a thin strip of seal region that has clearly defined boundaries. This seal section seems to contain an additional thinner feature. From a 2 dimensional microscopic image it seems that the inner feature, ***A***, has a hemispherical profile. This may be a result of the tool used. However this is not a single layer, it is a combination of heat seal coating and aluminum film. There is also a possibility that the heat seal coating melts and flows away from the central section of the tool. It is possible that there is an aluminum to aluminum contact or no bonding under the exit seal line. Figure 16 indicates a sharp definition B, which may have been caused by the lid film pressing against the dome film. On the other hand, an image of the lid film under the microscope is indistinct at the boundary B.

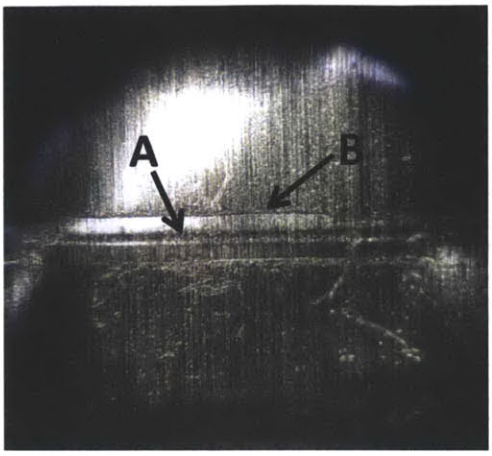

Figure 16: Exit Seal Dome film Bottom Layer under the Microscope

5.8.2.2 Thermal Analysis

The heat seal coating on the films is sensitive to heat. For both peel protocols, the lid film and the dome film were subjected to heat from an open flame. The heat melts the coating, turning the heat seal coating brown. Areas of the film where the coating is missing exposing the aluminum underneath become clearly visible with this test. Experiments indicated that the coating on the dome film is completely intact when the lid film is peeled (Figure 18) however there is a distinct line of aluminum when the dome film is peeled. (Figure 17) On the other hand both peel protocols indicate that an aluminum line is exposed on the lid film. A distinct line under the exit seal would have been visible if the coating flowed away from the exit seal, irrespective of the sealing protocol. It can be deduced that the coating on the lid film flows away under the pressure from the seal tool. On the other hand, the coating on the dome film does not flow away. The coating bonds the exposed aluminum on the lid film to the dome film creating the exit seal.

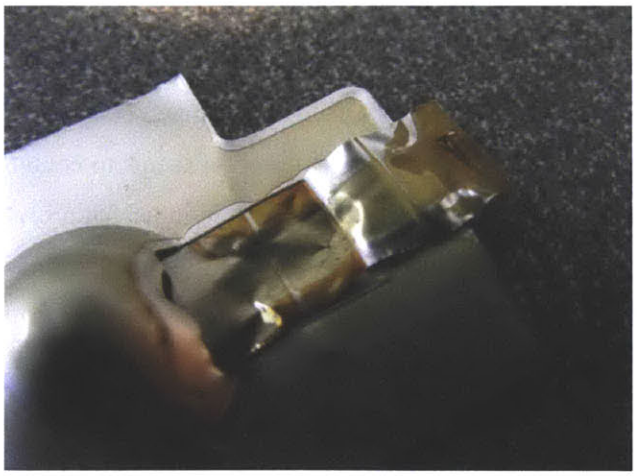

Figure 17: Dome Film - Aluminum exposed across seals on both films

Figure 18: Lid Film - Aluminum exposed across Exit Seals on Lid Film only.

5.8.2.3 Chemical Analysis

The exposed aluminum hypothesis was further validated using chemical analysis. A mixture of Hydrochloric Acid, Copper Sulfate and DI water detects the presence of aluminum. The mixture when applied to the peeled reservoir pack turns areas where aluminum is exposed, black (Aluminum Oxide). The experiment clearly indicated a black line forming when the lid film was peeled and the lid film was tested. However, the dome film did not show a black line indicating that the surface was completely covered in the heat seal coating.

5.8.2.4 Interferometry

An interferometer was used to scan the topography surrounding the exit seal regions. Scans were taken for both peeling protocols as well as an unpeeled reservoir pack. The scans provide valuable insight about the topography and bonding of the exit seal area. The peeling protocol also allows understanding the effect of peeling. The scanned images validate some earlier hypotheses from analyses conducted using microscopy, thermal and chemical methods.

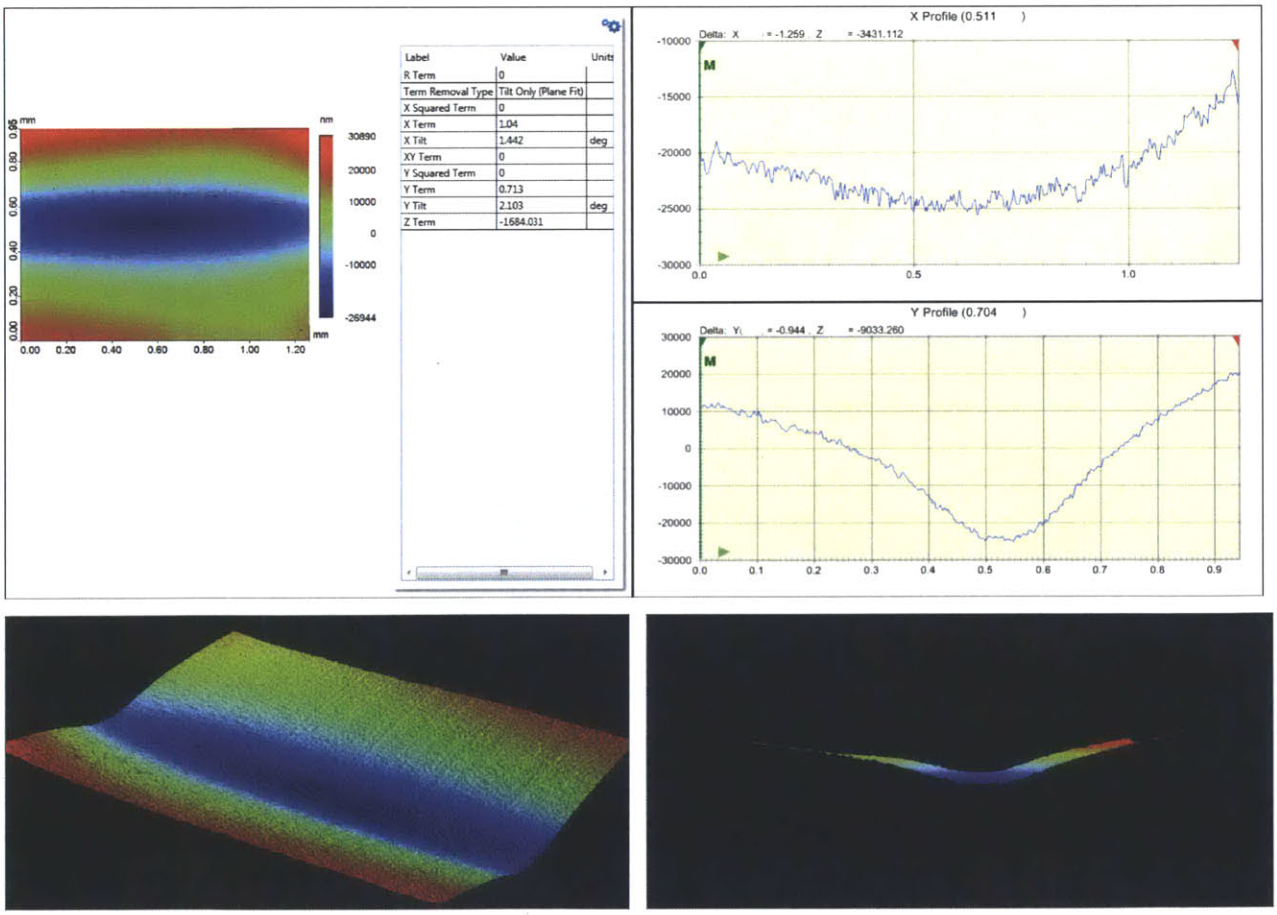

Figure 19: Lid film External Topography – Lid film Peel

In Figure 19, the deformation of the lid film that creates the exit seal is clearly seen. Scanned from the external surface of the lid film, the film deforms, drawing material from around the maximum depth of deformation. The aluminum layer in the lid film is less than the maximum deformation indicating that aluminum deforms with a possibility of being exposed for contact with the dome film. This deformation profile shape indicates the tool profile providing insight for the tool design. The convex surface in the bottom right image is the heat seal coating while the concave surface is the stove lacquer that bonds with the hot melt and the backbone.

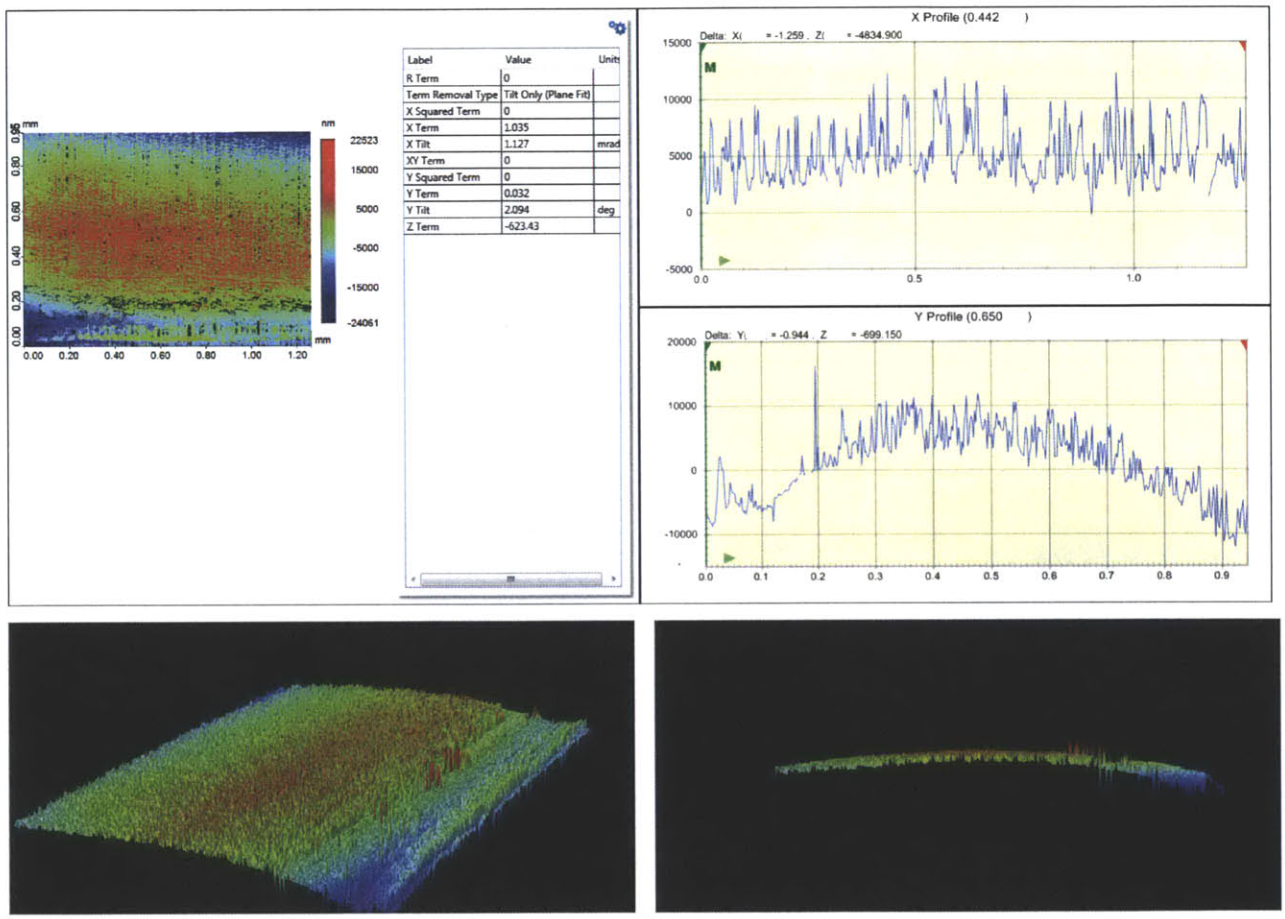

Figure 20: Dome Film Internal Topography – Dome Film Peel

The scan of the dome film peel when the dome film is peeled reveals an abnormally flat topography (Figure 20). However, the limited deflection could also indicate that the significant portion of the curvature could be aluminum exposed as a result of the peel process. The thermal analysis experiments have indicated that there is aluminum exposed on the dome film peel during the dome film peel protocol because the heat seal lacquer stays bonded to the lid film .

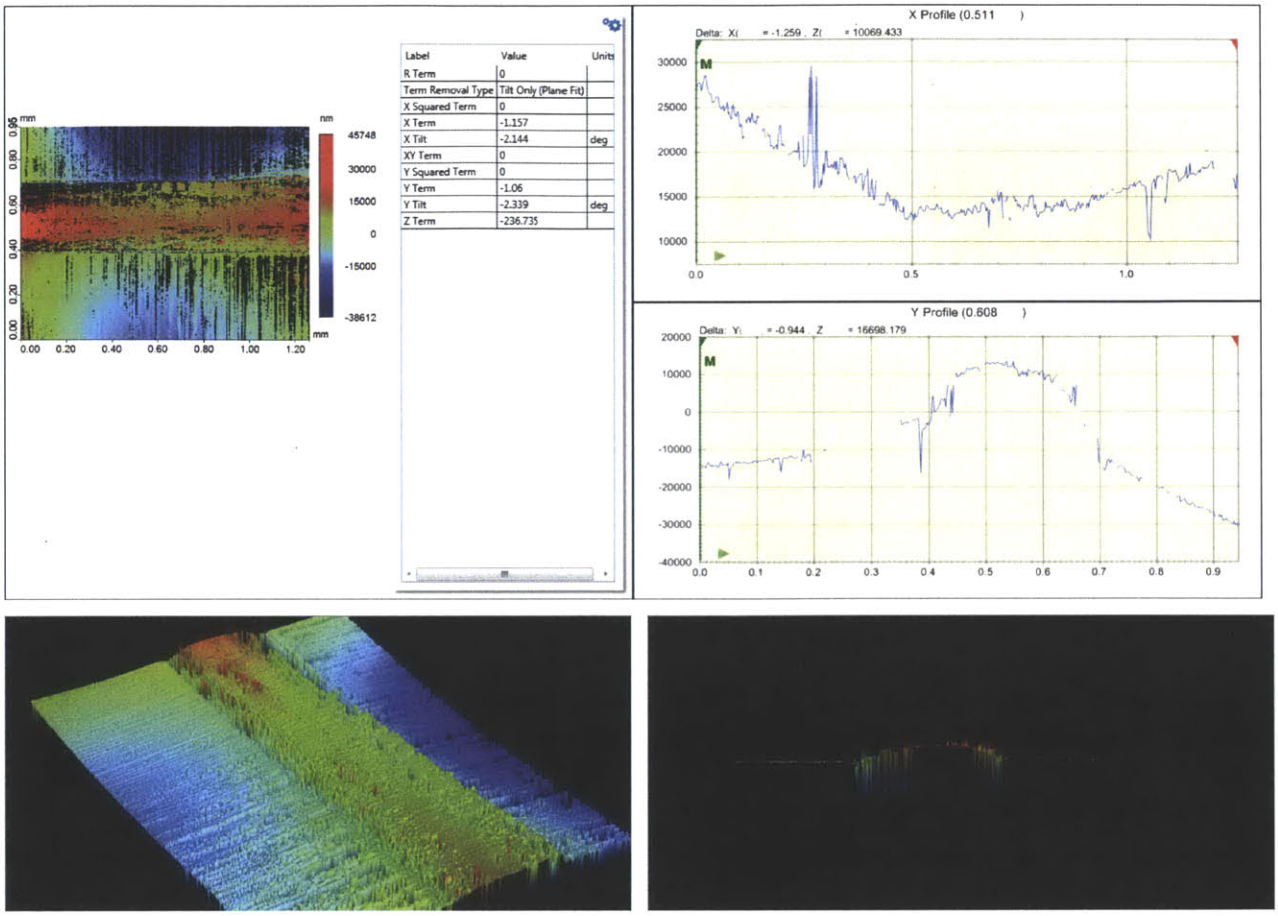

Figure 21: Lid film Internal Topography – Dome Film Peel

The Y Profile again indicates the nature of the tool profile (Figure 21). The profile appears inverted because of the orientation of the film under the scanner. The clear demarcation at the edge of the hemispherical surface suggests that the hemispherical profile may be exposed aluminum surrounded by heat seal coating as was discovered in the thermal analysis

The Lid film, dome film scan clearly indicates the impact of the tool on the inside of the dome film surface (Figure 22). The valleys and hills in the scan indicate the existence of flow of the heat seal coating away from the central portion. It may be possible that the coating melts and flows under pressure from the tool. The two valleys in the Y profile may be heat seal material. The two peaks next to the two valleys are slightly higher than the maximum deformation, which means that the heat seal coating has not been completely penetrated to expose aluminum. This validates initial findings from thermal experiments for the lid film peel protocol. The tool also draws material from the maximum depth of deformation.

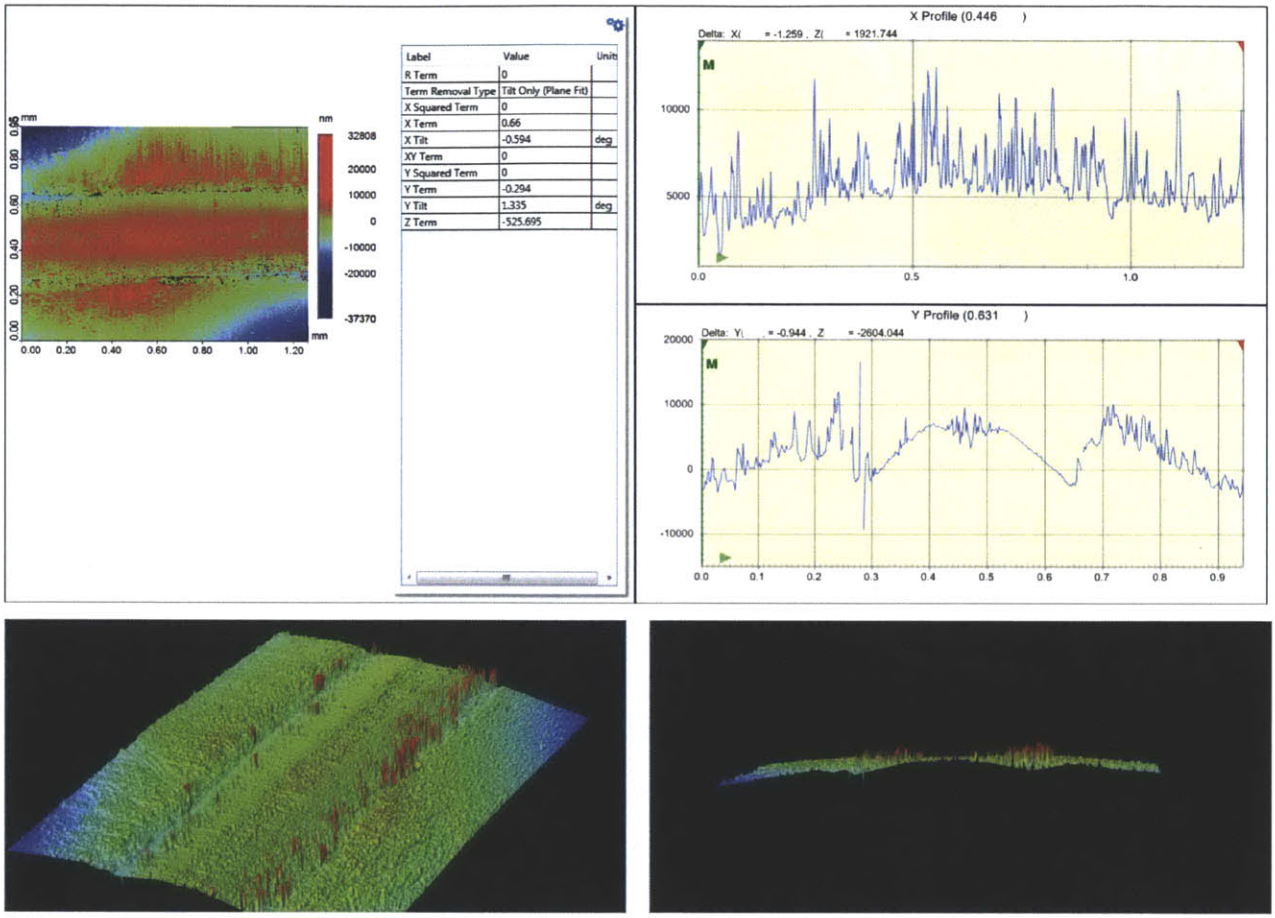

Figure 22: Dome Film Internal Topography: Lid film Peel

The research on breakable seal patents provides a direction to design and experiment with alternative seals to improve flow patterns by eliminating anomalies. Investigations on Daktari's present seal suggest that the seal is in fact a bond between the aluminum film on the lid film and the heat seal coating on the dome film. The next chapter describes the design, development process and tools used to create alternative seals.

Chapter 6: Exit Seal Development

This research explores various aspects of exit seal design and manufacturing process. This thesis also revisits the selection of the exit seal design. A tool used to create the seal will be redesigned and tested for different seal designs. The process parameters – Temperature, Time and Pressure* that determine the strength of the seal will be studied through a series of bonding experiments followed by flow tests and force tests that measure anomaly characteristics.

6.1 Exit Seal Design

Currently, the exit seal is a bond along a straight thin line. The exit seal tool is hemispherical in profile. Variations in the current design will be explored to determine the most optimal design. A fixture platen setup is designed to allow modifications in the location and profile of the exit seal. Simply in terms of design, the following alternative designs (Figure 23) are selected to test –

1. Chevron
2. Line

The study also considers the tool profile formed by changing the cross section across the exit seal.

1. Hemisphere
2. Flat

6.2 Process Characterization

The exit seal as mentioned previously is a key feature that regulates the flow of reagents at the point of exit from the reservoir dome. The strength of the exit seal may influence flow anomalies, to a certain extent. In order to fully characterize the process parameters and identify a process window is essential to establish manufacturing protocols that ensure repeatability in reservoir operation.

There are several important parameters that deserve consideration. The material used to create the reservoir packs. The mechanical, chemical and surface properties associated with the materials play a crucial part in the reagent delivery operation of the reservoirs. The gap between the two films which is a pressure dependent factor in the sealing operation also influences the strength of the reservoir pack. Operating parameters for the exit sealing operations were the control opportunities available to influence the reservoir manufacturing process.

*All parameters described in this thesis are dimensional units, concealed to protect Daktari's IP

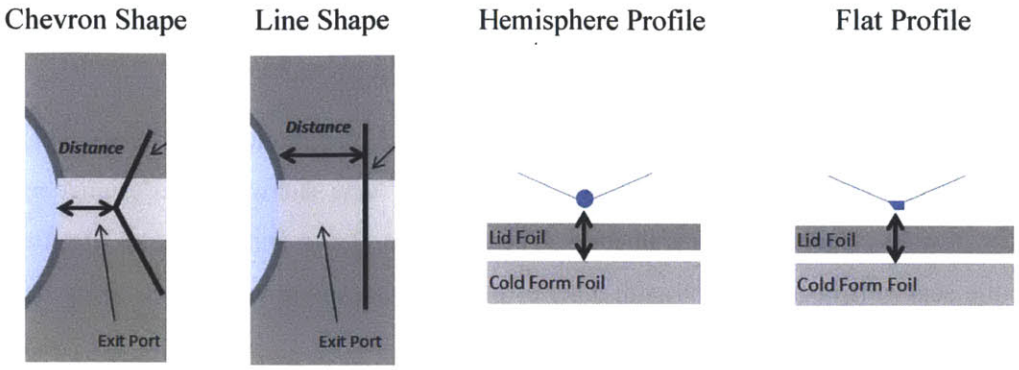

Figure 23: Exit Seal Design Considerations

Consequently, the three important factors taken into account in this study are – Temperature, Time and Pressure. Although all three factors generally contribute positively to the strength of a bond, it is expected to fail under a predetermined pressure applied by the plunger.

Earlier experiments conducted [28] on the bonding characteristics of a two layers of the dome film indicated that Temperature was the most significant factor in the bonding process. Time followed by Pressure was also a significant factor in the bonding process.

Preliminary experiments will be carried out to get a general understanding of the design space for the parameters. This will be followed by a parameter scoping exercise for the three factors – Temperature, Time and Gap at the best seal pattern. These reservoirs would then be filled up and sealed in batches and tested using a flow measurement setup to measure flow rates and identify and record the changes in flow pattern for different seal designs.

6.3 Platen Press

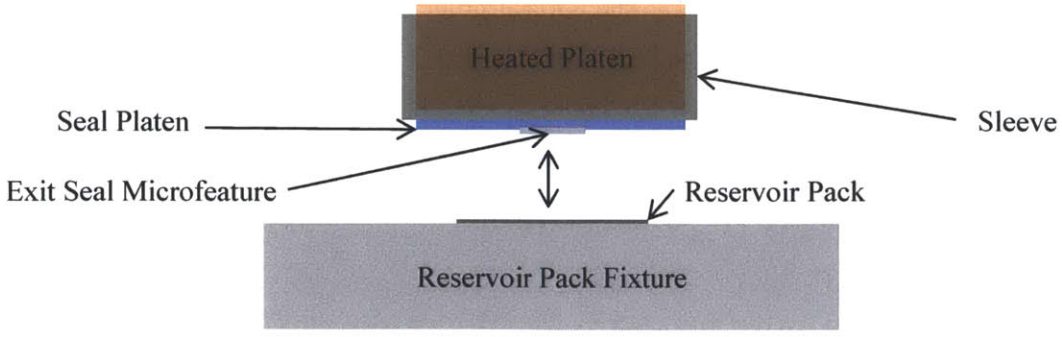

Figure 24: Platen Press Schematic

6.3.1 Existing Fixture for the Fill Port Seal

Daktari operations have been geared towards establishing a pilot line and several operations are being performed in-house, one of which is the area sealing operation. Daktari has a platen press fixture that houses the reservoir packs and heats the platen, sealing the reservoirs. A platen heater, with three integrated features, the reservoir base plate and connectors that can connect the heating platen to the press are also available. Keeping the existing fixture intact the setup is modified to create an exit seal platen. This fixture is added to the manual press to move the platen head vertically. The manual press allows height adjustment and travel adjustments (Gap) as a substitute for constant pressure.

6.3.2 Sleeve

A sleeve is designed to protect the pre-existing features on the platen heater and affix the sleeve to the platen heater using allen screws. A thermal expansion allowance is factored into the clearance fit designed for the sleeve. The sleeve also has a provision for attachments which allow greater variation in exit seal design experiments. Platens with different profiles can be easily attached without the need for creating multiple platen heaters. (Figure 24)

6.3.3 Platen

The platen is a thin plate with single feature integrated into it. These features determine the profile of the exit seal as discussed in the earlier section. The plate is unscrewed from the sleeve and is replaced by another platen to test different designs. These features on the platen are at the scale of 10-100 units and ensuring dimensional accuracy is challenging. A few but distinctly different profiles (Figure 27-30) were designed to experiment and optimize the exit seal. For the purpose of defining a nomenclature, the macro scale feature of the seal tool is referred to as the shape while the micro scale cross-sectional feature is referred as the profile.

6.3.3.1 Shape

The following shapes were proposed to test the hypothesis that the point of rupture will have an impact on the flow pattern.

6.3.3.1.1 Chevron

The shape is chosen to study if notch propagation becomes easier if the seal is broken at a single point first instead of a line. The intersection of the two arms is aligned with the center of the exit channel. (Figure 26) The chevron shape also allows gradual rupture of the exit seal. Two possibilities are predicted as a result of this change – The chevron shape may only rupture at the intersection of the two lines without propagating the rupture along the two arms. This may not be a desirable outcome of the experiment and instead a line would be a better alternative. The other possibility is that this shape

provides a more predictable and consistent failure eliminating flow anomalies. The rationale behind such a hypothesis is that a point based failure initiation reduces variability compared to a line based failure simply because identical multiple points may or may not rupture concurrently every time. A better flow pattern associated with the chevron seal would validate this hypothesis.

6.3.3.1.2 Line

This is fundamentally a thin line which stretches across the exit region (Figure 25). Although this is the shape of the current seal, this platen shape was designed to eliminate variations in operational practice vs. the present study arising from parameters and equipment.

Figure 25: Line Shape

Figure 26: Chevron Shape

6.3.3.2 Profile

These micro scale features determine the topography of the lid film and the dome film as a result of the sealing operation. The following profiles were constructed and tested for flow pattern.

6.3.3.2.1 Hemisphere

The hemispherical profile was chosen to eliminate the impact of angular misalignment. This profile creates a distinct topography which will be explored more in the section on exit seal investigation. It is worth exploring if this is indeed the best profile if we assume accurate angular alignment. The diameter of the hemisphere is designed to be 200 units.

6.3.3.2.2 Flat

The flat face of the sealing feature is designed to understand how a planar seal interface affects the rupture mechanics. The flat feature is also provided with a taper at the end to gradually (not slowly) release fluid pressure through the exit region instead of an abrupt opening. The influence of such a taper or its position with respect to the flat surface is worth exploration. The author postulates that this would result in reducing pressure waves and minimize Anomaly 1 spike. The flat face is designed to be 100 units with 100 units in height with a slope of 45°.

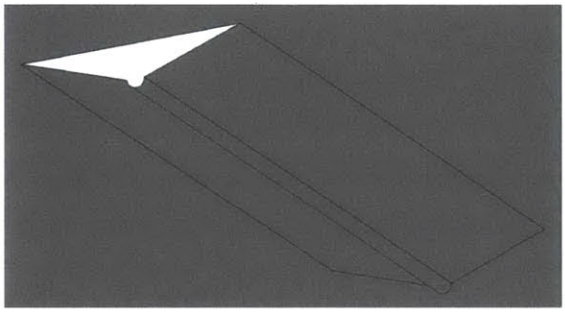

Figure 27: Line Hemisphere

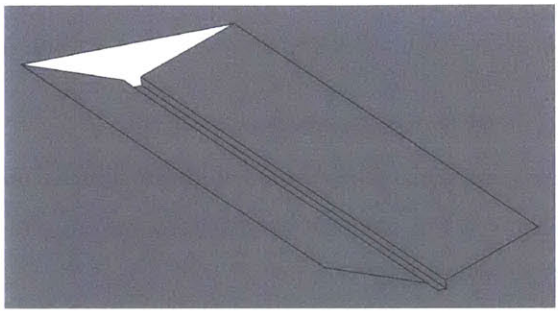

Figure 28: Line Flat

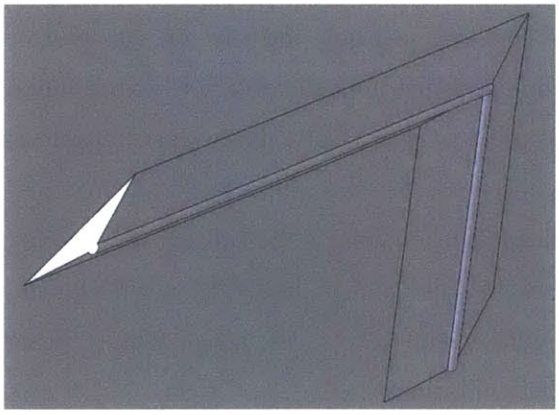

Figure 29: Chevron Hemisphere

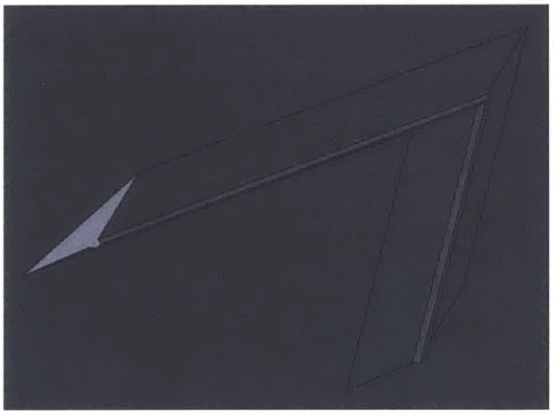

Figure 30: Chevron Flat

A combination of these platens results in 4 different patterns for the exit seal platens – chevron hemisphere, chevron flat, line hemisphere, line flat.

6.3.4 Connectors

The connector plates allow the attachment of the linear stage to the other parts of the fixture. The top plate connects the top reservoir housing plate to the linear stage. The bottom plate connects the linear stage to the Base plate.

6.3.5 Linear Stage

The linear stage allows changing the position of the reservoir pack relative to the position of the platen. The exit sealing is performed one reservoir at a time. Moving from B1 to B2 and B3 is possible with the stage. Additionally, the stage also allows changing the location of the exit seal relative to the reservoir to explore the most optimal location.

6.3.6 Heating System

The heating system uses a 200 W Cartridge Heater and a thermocouple to sense temperature of the platen. The temperature ranges from 80 to 120 units. A temperature controller is also integrated into the system that allows detection and control of the sealing parameters.

6.4 Interferometer Scans

The new seals are scanned with an interferometer to inspect the resultant geometry of the film. Two designs – the chevron hemisphere design and the line flat design and the scans are discussed in the following section.

6.4.1 Chevron Hemisphere

The scans below (Figure 31-34) are taken from the Lid film side and help identify the diameter of the hemispherical tool and the sharpness of the corner which is designed to be the point of rupture initiation. The X axis profile shown in the (top graph) of all figures gives an idea of how the two arms meet toward the tip of the chevron. The two valleys in the top left image are the two arms of the chevron and are caused by the hemispherical profile on the chevron and keep coming closer in the subsequent images until they converge to the tip. The y profile remains constant as we move along a straight line towards the tip, but it indicates the diameter of the impression caused by the micro-feature. The micro-feature is around 200 units as expected and draws film around the hemispherical feature.

6.4.2 Line Flat

An interferometer scan of the lid film from the inside taken after peeling the dome film, clearly shows the presence of a slope followed by a flat and a straight drop in the Y profile (Figure 35). This scan confirms that the Line Flat exit seal creates seal with a slope on the reservoir dome side. The raised feature is a result of the orientation of the peel under the scan. The flat face seems to be more than 100 units and could be a result of the lid film being drawn from surrounding the micro-feature.

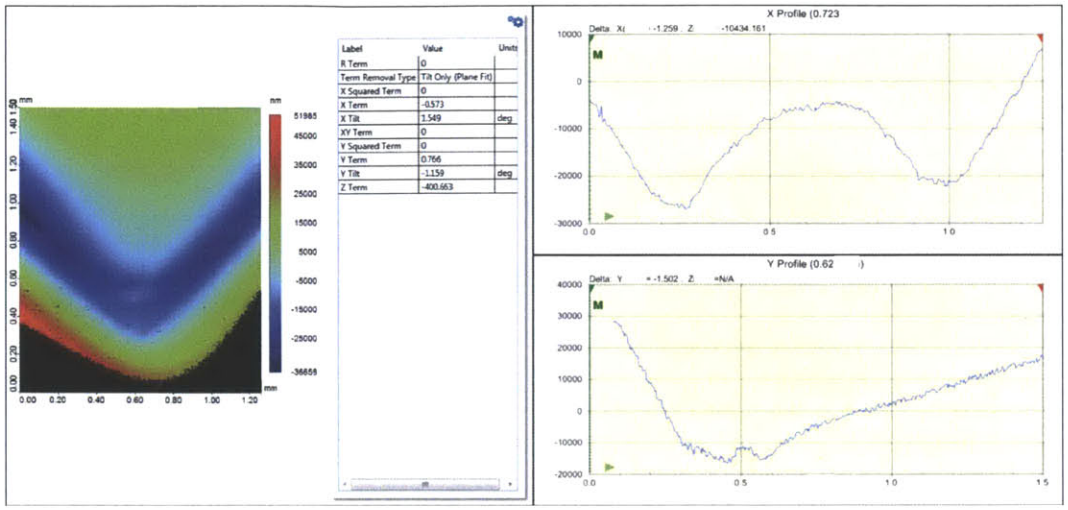

Figure 31: Chevron hemisphere Interferometer Lid film Scan at y = 0.723

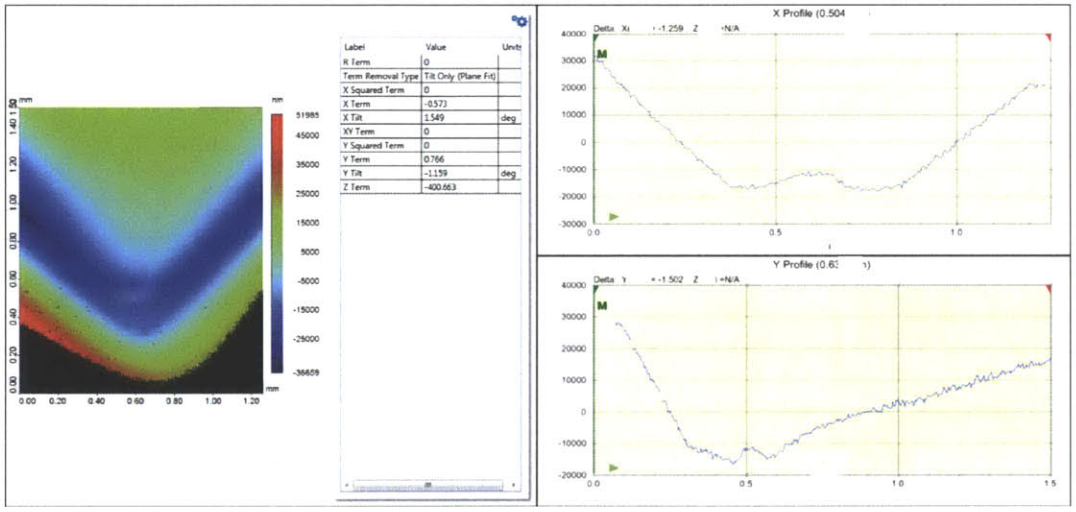

Figure 32: Chevron hemisphere Interferometer Lid film Scan at y = 0.504

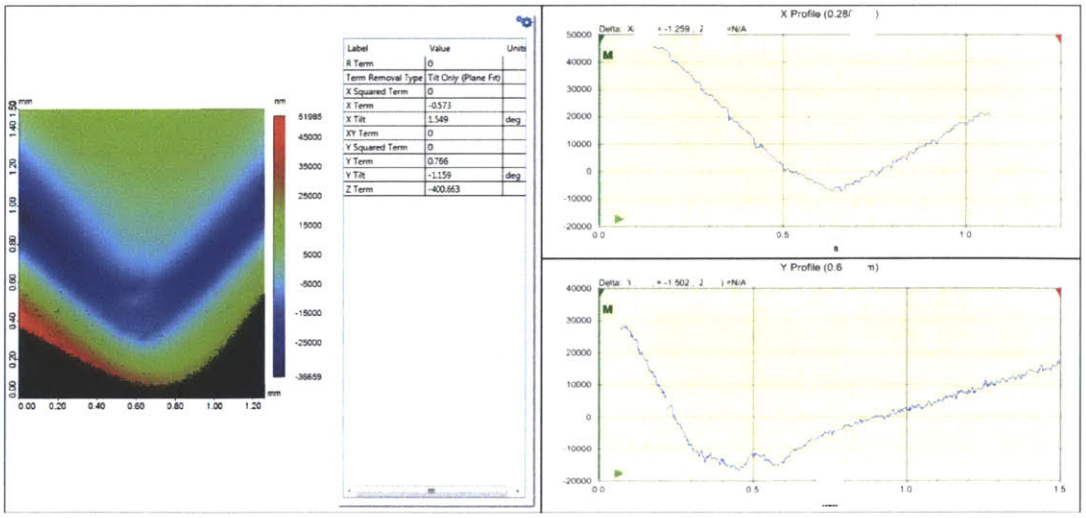

Figure 33: Chevron Hemisphere Interferometer Lid film Scan at the corner (y = 0.288)

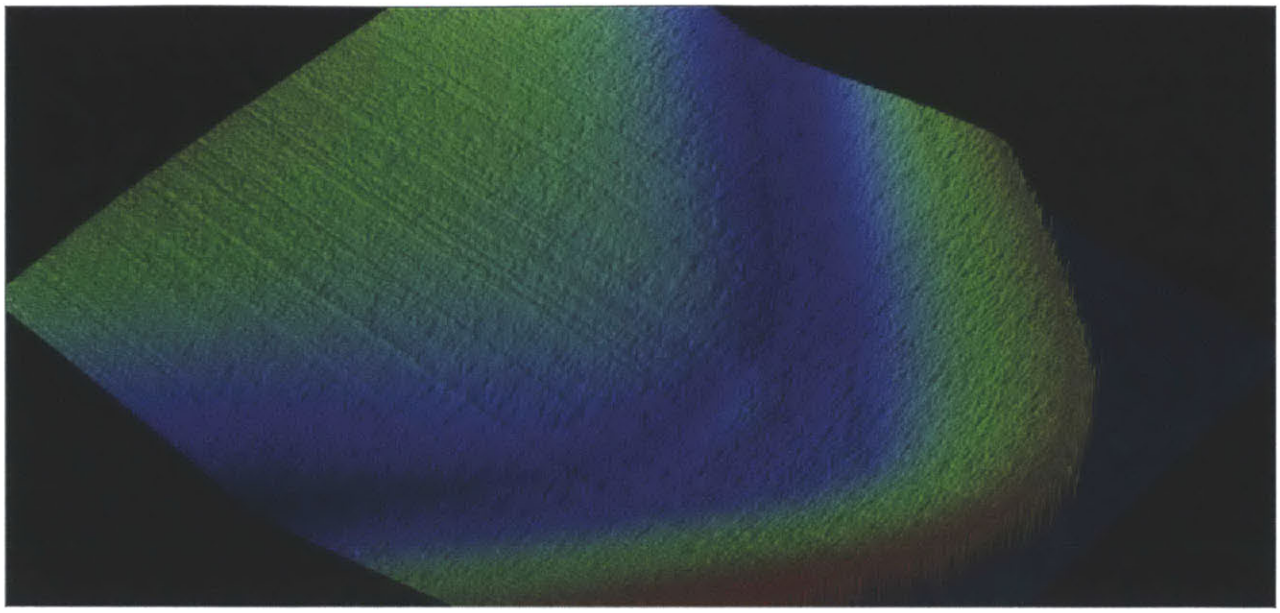

Figure 34: Chevron Interferometer Lid film Scan

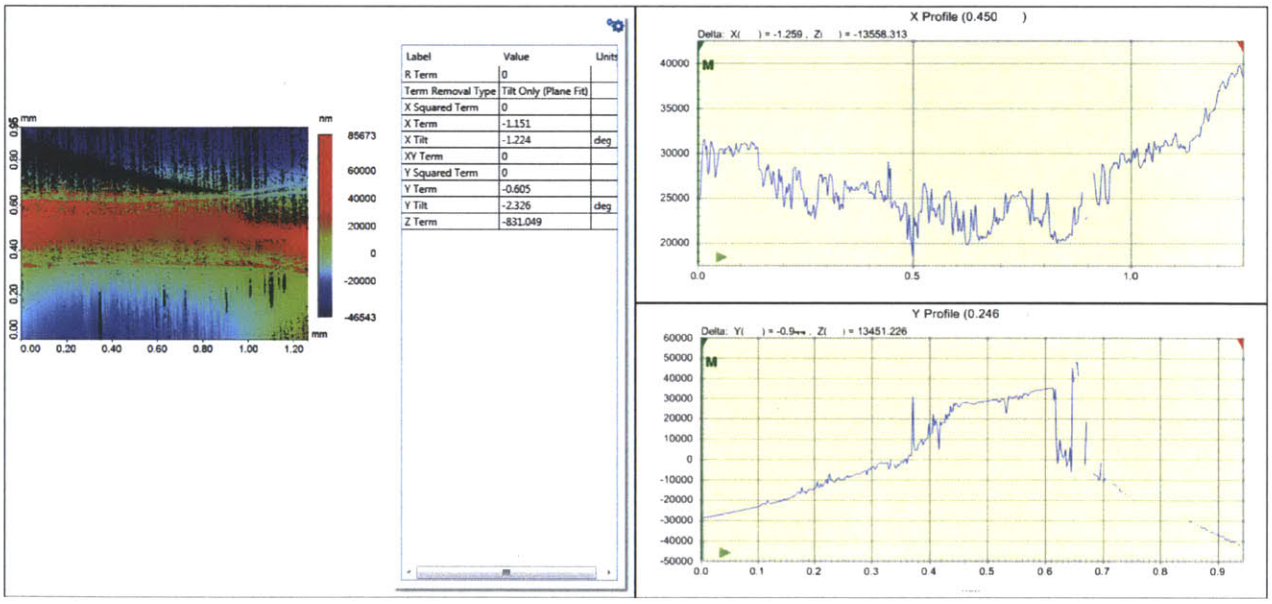

Figure 35: Dome film Peel - Lid film Scan

The interferometry scans provide a confirmation of the shapes and profiles designed for the exit seal. These two designs cover the both the chevron and the line shape as well as the flat and hemispherical profile. Next, a discussion on the methodology of experiments to test the exit seals for flow patterns and force patterns to discover the nature of seal rupture.

Chapter 7: Methodology

This chapter discusses the methodology for experimentation of the impact of exit seal design on the flow patterns. The parameter space is explored through preliminary experiments followed by a discussion about the sealing protocols, peel tests, scoping for parameters, force measurement and the flow measurement technique.

7.1 Exit Sealing Parameters

The exit sealing process was carried out using the platen press described in Chapter 6. The process involved using a manual press to press the heated seal plate onto the lid film face of the reservoir pack to create the exit seal. A set of parametric settings influence the behavior of the exit seal. It is important to identify these factors and find optimal levels that ensure repeatability of flow pattern without the flow anomalies mentioned in section 4.3 on Reservoir Dynamics. The following section enumerates on these factors and defines a method for scoping the said parameter.

7.1.1 Temperature

Earlier experiments in film bonding [28] had clearly established the significance of temperature in the sealing strength. Temperature is positively correlated with strength of the seal. However, the exit seal breaks to allow reagent to flow and yet is hermetically sealed to prevent loss of reagent through evaporation or leakage.

The exit seal plate was heated through the sleeve and the existing platen heater using a 200W cartridge heater. The heat seal coating on the film which creates the bond has a melting temperature of 75 units. Any temperature below the melting temperature of the heat seal coating may fail to create any sort of bond between the dome film and the lid film. A higher temperature will create a stronger seal but could also result in bonding areas adjacent to the exit seal due to heat conduction through the film. A process of trial and error was adopted to identify a working range of temperatures measured in arbitrary units. Preliminary experiments led to the parameter scoping exercise using 5 replicates for each condition.

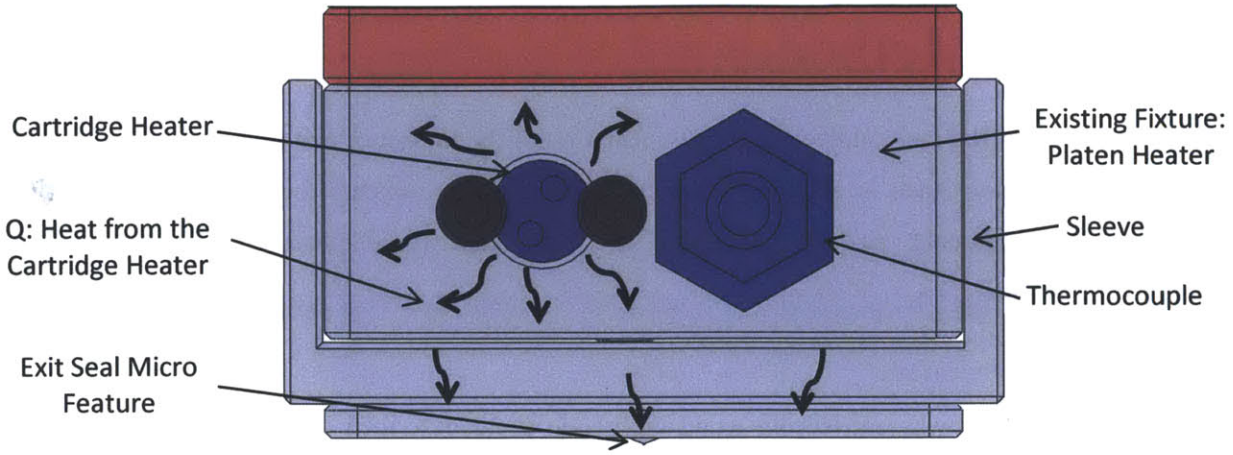

Figure 36: Platen Press Head: Side View

The Platen Press designed had one severe limitation. (Figure 36) The cartridge heater and thermocouple were both located in the platen heater in the existing fixture. The temperature recorded by the thermocouple was from the vicinity of the cartridge heater. However the heat supplied by the cartridge heater must go through the sleeve which is attached using fasteners resulting in some air gap followed by the actual platen plate which has a micro-feature milled on its bottom surface. As a result, the effectiveness of heat transfer was severely limited. The platen plate temperature was measured using a different contact thermocouple and was found to be lower than the temperature indicated by the thermocouple. We found that there was a difference of about 15 units. This temperature difference was further amplified after a few samples due to heat transfer from the micro-feature to the film and to the colder aluminum base. The recovery time to base level is 30-60 units. These findings made it necessary to continually monitor the temperature of the feature independently to ensure uniformity in sealing parameters. The selection of parameters for scoping is explained in the preliminary experiments section

7.1.2 Time:

Earlier bonding experiments [28] indicated Time as the second most significant parameter after Temperature in film bonding processes using heat seal coating. The dwell time is the time the plate continues to be in contact with the film after reaching the maximum travel of the lever on the manual press. The pressure applied is determined by the travel of the lever. In addition to melting the heat seal coating more effectively, the dwell time also affects the heat distributed around the seal which resulting in undesirable bonding around the exit seal. Not only does this result in a higher overall force needed to push reagents through the reservoir, it also results in noisy flow patterns due to topography variations. The dwell time or press time was varied over extremes and studied in preliminary experiments. The selected dwell time parameters for scoping are enumerated in the preliminary experiments section.

7.1.3 Pressure/Gap

The use of a manual press makes it difficult to accurately measure the applied pressure. Given the constraint it was decided to adopt Gap as a substitute for pressure. The gap is actually the compression of the micro-feature into the film. (Figure 37) Varying this distance allows us to vary how deep the micro-feature will travel after it makes contact with the lid film surface in effect changing pressure.

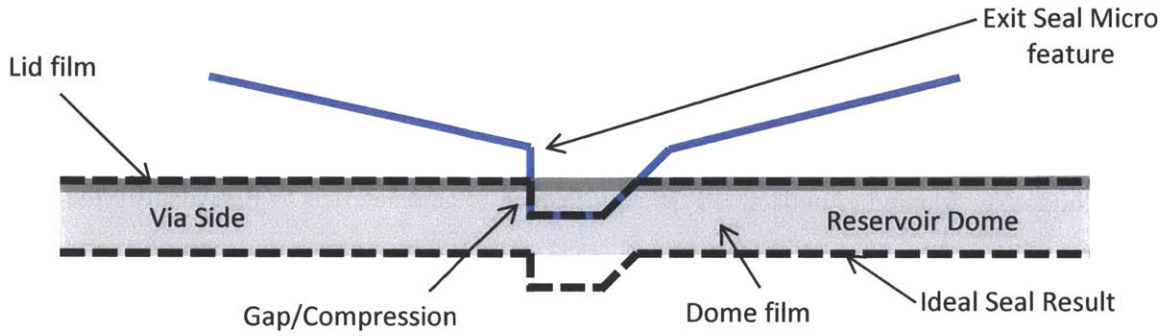

Figure 37: Exit Sealing Process for "Line Flat"

The manual press has a micro travel adjustment with a least count of 20 units. Pressure/Gap is decided by make contact with the lid film using the micro travel adjusting mechanism. It is much easier to keep track of compression from point of contact and hence Gap is actually measured as the maximum compression. The thickness of the reservoir pack is 100 units in areas where the lid film is bonded to the dome film. The micro-feature embosses a line from the lid film side, and protrudes the dome film on the other side. The expansion of the platen heater, the sleeve, the plate and the micro-feature must be taken into account when the distance adjustments are at such micro scales. Once different temperatures were selected through the preliminary experimentation process, each of the temperatures was assigned a contact distance, the Gap parameter was maintained by keeping the depression constant over the different temperatures. Certain low compression depths failed to produce any sealing, on the other hand high compression depth damages the micro-features due to direct contact and high pressure at the lowest point when the feature makes contact with the rigid aluminum base.

7.1.4 Distance

Distance is important; however, it is necessary to optimize other parameters by isolating the parameters – Temperature, Time and Gap as these directly affect seal strength. (Figure 36) The addition of a fourth optimizing parameter influenced by an uncontrolled feature such as the exit channel will add more variation in results. An optimal distance setting was found and kept constant throughout the parameter scoping exercise. Preliminary experiments on distance variation were used to find the best location for the exit seal.

7.1.5 Exit Seal Design

Different plates used for different exit seal shapes and profiles are changed and attached to the sleeve using fasteners. The plates were made from aluminum. However, preliminary experiments especially with the Line-hemisphere design resulted in the micro-feature being damaged, losing its hemispherical profile. This damage prompted a revision of the material. Another plate was machined in Carbon Steel to reduce wear due to repeated impact with the base. Preliminary experiments using the four shape-profiles indicated some clearly weak designs while some performed exceedingly well in flow tests prompting further parameter scoping for the best shape-profile.

The methodology adopted to understand the significance of parameters is to first identify the best shape-profile combination through preliminary experiments, followed by a parameter scoping exercise using the best plate for parameters- Temperature, Time and Gap with 5 replicates. Distance Optimization is carried out based on the findings in preliminary experiments. The best parameter combination would again be tested with different shapes and profile to complete a validation of the selection for the best plate. The system is isolated to study phenomenon directly. Only one reservoir - B2 is analyzed for all experiments.

7.2 Filling Reagents

Although Daktari's final product will contain reagents R1, R2 and R3 of varying ionic concentrations, all experiments use Deionized water (DI water) to test flow from the reservoir. Reagent properties such as viscosity do not vary much from DI water and hence can be used as an effective substitute. A calibrated pipette is used to fill Reservoir 2 with a fixed volume of DI water. Once filled the fill port is either immediately sealed or placed in a fixture ensuring no leakage of the reagent/DI water held within the reservoir dome. (Figure 38)

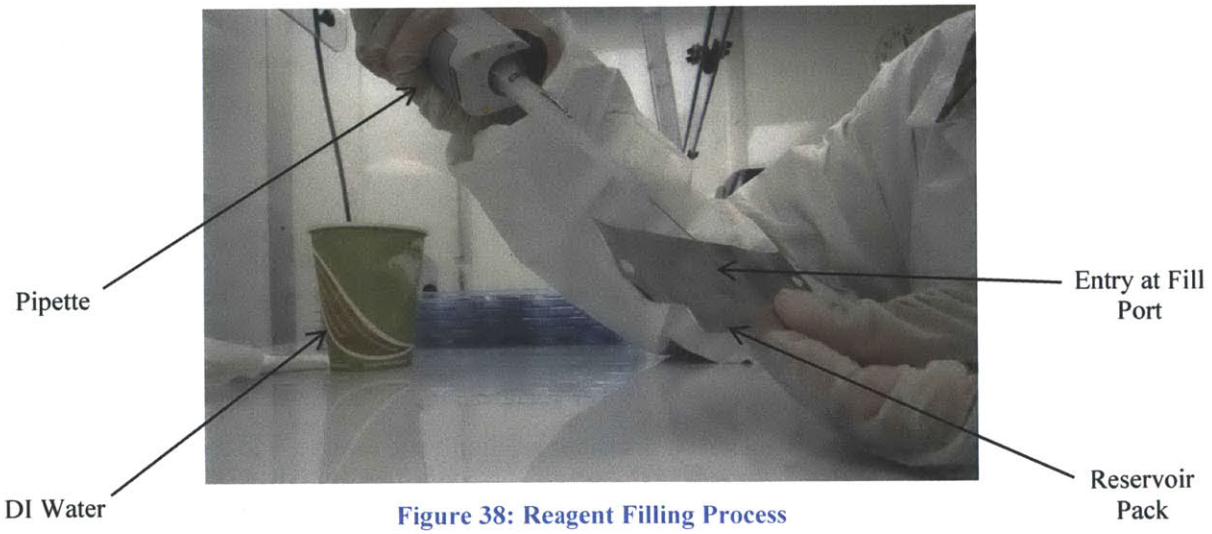

Figure 38: Reagent Filling Process

7.3. Fill Port Sealing Process

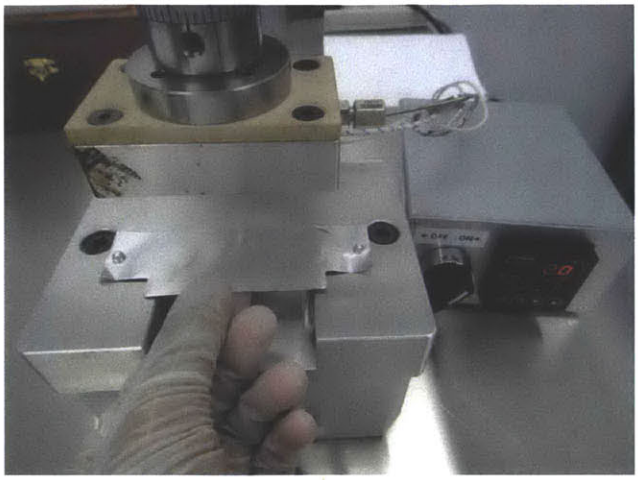

Figure 39: Fill Port Sealing Protocol

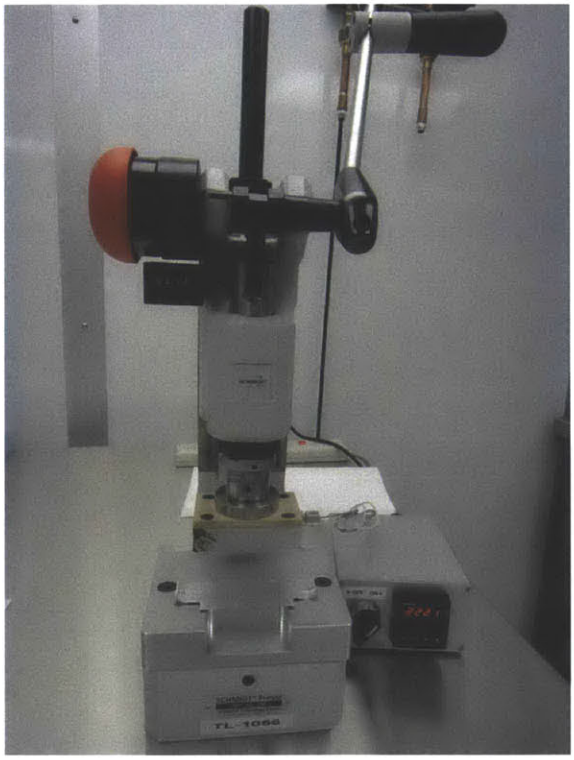

Figure 40: Manual press lowers the heated platen on the Lid film surface

Following the protocol the platen is heated and the lever is manually operated creating a stronger seal than the exit seal. (Figure 39, Figure 40)

7.4 Exit Sealing Operations

After the fill port has been sealed, the blisters are sealed at the exit channel. Care must be taken to avoid any leakage of reagents. The sealing fixture described in section 6.3 is then used to complete the sealing process. The platen is heated to specific temperatures, adjusted for a predetermined gap setting and pressed manually for a fixed dwell time. The process is illustrated in the figures below (Figure 41 - 44)

Figure 41: Manual Press

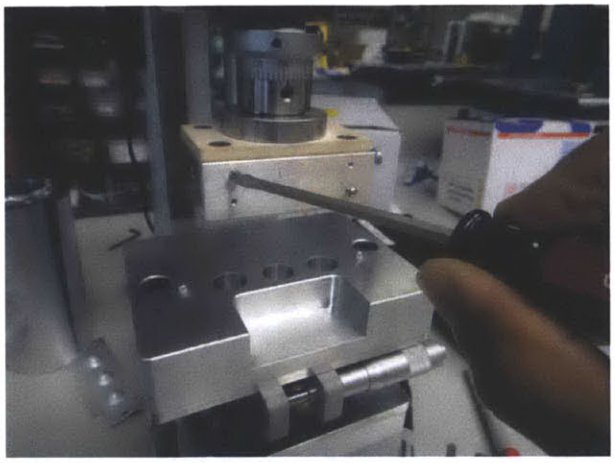

Figure 42: Set up the Exit Seal Fixture on the base

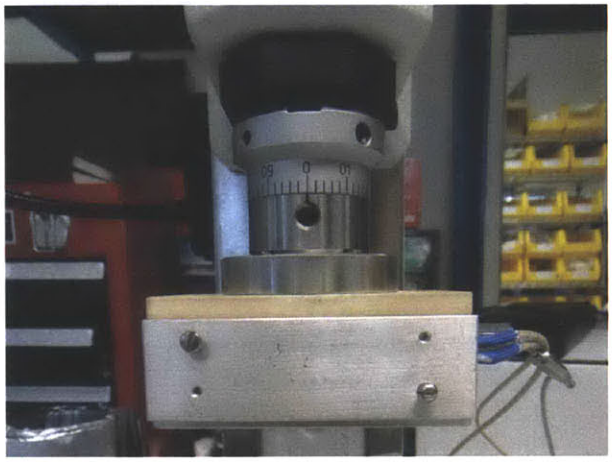

Figure 43: Adjust the gap setting.

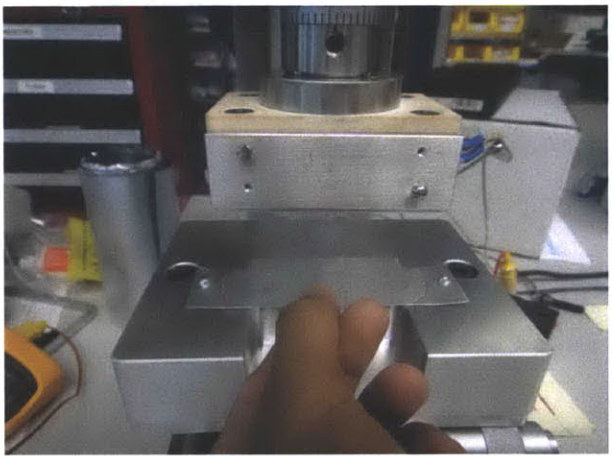

Figure 44: Place the Reservoir Pack

7.5 Backbone bonding

The sealed and filled reservoir pack is then bonded to the backbone ensuring that reservoir opens directly opposite the reservoir via (flow outlet hole) in the backbone. A thin layer of hot melt is positioned on the backbone. The reservoir pack is then placed on the hot melt and bonded. The press is heated and pressed with a pressure of 1.5 units for a fixed duration of 1.5 units.

7.6 Flow Testing

The purpose of this thesis is to characterize Daktari's exit seal to improve flow pattern repeatability by eliminating flow anomalies such as Anomaly 1, Anomaly 2 and Delamination. A custom flow setup at Daktari acts as a substitute for actuating mechanism in the Daktari CD4 instrument. This custom fixture houses servo motors which actuate the plungers based on a predefined script adjusting the plunger motion to achieve uniform flow rates. A flow sensor is also used in conjunction to measure reagent flow rates out of the reservoir via. The following section outlines a protocol for flow testing operations.

7.6.1 Flow Testing Operations

After the backbone bonding is complete, the reservoir pack bonded on to the backbone is tested for flow pattern using Daktari's custom flow setup. (Figure 50) The backbone is placed in the plunger setup using locating pins with the reservoirs facing inward towards the plungers. (Figure 47) The backbone is then locked in place using a backing plate held by clamps. (Figure 48) A plunger actuation script is loaded onto the instrument memory using a computer. The script parameters are described in the next section. The flow sensor is attached with pipette tips and connected to a syringe. (Figure 49) The syringe is used to prime the entire tubing with DI water. The pipette tip is then stuck into the reservoir via. The flow measurement program is loaded followed by initiation of the servomotor script. The plunger moves in and stops according to predefined steps in the script, popping the Exit Seal along the way and pushing the reagent through the reservoir via and the pipette tip and finally through the flow sensor where it is measured and the readings transmitted back to the computer.

7.6.2 Flow Testing Parameters

The script adopted for flow testing is restricted to Reservoir 2 to isolate systems and better characterize exit seals. According to the script, the plunger completes a self-test and actuates the plunger proceeding to pop the reservoir. Once the reservoir is popped the plunger continues its travel, compressing the reservoir for 30 units. The flow rate jumps higher than 40 units as soon as the exit seal is ruptured. The Plunger then stops moving resulting in the flow rate dropping precipitously in the ideal situation. The reservoir popping stage is followed by a period of sleep for 30 units where the flow rate should drop down to zero. After the sleep stage the plunger starts compressing the reservoir again adjusting the speed to achieve the desired flow rate of 20 units. Any anomalies present in the reservoir become clearly visible at this stage. Flow at 20 units continues for 60 units and is followed by a period of sleep for 60 units during which the flow rate drops down to zero. Another flow wave is designed into the script to test repeatability of flow within the reservoir. This second flow wave is again initiated by restarting the plunger motion pushing reagent/DI water at 20 units for another 60 units. Once completed, the plunger stops compressing the reservoir pack and rests/sleeps for a period of 30 units. Finally the plunger retracts to its home location within the instrument/setup. (Figure 45)

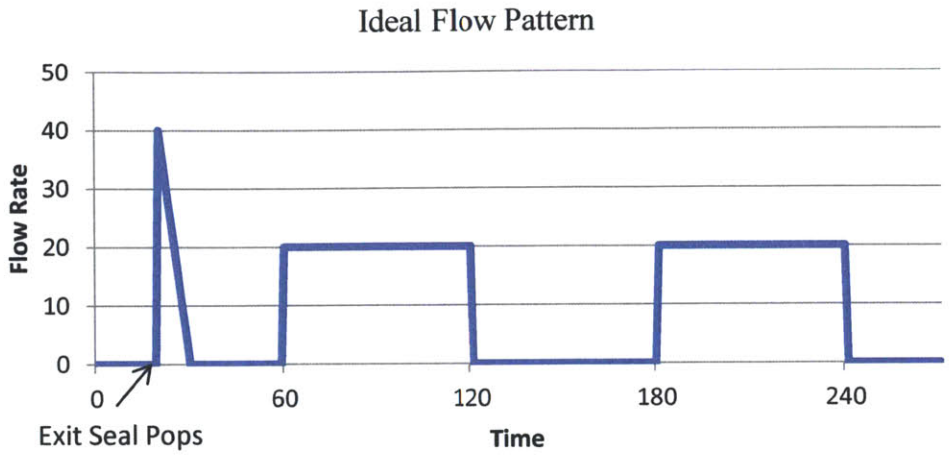

Figure 45: Ideal Flow Pattern for the Script

7.7 Force-Flow Testing

Understanding Force and Flow in an isolated manner does not fully reveal the true nature of the exit seal in its natural condition in the reservoir pack. A setup was developed combining the force testing capabilities of the tension testing instrument and the flow sensor. (Figure 54) A reservoir-pack bonded backbone was tested for flow and force simultaneously. Although, the plunger cannot be manipulated to achieve the same flow rates achieved with the flow setup Instrument, the data is extremely helpful in understanding Anomaly 2 and its relation to the strength of the exit seal.

A reservoir pack bonded backbone is attached on to an elevated platform using a double sided tape. (Figure 52) The elevated platform supports the backbone under the reservoir dome, however leaves space underneath open to attach a pipette tip to measure flow exiting the B2 reservoir via. (Figure 51) The tension testing force gauge has a plunger attachment connected to it which presses down on the reservoir emulating the action in the instrument. (Figure 53) The orientation of the backbone is horizontal as opposed to vertical in the instrument, while the plunger acts vertically as opposed to horizontally in the instrument. It is assumed that gravity does not have a major influence on micro-scale flow. The pipette tip is connected to the flow sensor using tubing and is fully primed before its insertion into the reservoir via. The plunger is set to move at a speed of 16.67 units.

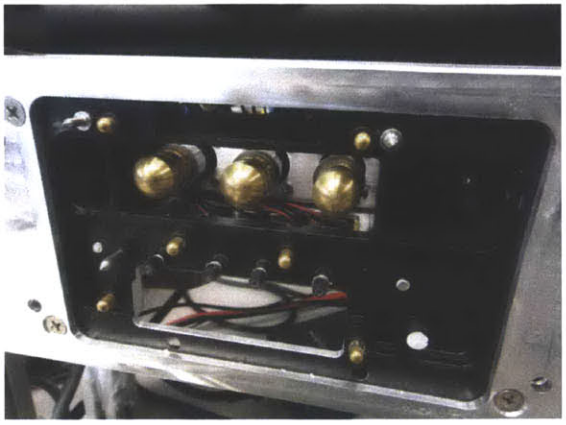

Figure 46: Servo actuated plungers in the instrument

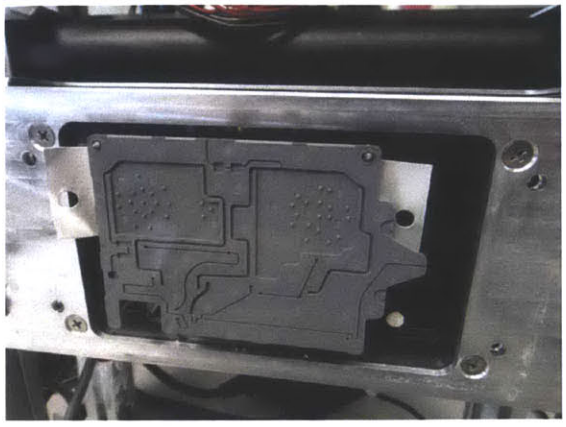

Figure 47: Locate Backbone in the flow setup

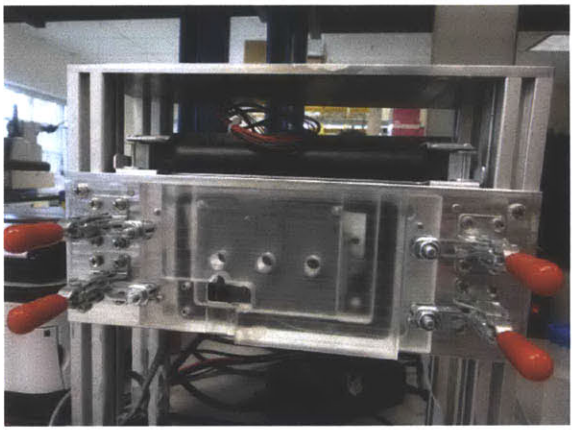

Figure 48: Clamp cover against the backbone

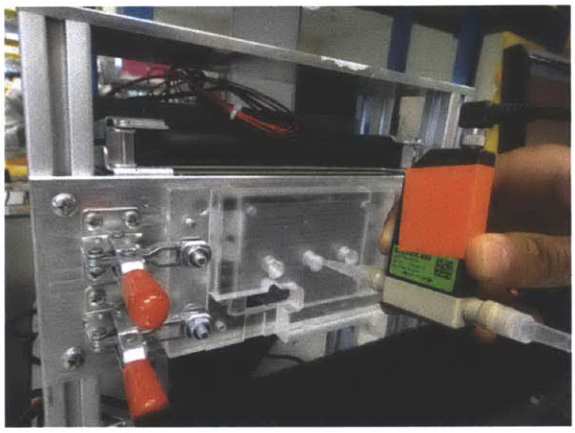

Figure 49: Insert pipette tip into B2 reservoir via

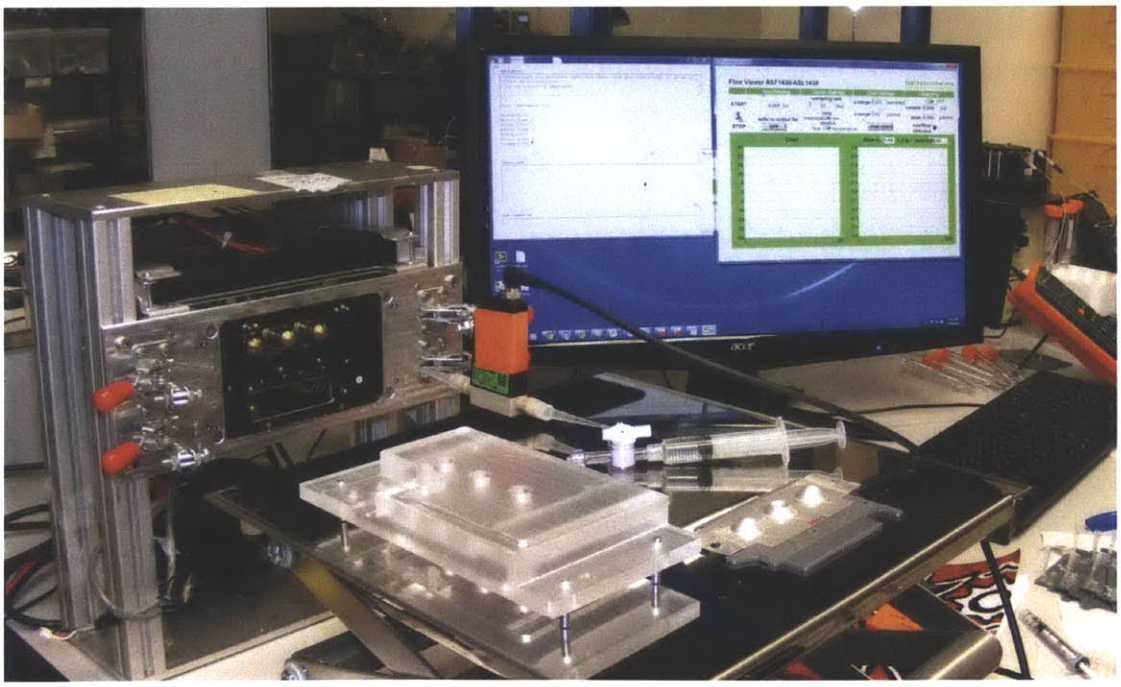

Figure 50: Flow Setup

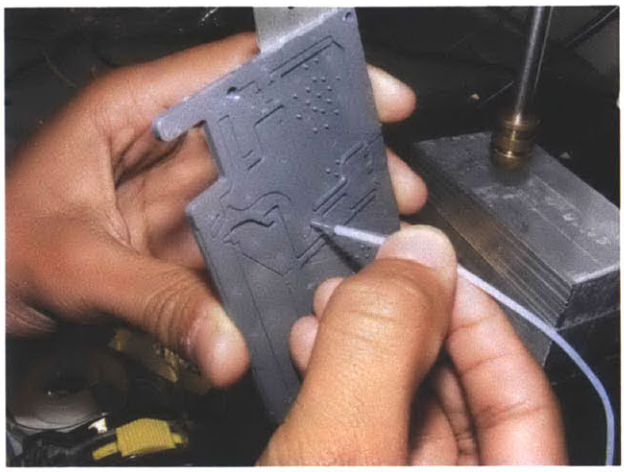

Figure 51: Pipette tip attached to reservoir via

Figure 52: Backbone attached to standoff with double sided tape

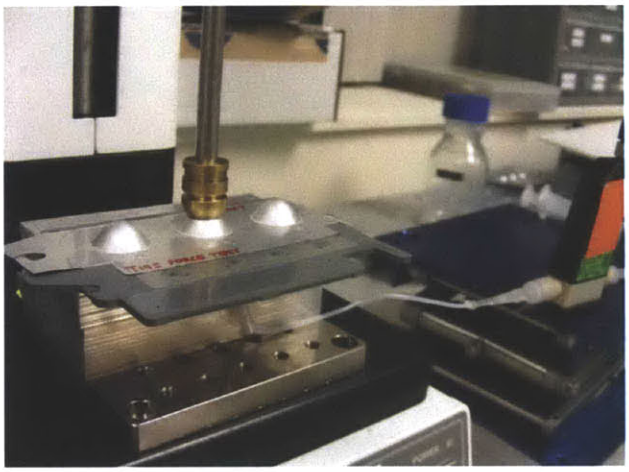

Figure 53: Plunger attached to force tester acting on the reservoir

Figure 54: Force - Flow Measurement Setup

7.8 Preliminary Testing

A series of preliminary experiments were carried out to understand the parameters in the design space for effective exit seals. The preliminary tests were run at a flow script with 30 unit flow cycles. The following section describes preliminary experiments and the results obtained from the experiments. Building on the preliminary experiments, a parameter scoping exercise is conducted for a more detailed study of the impact of temperature, time and gap on flow pattern.

7.8.1 Distance Experiments

The distance of the Exit Seal was varied between 750 to 4000 units from the dome. All distance experiments were carried out with a Line Hemisphere Exit Seal design. The characterization of distance is very important to limit delamination.

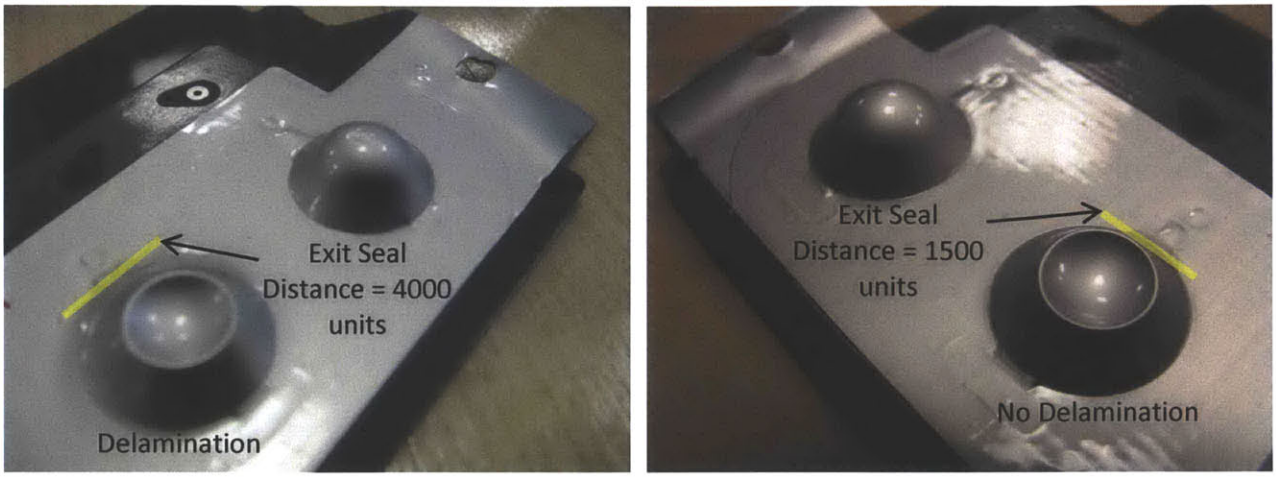

Figure 55: Exit Seal Delamination

Delamination increases as the Exit Seal distance is increased and occurs along the entire periphery. (Figure 55) At higher distances above 1000 arbitrary units the Exit Seal delaminates and fails to rupture, (even at the end of the script) irrespective of the strength of the seal as created by the different parameters – temperature, time and gap. In some cases around 2000 - 3000 units the Exit Seal delaminates up to the Exit Seal and ruptures very late in the script, when the script actually asks the plunger to pump reagents at 20 units. At closer distances 750 to 1000 units the Exit Seal pops at the right time, during the script. Delamination also results in Anomaly 2 due to pressure build up prior to the delayed rupture. The escaping reagent through the long exit channel may not be able to apply pressure on the Exit Seal to pop causing delamination. These findings led to the selection of a fixed distance setting of 1000 units for the parameter scoping exercise. The preliminary experiments suggest that a closer Exit Seal is better to reduce flow anomalies and will be optimized after the temperature, time and gap are identified.

7.8.2 Temperature Experiments

A wide range of temperatures from 85 – 120 units were experimented on film strips and tested for bonding manually. Temperatures below 85 units failed to produce any kind of bond even after significant pressure and time. At higher temperatures above 105 units, the exit sealing plate resulted in bonding areas around the micro-feature. This led to the selection of 5 Temperatures - 95, 97.5, 100 and 102.5 units. In (Figure 56), shows flow tests at a second flow script. Anomaly 1 is minimized at 100 units. Hence, a temperature of 100 units was selected as the base temperature in experiments where other parameters were varied.

The lack of bonding at below 90 units is a result of the presence of a temperature difference. The heating platen, the sleeve and the exit seal plate results in the micro-feature are about 30 units below the

thermocouple temperature. A set temperature, representative of the micro-feature temperature at temperatures recorded by the thermocouple in the platen heater was maintained for all replicates. For the parameter scoping exercise micro-feature temperatures were ensured to be at 73, 76, 79 and 82.5 units for 95, 97.5, 100 and 102.5 units respectively.

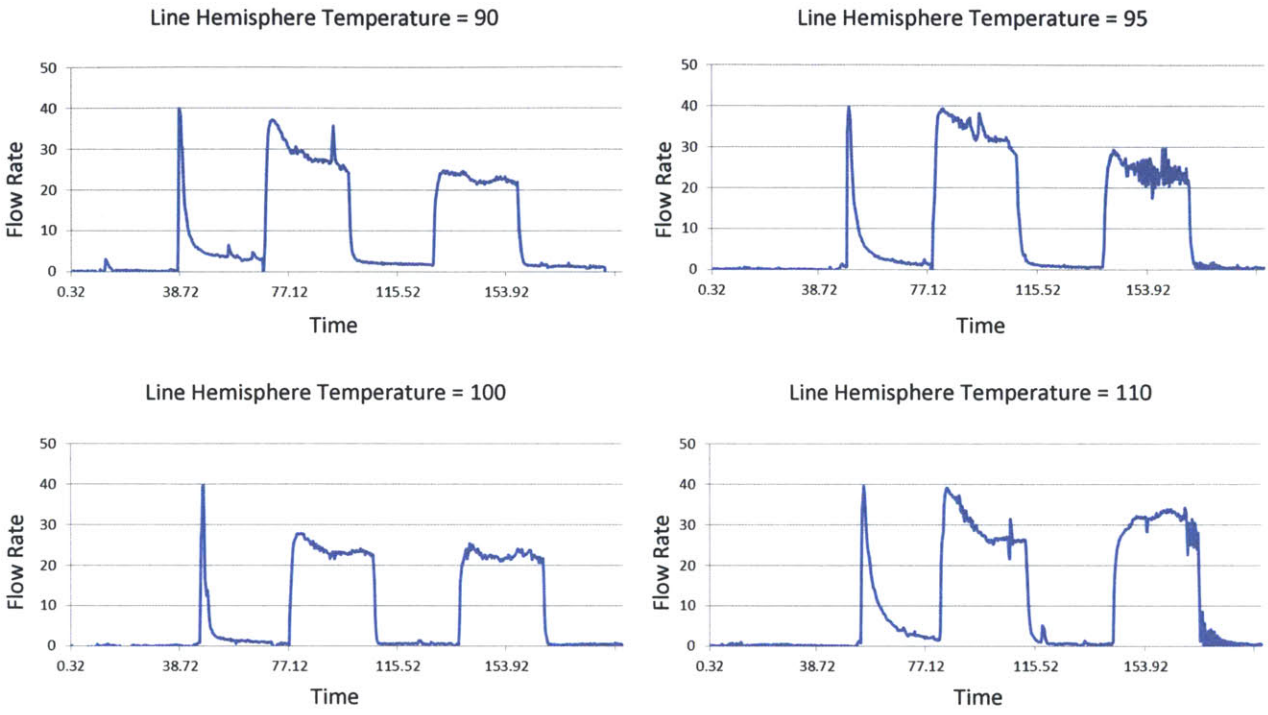

Figure 56: Line Hemisphere - Temperature Variation

7.8.3 Time Experiments

A wide range of times, 0 units (contact) to as long as 10 units were used to test the bonding phenomenon. Although higher strengths were observed at higher temperatures, unwanted bonding in surrounding areas created a problem of pressure build up and of inconsistent flow pattern.

It was also observed that it took different time periods for the bonding to take place. For instance at 90 temperature units bonding took 5 units, at 100 units the bonding took 2-3 units, at 102.5 units the bonding was instantaneous, simply requiring contact and at 105 units the bond was also instantaneous, creating a strong bond on contact. The preliminary experiments led to the selection of 4 different time settings – contact, 1, 2 and 3 time units with 2 units being the baseline parameter.

7.8.4 Gap Experiments

Accounting for the thermal expansion and a film thickness of 100 units a set of different gap settings were tested on film strips and on the tension testing force gauge. Gap clearly has an impact on the strength of the seal. A setting for 140 units at 200 units and time 2 units for the film strip required a force of 12 units and on the other hand a gap setting for 80 units at the same temperature and time required 8 units. Gap settings of 60, 80 and 100 units were selected with 60 units as the baseline parameter. The impact of gap settings on flow is tested in the parameter scoping exercise.

7.8.5 Shape-Profile

The preliminary exercise also looked at different exit seal designs – shapes and profiles. The four designs – line hemisphere, line flat, chevron hemisphere and chevron flat were tested at different parameters.

7.8.5.1 Line Hemisphere

The line hemisphere profile is prone to deformation given its micro scale hemispherical dome. The Line Hemispherical design gave good results but resulted in Anomaly 1 and Anomaly 2 in some instances as seen in (Figure 57). There is significant variation and unpredictability associated with this design.

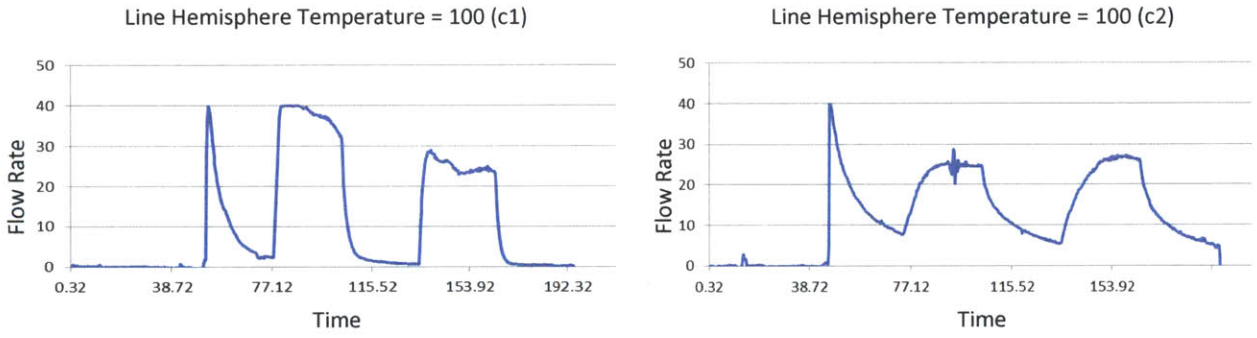

Figure 57: Line Hemisphere Flow Variation in 2 samples at the same parameters

7.8.5.2 Line Flat

The Line Flat Shape gave the best results vis-à-vis flow anomalies. A variation of Line flat was also attempted, turning the slope away from rupture initiation (or on the reservoir via side). The Line Flat away experiment gave poor results having higher Anomaly 1 levels. (Figure 58)

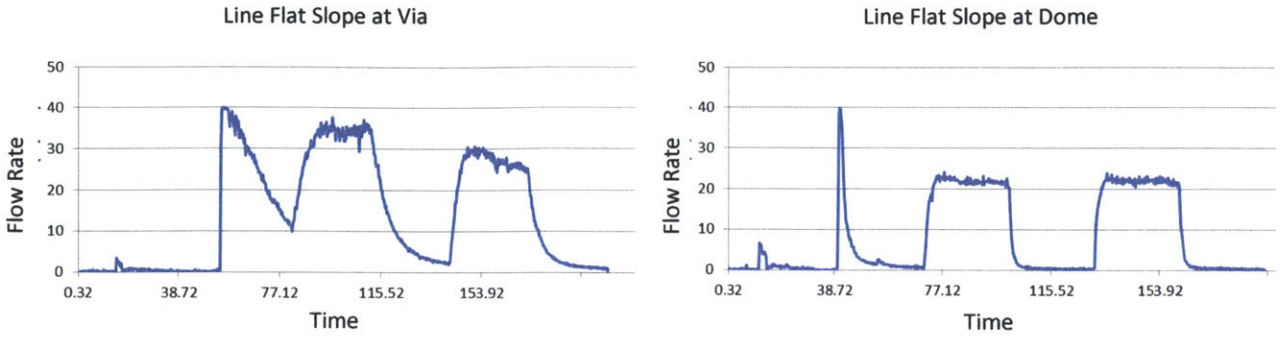

Figure 58: Line Flat Preliminary Experiments at 100 units

7.8.5.3 Chevron Hemisphere

The Chevron Hemisphere shape resulted in large amounts of Anomaly 2. Even changing parameters continued to result in both anomalies in all instances. (Figure 59) Certain cases also resulted in delamination due to increase in distance from the Chevron arms. Therefore, the distance of the vertex was minimized as far as possible to avoid delamination. A case of inverted chevron was also experimented. However, the distance from the reservoir increases making the reservoir more susceptible to delamination. Even in this case, high Anomaly 2 was observed.

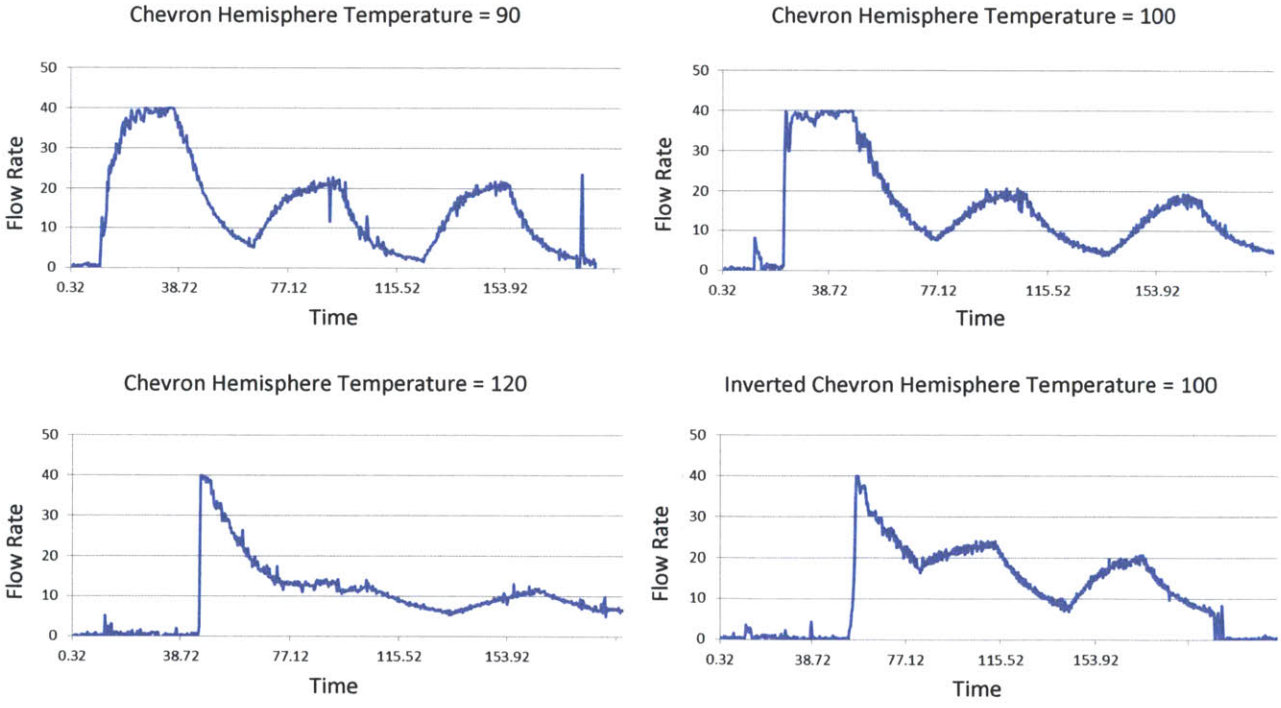

Figure 59: Chevron Hemisphere Preliminary Experiments

7.8.5.4 Chevron Flat

Similar to the Chevron Hemisphere case, the Chevron flat shape also results in large amounts of Anomaly 2. The Chevron flat design had the slope facing away from rupture initiation. A variation where slope was facing the rupture initiation was not tried owing to geometrical limitations. The change in orientation would result in an inverted Chevron shape.

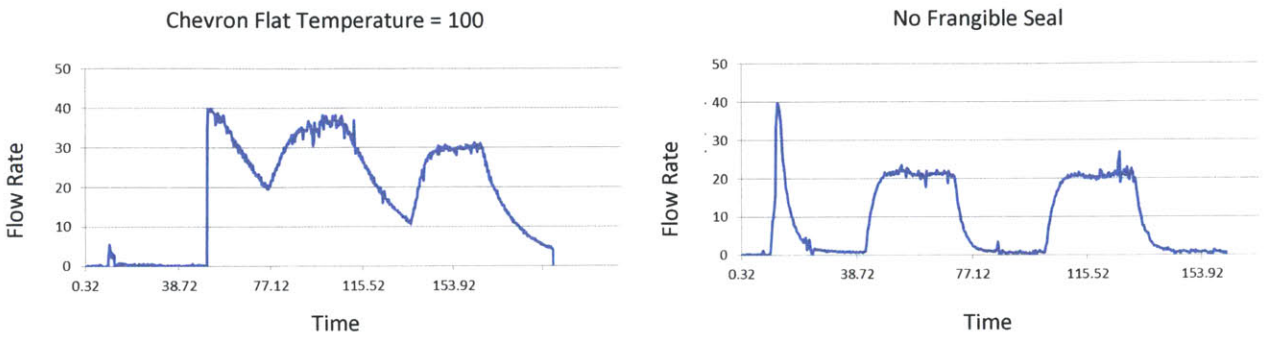

Figure 60: Chevron Flat and No Exit Seal Cases

7.8.5.5 No Exit Seal

A case for unsealed flow was also evaluated after filling, sealing the reservoirs and bonding the reservoir pack to the backbone without the exit seal. The figure above suggests that there is no Anomaly 1 presence in the flow pattern. One of the reasons for lack of Anomaly 1 may be the absence of pressure build up prior to rupture. However, Anomaly 2 continues to be present. Despite these flow anomalies, the flow pattern seems to be similar to a square wave.

Of all the exit seal variations tried during preliminary experiments, the Line Flat design seemed most promising and was used for all parameter scoping experiments

7.9 Parameter Scoping

Keeping the Line Flat exit seal design constant, flow patterns are explored at different parameter regions. Selecting a base set of values for Temperature, Time and Gap, one parameter is varied at a time keeping the others constant with 5 replicates at each set. (Figure 61) The variation range is set based on the observations in the preliminary experiments. While the author understands the possibility of interactions between these parameters may have an effect on the flow characteristics, the optimization of the three parameters – Temperature, Time and Gap using a 3 Factor Design of Experiment would be the next stage in this direction of research on the Daktari exit seal.

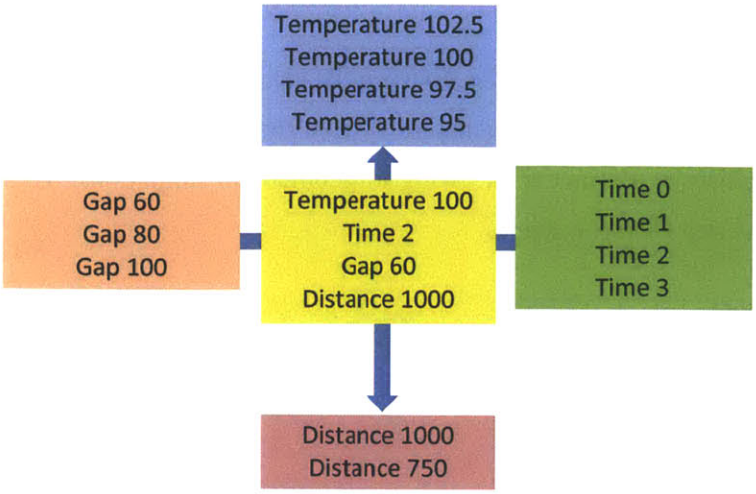

Figure 61: Parameter Scoping with Line Flat Exit Seal Design (5 Replicates for each case)

Following the parameter scoping exercise for Temperature, Time and Gap, the best combination of parameters is selected and used to determine the influence of distance on the flow pattern. These parameters are then again used with the Line Hemisphere pattern and the Chevron Hemisphere Pattern to confirm observations from preliminary analysis. The next chapter will discuss the results obtained from Flow tests, Flow Force Tests and the Interferometry Scans for all the exit seal designs.

Chapter 8: Results and Discussion

This chapter discusses the Flow and Force Results obtained for the parameter scoping exercise. Results from each of the 5 replicates at an individual set of parameters are plotted and analyzed. Postulates are also drawn about the nature of the exit seal rupture and the relationship between force and the flow pattern observed. It must be noted that many of the characteristics of these force plots remains unanswered and needs further research. These results help identify the design space to optimize the Exit Seal for higher flow predictability while minimizing flow anomalies.

8.1 Time Variation

At the base set of parameters, (Temperature = 100 units, Gap 60 Units and Distance = 1 unit) Time for sealing is varied from contact to 3 units. Although 5 replicates is a small number from which to draw effective conclusions, the consistency of results in some cases cannot be ignored. The Time Contact experiment produced the best flow pattern with minimal Anomaly 1 and Anomaly 2 instances.

8.1.1 Time = Contact

Increases in dwell time also increase in heat transfer from the micro-feature to the film. At time = contact heat transfer was minimized preventing unwanted bonding around the exit seal. The seal consistently ruptured around 30 units in each of the replicates establishing repeatability in operation. Although the first card (c1) has a spike in the second flow wave, it is not characterized as Anomaly 1 because of its extremely short duration. Anomaly 1 anomalies were generally observed in the first flow cycle and the c1 case seems to be sensor noise or accidental flow spike. Card 3 (c3) has some degree of Anomaly 1 lasting 10 units. However, cards - c2, c4 and c5 exhibited almost no anomalies. (Figure 62)

The Force flow test for Time = Contact in Figure 62 shows that the Exit Seal ruptured at a load of 8 units at the 1st peak. The slope leading to the 2nd peak is the flow and film deformation resistance. The slope is almost constant as seen during the rise up to the 3rd and the 4th peaks. At the first peak the flow and plunger motion is stopped, emulating the script which results in a drop in the force on the plunger. Once the plunger starts moving again, the force must rise to a threshold level along the flow and film deformation resistance slope. The rise up to the third and the fourth peaks signify the force on the plunger during the first and the second flow wave. Their peaks are termination of flow achieved by stopping the plunger. After the drop from the fourth peak, the plunger retracts dropping the load to zero.

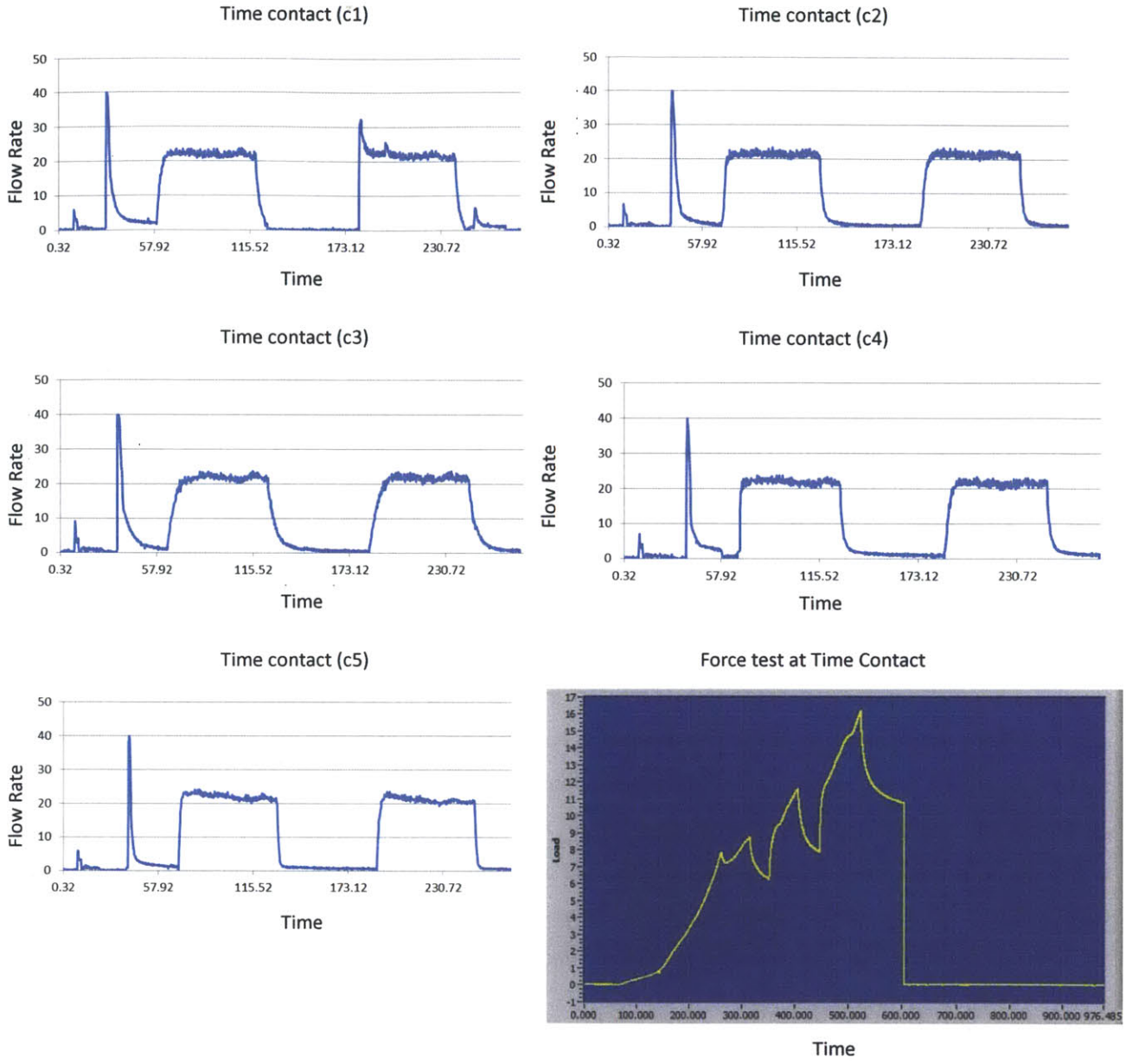

Figure 62: Flow Tests and Force Test at Time Contact

8.1.2 Time = 1

The Flow and Force experiments at Time = 1 unit indicate Anomaly 1 in some samples; however there are no instances of Anomaly 2. (Figure 63) It can also be observed that the second flow wave rarely has any flow anomalies. The existence of flow anomalies can be predicted from the flow drop after the Exit Seal is ruptured. Anomaly 2 after rupture will influence all other flow waves which follow. It must also be noted that the exit seal at Time = 1 units is stronger as expected and ruptures at 13 units (Figure 63). Here the drop from the exit seal is significant; the second peak in the force graph corresponds to the 40 units flow after the exit seal ruptures.

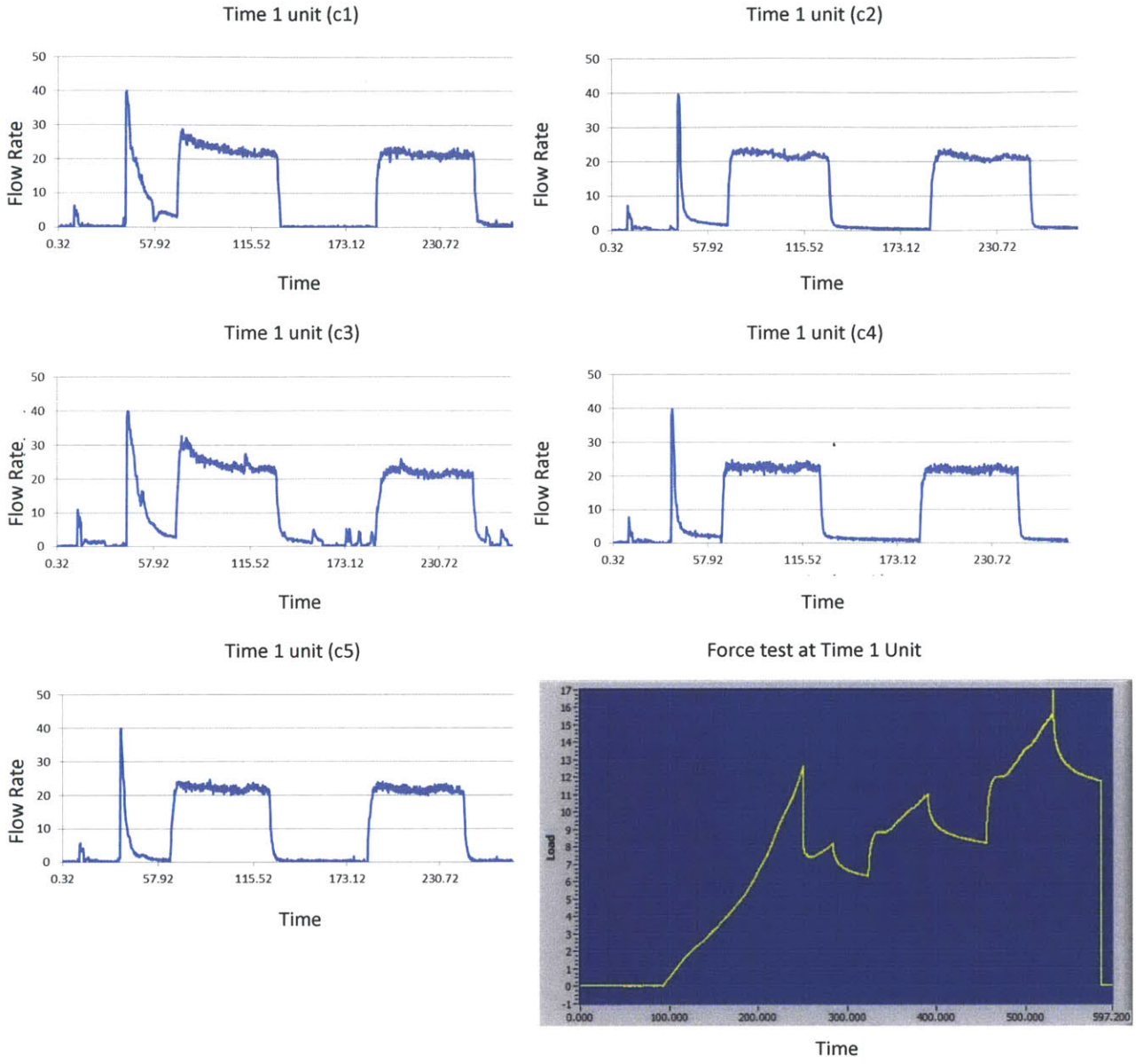

Figure 63: Flow Tests and Force Test at Time 1 Unit

8.1.2 Time = 3

Experiments with Time = 3 units keeping all other parameters constant, clearly showed the existence of Anomaly 1 in all 5 replicates (Figure 64). However, these results did not have high Anomaly 2. Card 4 (c4) and card 5 (c5) are classic cases of Anomaly 1 where the duration of the Anomaly 1 cannot be predicted. C4 has a short initial surge but the flow surge in c5 continues for most of the first wave. An estimation of the duration would allow us to circumvent the initial flow surge to a waste channel. Such predictability through process control will go a long way in establishing repeatable results.

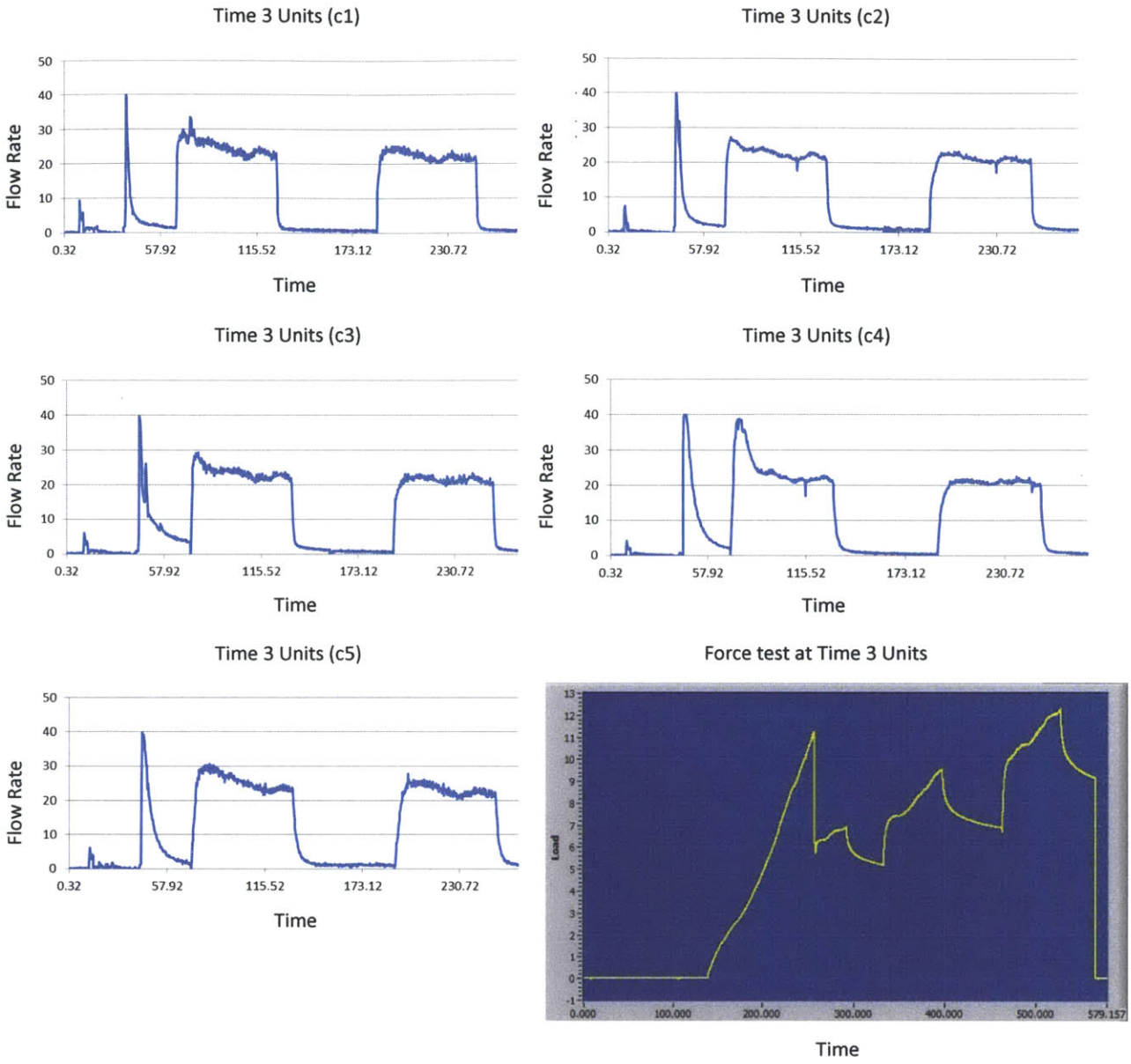

Figure 64: Flow Tests and Force test at Time 3 Units

The Force curve (Figure 64) shows that the exit seal ruptures at just over 11 units. The strength of this seal appears to be weaker than time = 1 unit. However, this could be a result of statistical variation. It may be possible that the seal is weaker than time = 1 unit, in either case, further experiments are needed.

The above time scoping exercise has yielded little flow anomalies in almost all cases. However, the time = contact experiment provided the most reliable, repeatable and predictable results. It is also worth noting that the contact case creates the weakest exit seal, popping at 8 N. This strength must however be optimized against the hermeticity needed to contain the reagents. The facet of hermeticity has not been explored in this thesis and must be performed as a part of future work.

8.2 Temperature Variation

The base set of parameters were again kept constant (Time = 2 units, Gap 60 units, Distance = 1 units) and the Temperature was varied within the bonding range from 95 to 102.5 units. The temperature difference between the micro-feature which actually seals and the temperature read by the thermocouple must be noted. The following temperatures are those recorded by the thermocouple which is in general about 15 units higher than the micro-feature temperature. The base parameter or Temperature at 100 units experiment gave the best results compared to the other temperatures.

8.2.1 Temperature = 95

The sample set at 95 units is erratic and unpredictable. Although card 2 (c2) shows no flow anomalies, 4 of the 5 cards show presence of Anomaly 1, the duration and amplitude of Anomaly 1 is inconsistent. 2 of the 5 replicates also show considerable Anomaly 2. Card 4 shows a high degree of noise and random flow behavior and is regarded as a bad sample. In sum, the high variation rules out this temperature. Figure 65

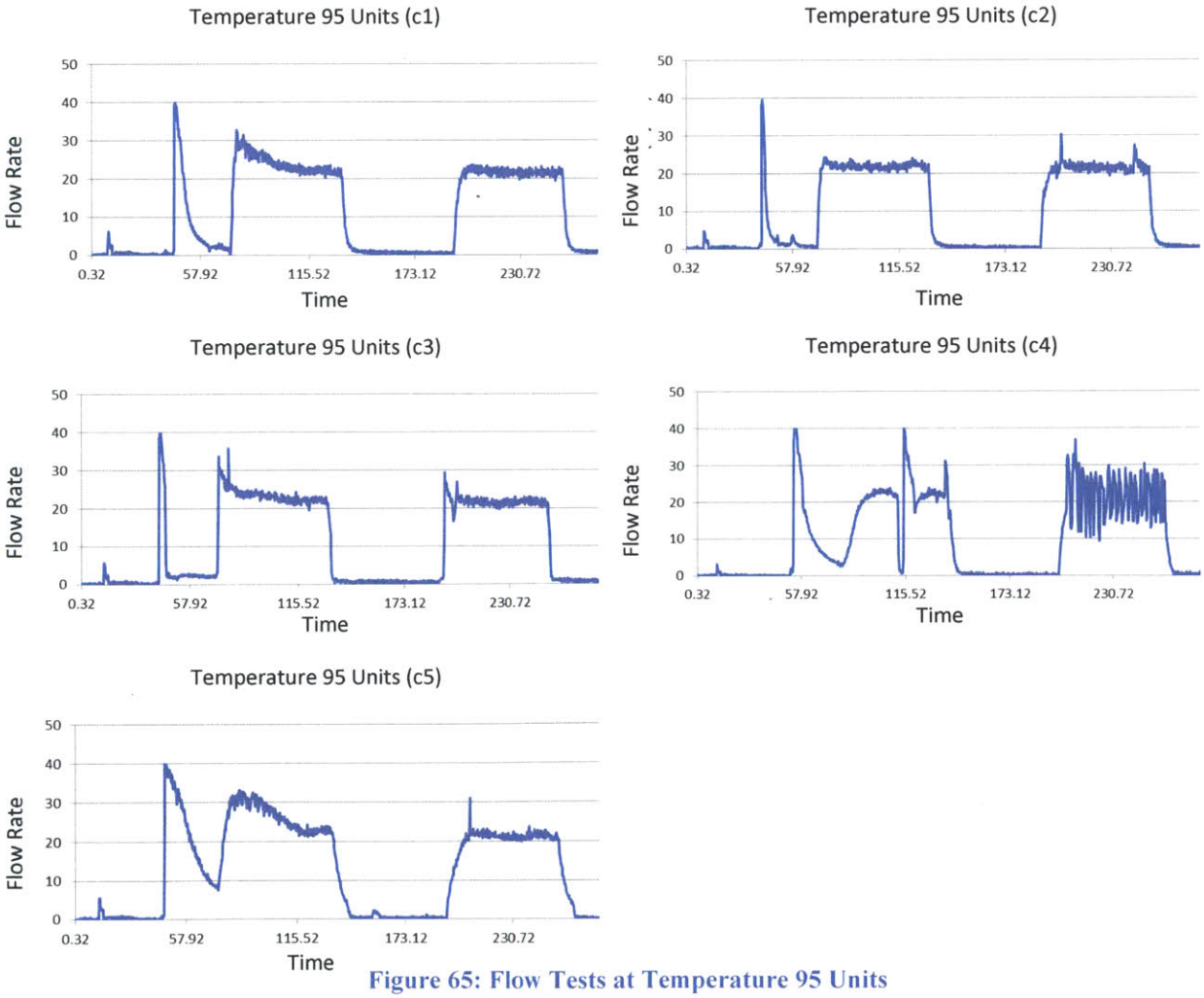

Figure 65: Flow Tests at Temperature 95 Units

8.2.2 Temperature = 97.5

Similar to the previous set of experiments, temperature at 97.5 units also results in unpredictable flow patterns. (Figure 66) Most cases of the 5 replicates have heavy Anomaly 1 as well as Anomaly 2. Only one sample (c1) provides an ideal flow pattern. The source of this unpredictable behavior at both these temperatures is unknown. Speculations about the sealing process lead to the possibility of variation in micro-feature tip temperature, since all other factors are not varied during the batch of replicates.

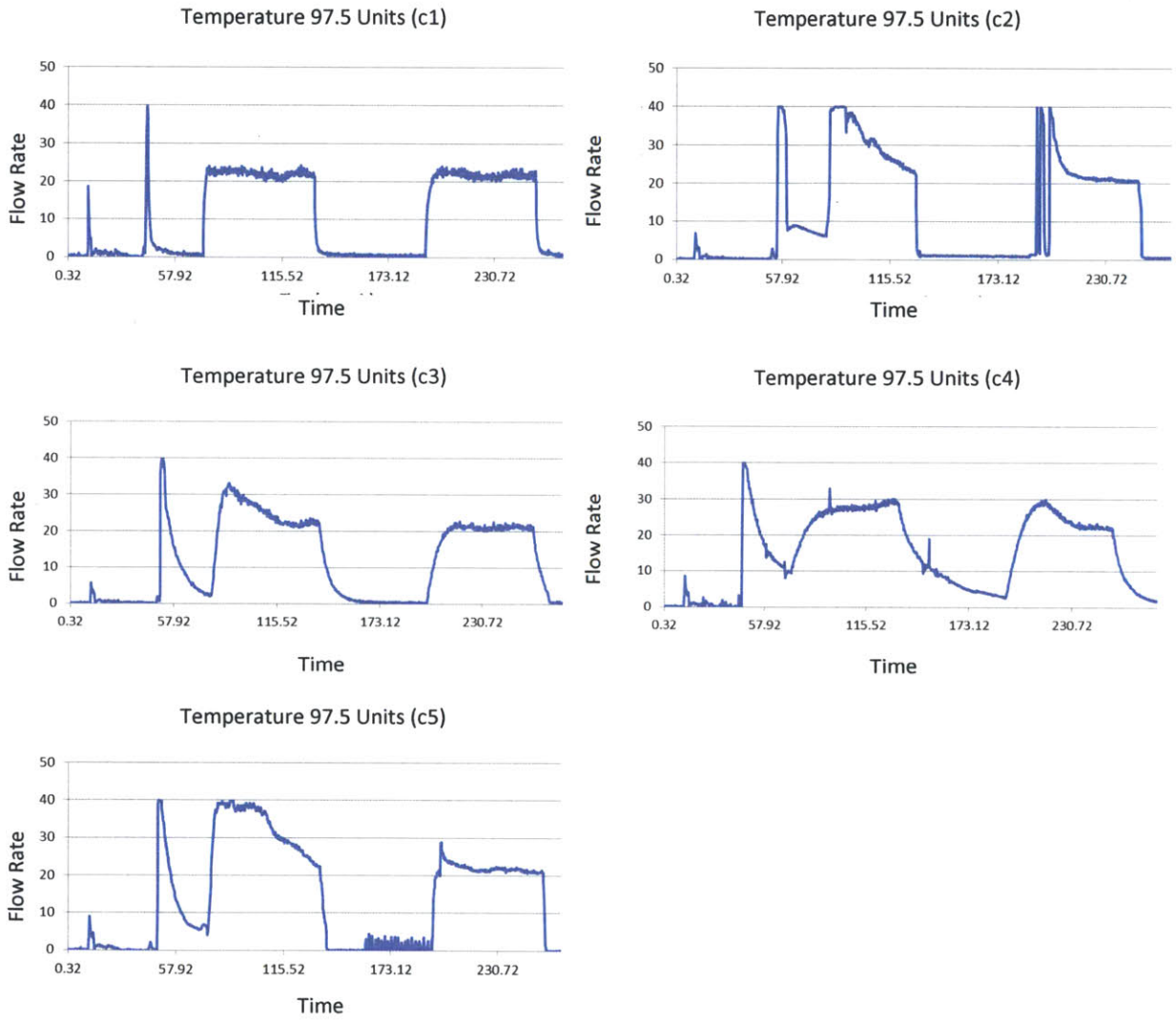

Figure 66: Flow Tests at Temperature 97.5 units

8.2.3 Temperature = 100

Experiments at 100 units (Figure 67) resulted in the least flow anomalies among the temperature scoping experiments. Card 2 (c2) and card 3 (c3) show high flow sensor noise and seem to vary. However, this was more of a sensor issue than a flow anomaly. Cards 1 (c1) and card 4 (c4) have 10 and 15 units of Anomaly 1 respectively. There is very little Anomaly 2 behavior in all 5 replicates.

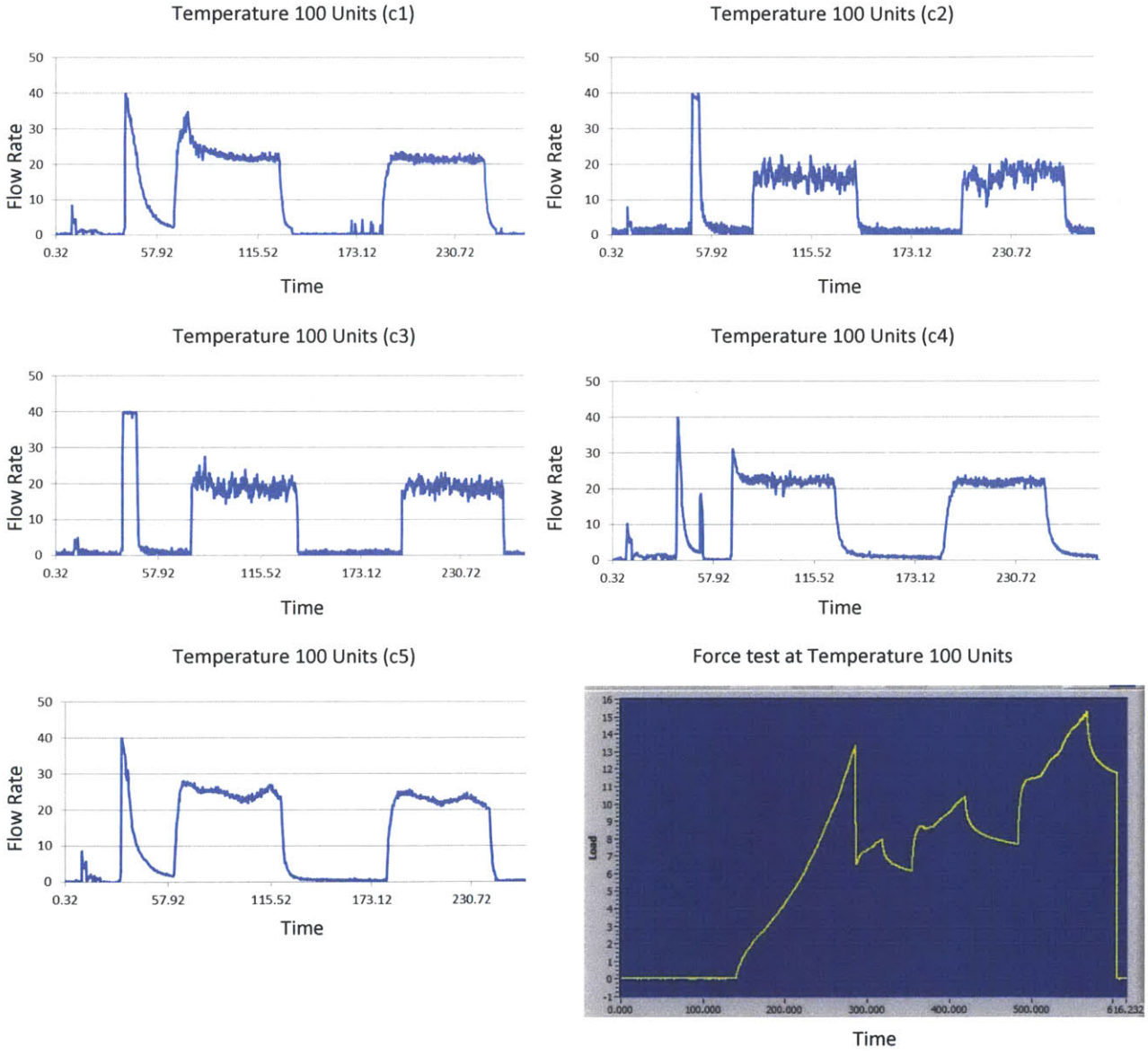

Figure 67: Flow Tests and Force test at Temperature 100 Units

The Force graph (Figure 67) indicates that the load on the plunger increases exponentially after contact with the reservoir dome and finally ruptures the exit seal at 13.5 units leading to drop until flow resistance comes into play. An interesting observation from this graph is that the drop in force after the 2nd, 3rd and the 4th peaks becomes increasingly steep in that order indicating that the exit seal continues to open up, reducing flow reactive force after each flow wave. This drop provides insight into the different Anomaly 2 seen in the 1st and the 2nd flow waves. A steeper force drop indicates little or no stored pressure acting on the reagents, thereby reducing Anomaly 2. On the other hand resistance caused by partial opening results in energy storage which continues to act once the plunger stops, causing Anomaly 2.

8.2.4 Temperature = 102.5

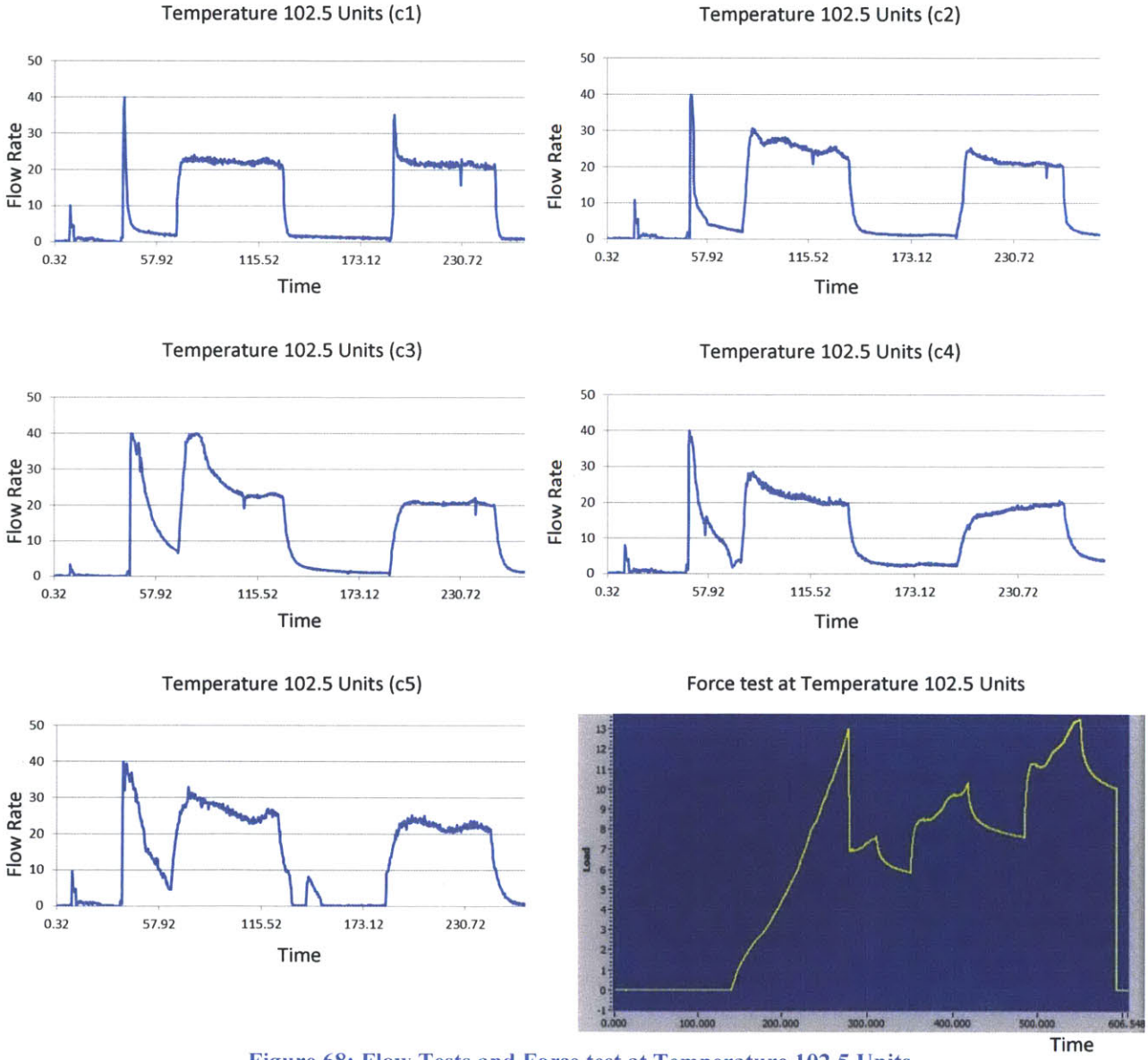

Figure 68: Flow Tests and Force test at Temperature 102.5 Units

Although card 1 (c1) has no flow anomalies apart from a uncharacteristic flow spike, all other replicates at 102.5 units have 10-20 units of Anomaly 1 with 10 units of Anomaly 2. The Anomaly 1 duration for all the cards lasts the entire duration of the first flow wave. (Figure 68)

Interestingly, the Force required to rupture an exit seal created at 102.5 units does not vary significantly. (Figure 68) The seal ruptures at 13 units and similar to the case with 100 units, the drop in force after the 4th peak is much steeper than the 3rd peak and is reflected in the second flow wave, which appears to have significantly less Anomaly 1 and Anomaly 2. (Figure 68)

8.3 Gap Variation

Gap variation is actually measured as the compression of the film under the micro-feature. Keeping all other parameters at the base level (Temperature = 100 units, Time = 2 units, Distance = 1000 units) the gap is tested at 80 units and 100 units with 5 replicates each.

8.3.1 Gap = 80

Card 1 (c1) was the first experiment run in the parameter scoping exercise. The script for this individual experiment was for 240 units to calibrate the instrument for flow at 20 units. The first card indicates the presence of Anomaly 1 of 15 units lasting for 30 units. Similar to (c1), card 4 (c4) has 15 units of Anomaly 1 lasting almost the entire duration of the flow cycle and some Anomaly 2. Comparing this set with the base set in section 7.2.2, an increased depth of penetration of the tool results in Anomaly 1. (Figure 69)

The force graph indicates (Figure 69) that the exit seal at 80 units setting ruptures at the same force as the exit seal at 60 units setting. The rise to the 3rd peak was tested to see if the force plateaued as the duration of flow increased The geometry of the reservoir dome is such that it requires higher force to deform a higher surface area as the plunger moves in deeper into the reservoir, resulting in a continual rise in load to the 3rd peak.

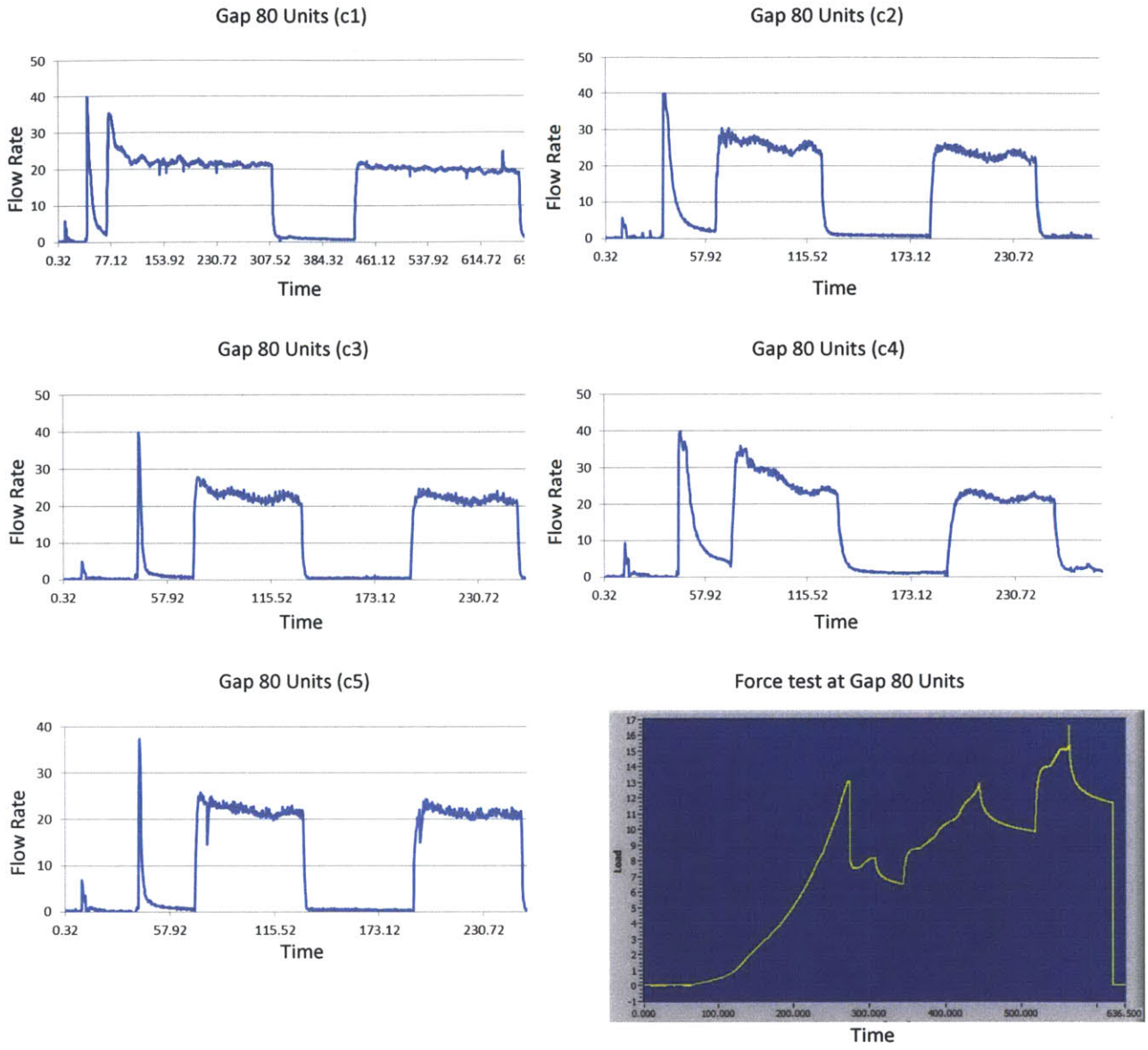

Figure 69: Flow tests and Force Test at Gap 80 Units

8.3.2 Gap = 100

The increase in depression of the micro-feature into the reservoir pack results in a higher degree of Anomaly 1 in general. All replicates except card 1 (c1) recorded Anomaly 1 ranging from 5 units to as high as 20 units. In cards 2, 4 and 5 (c2, c4, and c5) Anomaly 1 continues through most of the flow cycle (lasting 60 units). Although there is a high degree of Anomaly 1 this parameter setting produced no Anomaly 2. (Figure 70)

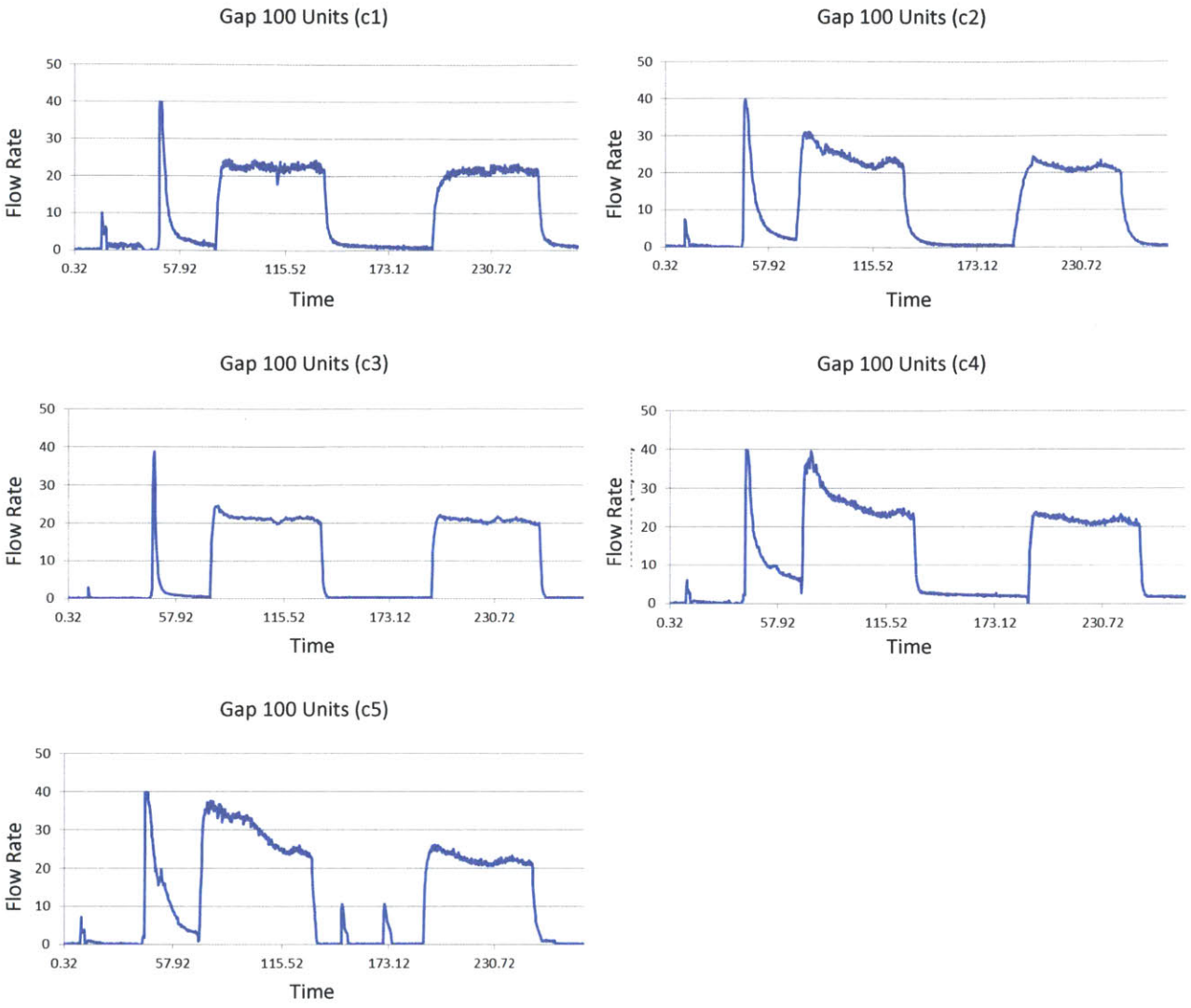

Figure 70: Flow Tests and Force test at Gap 100 Units

The parameter scoping exercise yields some key findings about the exit seal. A weaker exit seal reduces flow anomalies. A temperature of 100 units yields the best results and points to dramatic variation in flow patterns depending upon the Temperature. Time and Gap are also influential in seal strength is not heavily influenced by Gap settings. Based on the results, a combination of 100 units, contact time, 60 units at 1000 units distance give the best flow patterns with minimal Anomaly 1 and Anomaly 2.

8.4 Distance Optimization

The above experiments in relation to parameter scoping have been limited to Temperature, Time and Gap. Preliminary experiments had led us to believe that distance has a significant influence on the delamination prior to rupture. A few samples were tested at distance = 750 units instead of 1000 units keeping the Temperature at 100 units, Time Contact and Gap at 80 units.

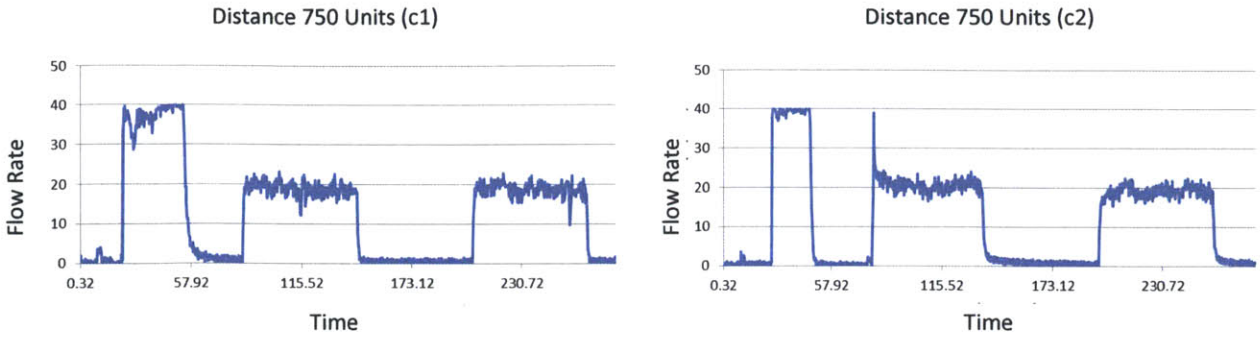

Figure 71: Flow Tests at Distance 750 Units

The flow plots above (Figure 71) indicate that Anomaly 2 reduces even further as the distance of the Exit Seal is reduced. Although there is a high degree of sensor noise, it is clear that the flow remains constant at 20 units. It should also be noted that a closer exit seal also ruptures earlier in the script, resulting in prolonged flow as compared to a rupture spike as seen in other cases. The spike in card 2 (c2) is not characteristic Anomaly 1 and may be regarded as sensor noise. Although only a few samples are tested for distance, the results seem promising to continue further optimization in future work.

8.5 Chevron Hemisphere Seal

The parameter scoping exercise yielded the best parameters for sealing the Line Flat exit seal pattern. Although the same parameters might not be optimal for a different exit seal design, an attempt is made at creating a Chevron exit seal using the same temperature (100 units), time (contact) and distance (1000 units) but varying the Gap setting. (Figure 72)

The results for the Chevron experiments show heavy Anomaly 2 in all 3 cases ranging almost the entire flow cycle. The experiment at 100 units also has significant Anomaly 1 in the first flow wave resulting from a high degree of Anomaly 2 after the exit seal ruptures. The force test was conducted at a depth of 80 units. The almost non-existent first peak indicates that the chevron exit seal does not fully rupture but only opens at the sharp corner and allows flow to begin. The notch propagation effect fails to open up the exit seal along the arms resulting in pressure buildup which is released as Anomaly 2 after the plunger stops its travel into the reservoir. (Figure 72)

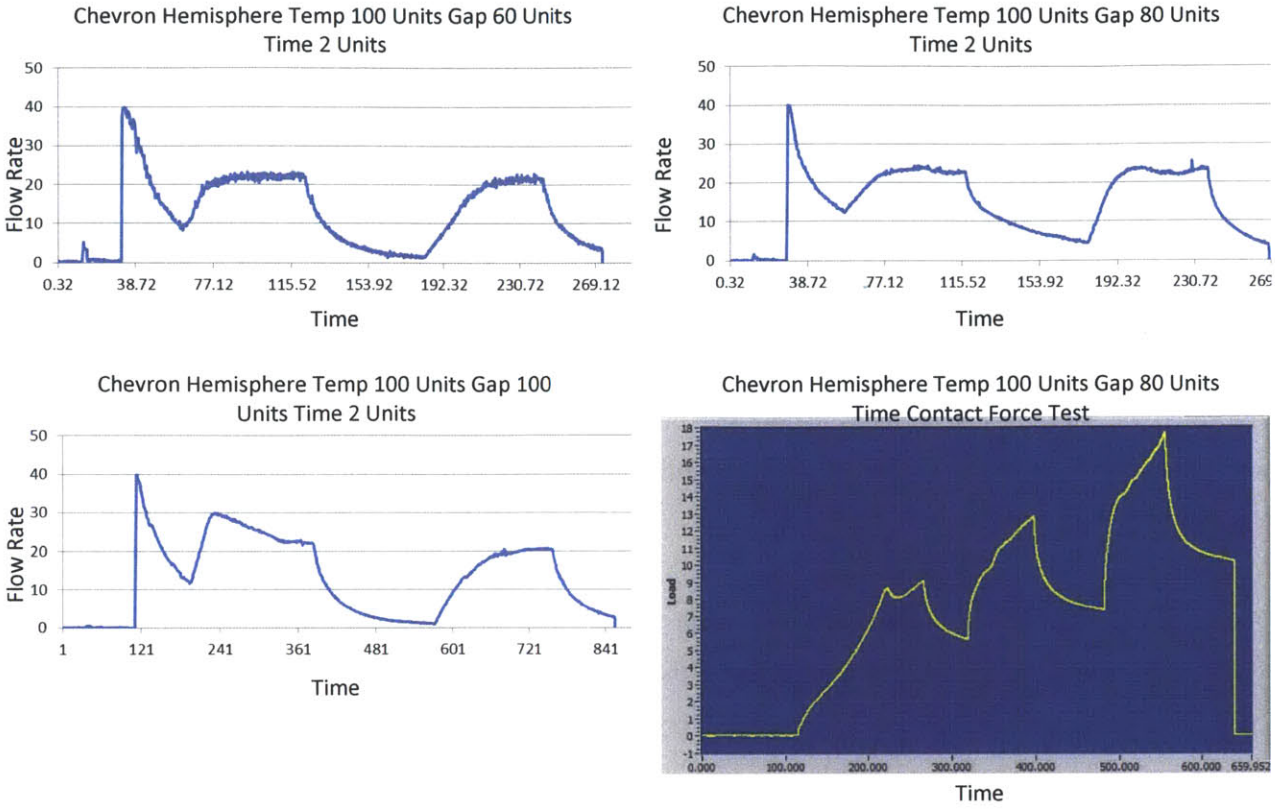

Figure 72: Chevron Hemisphere Flow Tests and Force Test

8.6 Current Exit Seal

Recent reservoir packs from alternative manufacturing processes have yielded good flow results. (Figure 73) Although reservoirs have some degree of Anomaly 1 for the first flow wave, the pattern is free from flow anomalies. The above flow test ran on a 240 units flow script. Analyzing the force plot for the current exit seal design, it seems that the exit seal ruptures at 14 units. However, it seems the distance and the strength has not been fully characterized. Another test resulted in the exit seal rupturing at 17 units.

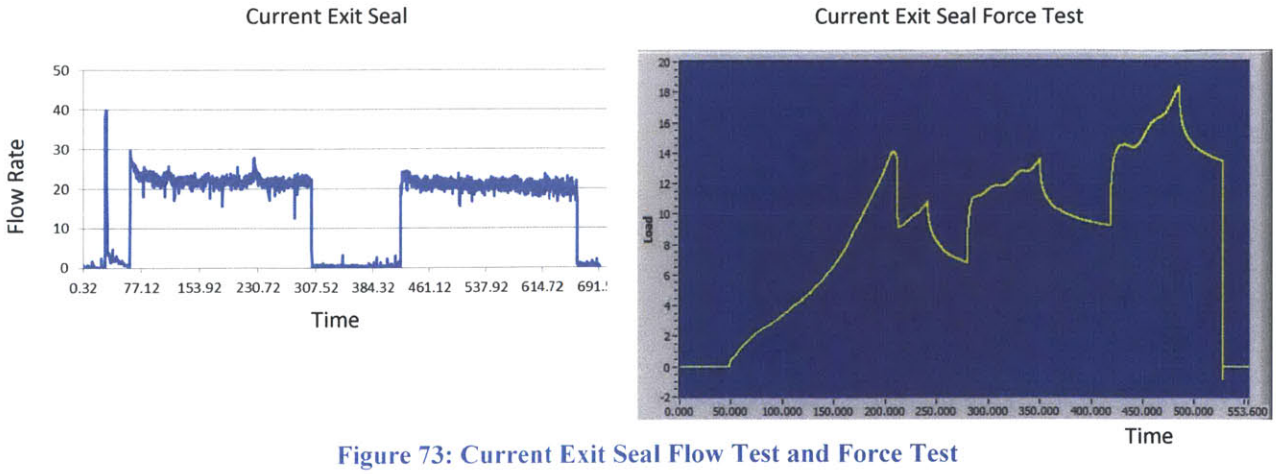

Figure 73: Current Exit Seal Flow Test and Force Test

The parameter scoping exercise followed by distance experiments reveal that a setting of Temperature = 100 units, contact time and a gap setting of 60 units yielded good flow results. However it is important to keep in mind that these results are based only on 5 replicates. Several factors such as micro-feature temperature and thermal expansion influence the consistency of the seals. It may also be possible that a set of parameters other than the one finally selected (Time = contact, Temperature = 100 units and Gap = 60 units) may deliver better flow results. For instance, a combination of time = contact and gap = 80 units or time = 1 units and gap = 60 units have not been experimented in this parameter scoping exercise. There is limited understanding of the complexities in these force plots. The influence of material properties of the reservoir pack during its deformation and the influence of fluid resistance have not been studied separately. The next steps to further experimentally characterize Daktari's exit seals are discussed in the chapter on Future Work.

Additional research, involving the mathematical modeling of the dome deformation phenomenon was undertaken and is integrated into the following thesis and presented in the next chapter. The model will help improve understanding of the reagent delivery process and help future design optimization. The two studies can be looked at independently.

Chapter 9: Dome Deformation Models

To completely understand the dynamics of reagent delivery, the author developed a mathematical model* predicting the dynamics just prior to the opening of the exit seal. This analysis proposes theories on delamination around the dome and the energy stored in the dome material to account for the volume lost during the Reservoir-Plunger Interaction. This study can be read independent of exit seal research.

9.1 Plunger-Dome Interaction

Daktari's reagent delivery system is actuated by a plunger deforming the reservoir dome. At a certain point, the pressure inside the reservoir dome can no longer be supported and the exit seal gives way allowing reagents to flow into the backbone. As soon as the plunger makes contact and starts deforming the dome, the volume available for the reagents starts decreasing. The pressure on the exit seal is correlated with the position of the plunger with respect to the dome. To understand when the seal gives way, it is important to calculate the volume lost during the plunger-dome interaction.

9.1.1 Geometry

In order to develop a model to quantify lost volume, it is necessary to make certain geometrical assumptions. For Daktari's reservoir dome, it is assumed that the dome is combination of a conical frustum and a spherical cap. The plunger analysis is performed assuming a spherical profile to keep the analysis simple. It is also assumed that the plunger intersects only with the spherical portion of the dome before the exit seal fails. These assumptions seem reasonable from experimental observations.

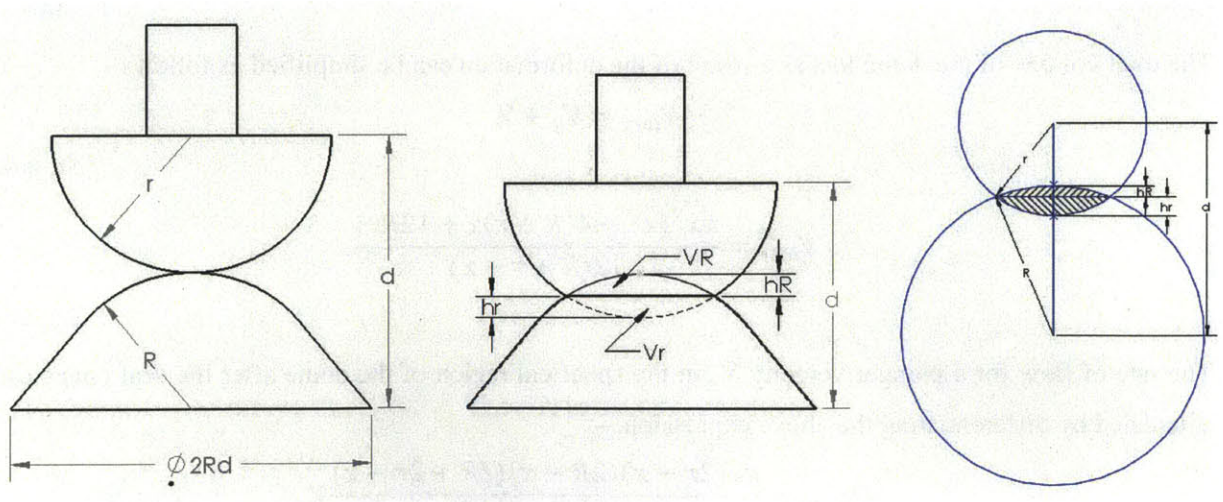

Figure 74: Plunger-Dome Interaction

*(A modeling nomenclature is included in Appendix A)

9.1.2 Volume Lost

The total volume in the dome lost as a result of the deformation is given by $V_R + V_r$ (Figure 74) This volume can be correlated with the position of the plunger. The distance between the center of the radius of the dome and the center of the plunger radius is denoted by d and keeps decreasing as the plunger moves into the dome. Both volumes V_R and V_r can be given as the volumes of spherical caps and are given by –

$$V_R = \frac{\pi(h_R)^2(3R - h_R)}{3}$$

Equation 1

$$V_r = \frac{\pi(h_r)^2(3r - h_r)}{3}$$

Equation 2

If x denotes the travel of the plunger inside the dome, it can be given by –

$$x = R + r - d$$

Equation 3

Both h_R and h_r can be calculated geometrically and are given by –

$$h_R = \frac{x(2r - x)}{2(R + r - x)}$$

Equation 4

$$h_r = \frac{x(2R - x)}{2(R + r - x)}$$

Equation 5

The total volume of the dome lost as a result of the deformation can be simplified as follows -

$$V_{lost} = V_R + V_r$$

Equation 6

$$V_{lost} = \frac{\pi x^2\{x^2 - 4(R + r)x + 12Rr\}}{12(R + r - x)}$$

Equation 7

The rate of flow for a plunger velocity V_p in the spherical region of the dome after the seal opens can be calculated by differentiating the above expression. –

$$Q_{flow} = \frac{\pi x(2r - x)(2R - x)(2R + 2r - x)}{4(R + r - x)^2} V_p$$

Equation 8

If the plunger radius and the dome radius are equal (R = r), the volume lost simplifies to -

$$V_{lost} = \frac{\pi x^2(6R - x)}{12}$$

Equation 9

If V_p is the velocity of the plunger, the rate of flow in the spherical region of the dome after the seal opens can be calculated by differentiating the above expression with respect to time –

$$Q_{flow} = \frac{\pi x(4R - x)}{4} V_p$$

Equation 10

Once the seal opens, the velocity of the plunger needs to be varied according to the plot given below (Figure 75) to get a constant flow rate. (Assuming the exit seal is fully open, the plot can be looked at in the section of travel after the seal opens) The change in velocity accounts for the change in dome volume (Figure 76) per unit travel of the plunger.

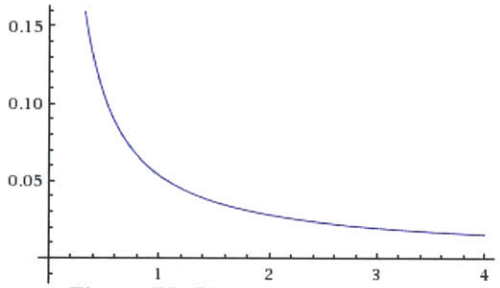

Figure 75: Plunger Velocity vs. Travel

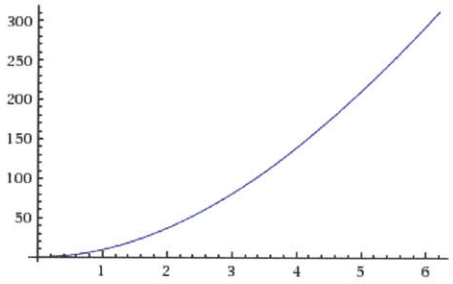

Figure 76: Volume vs. Travel

9.2 Dome Expansion

However, these liquid reagents are incompressible and the lost volume above must be recovered. Two theories are presented to reclaim the lost volume – Dome Delamination and Energy Storage. These theories are valid individually or together depending upon a multitude of different factors. The strength of the bond between the dome-film and the lid film, the elasticity of the film material, the strength of the exit seal and geometry all affect how the lost volume is actually recovered.

9.2.1 Dome Delamination

One of the ways, the dome might expand to account for lost volume is delamination around the periphery. Delamination increases as the plunger pushes in deeper into the dome. The work done in peeling the bond between the films is provided by the plunger. The following model attempts to predict the amount of delamination in relation to the lost volume calculated in the earlier section.

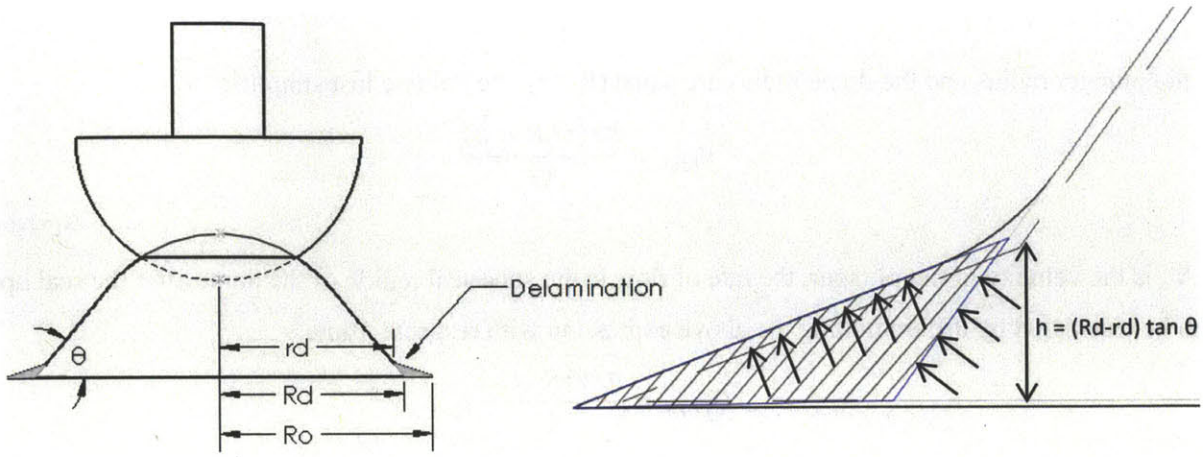

Figure 77: Delamination

The pressure first delaminates the periphery and then as the pressure angle changes Figure 77, it can no longer peel the bonding and starts stretching the foil. The change in volume can be calculated as the difference between two conical frustum volumes with base radii Ro and Rd.

The amount of expansion can be given by –

$$V_{recover} = V_{delaminatedfrustum} - V_{frustum}$$

Equation 11

$$V_{recover} = \frac{\pi h({R_o}^2 + (R_o)(r_d) + {r_d}^2)}{3} - \frac{\pi h({R_d}^2 + (R_d)(r_d) + {r_d}^2)}{3}$$

Equation 12

$$V_{recover} = \frac{\pi h(R_o - R_d)(R_o + R_d + r_d)}{3}$$

Equation 13

$$V_{recover} = \frac{\pi(R_d - r_d)(R_o - R_d)(R_o + R_d + r_d)tan\theta}{3}$$

Equation 14

$$V_{recover} = V_{lost}$$

Equation 15

$$\frac{\pi(R_d - r_d)(R_o - R_d)(R_o + R_d + r_d)tan\theta}{3} = \frac{\pi x^2\{x^2 - 4(R + r)x + 12Rr\}}{12(R + r - x)}$$

Equation 16

R, r, R_o and θ are known design parameters for the reservoir dome. R_d and r_d are both output variables of delamination and a relationship can be found by equating the recovery volume to the volume lost. This model can also be used to optimize the design parameters to reduce delamination. The energy involved in peeling or the work done has not been modeled and should be taken up in future work.

9.2.2 Energy Storage Theory

The energy storage theory reflects the idea that energy transferred from the plunger is actually stored in the reservoir film material. This energy appears as strain energy, expanding the dome volume to accommodate the volume lost at the plunger-dome interaction. In order to simplify stress and strain analysis, several assumptions are made about the geometry and physics of the phenomenon –

1. Dome is approximated as a hemispherical pressure vessel (radius is mean of R_d and R)
2. Pressure is uniform throughout the volume
3. Thickness of the film is much smaller than the radius of the dome.
4. Film material is isotropic and strains generated are uniform
5. Negligible variation in stress across the thickness of the film.

9.2.2.1 Stress Calculation

Elemental analysis is performed to calculate the stresses generated in an element by balancing forces. Hooke's law is then used to predict the strain generated in the element. Using, the surface area under strain, the foil thickness and strain and stress, the energy stored can be calculated as follows

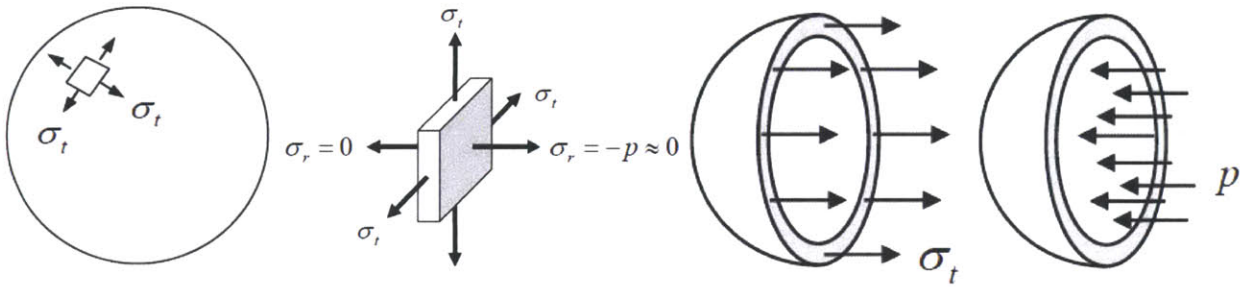

Figure 78: Stress Calculation [29]

Using force equilibrium for a hemisphere with film thickness - t, outside radius - r_o, inside radius - r_i, mean radius ($r_m = 0.5(R_d + R)$) internal pressure at rupture - p_r ; the tangential stress (σ_t) in a thin walled pressure vessel (Figure 78) is given by -

$$\pi p_r (r_i)^2 = \pi({r_o}^2 - {r_i}^2)\sigma_t$$

Equation 17

$$\sigma_t = \frac{{r_i}^2 p_r}{(r_o + r_i)t}$$

Equation 18

$$\sigma_t = \frac{p_r r_m}{2t}$$

Equation 19

The radial stress (σ_r) is negligible compared to the tangential stress (σ_t)

$$\sigma_r = -p_r \qquad t \ll r_m \qquad p_r \ll \sigma_t \qquad \Rightarrow \qquad \sigma_r \ll \sigma_t$$

As a result, of the three principal stresses, the maximum are the two tangential stresses and the minimum is the radial stress:

$$\sigma_x = \sigma_y = \sigma_t = \frac{p_r r_m}{2t}$$

Equation 20

$$\sigma_z = \sigma_r = 0$$

Equation 21

9.2.2.2 Strain Calculation

A thin walled spherical pressure vessel expands when internally pressurized and results in three principal strains – circumferential or tangential strain (ε_c) in two directions and radial strain (ε_r) along one. The strain in the film element can be calculated as follows (Figure 79) –

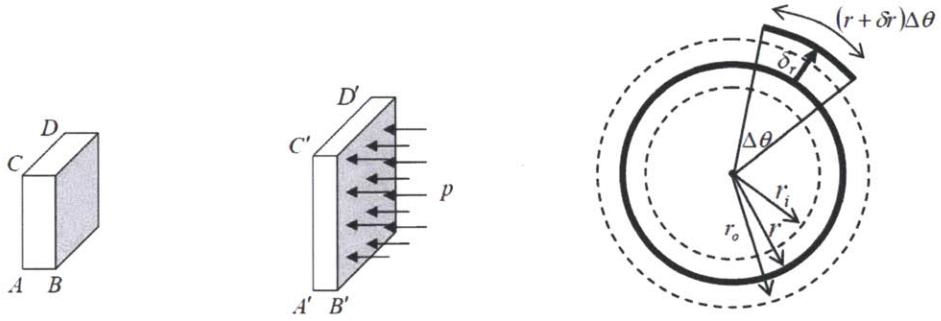

Figure 79: Strain Calculation [29]

$$\varepsilon_c = \frac{A'C' - AC}{AC} = \frac{C'D' - CD}{CD}$$

Equation 22

$$\varepsilon_r = \frac{A'B' - AB}{AB}$$

Equation 23

According to Hooke's law (where, Young's modulus, E and Poisson's Ratio, v) –

$$\begin{bmatrix}\varepsilon_x \\ \varepsilon_y \\ \varepsilon_z\end{bmatrix} = \begin{bmatrix}1/E & -v/E & -v/E \\ -v/E & 1/E & -v/E \\ -v/E & -v/E & 1/E\end{bmatrix}\begin{bmatrix}\sigma_x \\ \sigma_y \\ \sigma_z\end{bmatrix} = \frac{1}{E}\frac{pr}{2t}\begin{bmatrix}1-v \\ 1-v \\ -2v\end{bmatrix}$$

Equation 24

At rupture pressure p_r the strains can be given as -

$$\varepsilon_x = \varepsilon_y = \varepsilon_c = \frac{(1-v)}{E}\frac{p_r r_m}{2t}$$

Equation 25

$$\varepsilon_z = \varepsilon_r = 0$$

Equation 26

The amount by which a certain element or the dome expands can be calculated (Figure 79) -

$$\varepsilon_c = \frac{(r_m + \delta_r)\Delta\theta - r_m\Delta\theta}{r_m\Delta\theta} = \frac{\delta_r}{r_m}$$

Equation 27

$$\delta_r = r_m\varepsilon_c = \frac{(1-v)}{E}\frac{p_r {r_m}^2}{2t}$$

Equation 28

The volume created by this expansion of the dome is given by –

$$V_{expansion} = A_s\delta_r = \frac{(1-v)}{E}\frac{p_r {r_m}^2}{2t}A_s$$

Equation 29

Although stresses have been calculated based on a hemispherical dome profile, $V_{expansion}$ can be better approximated by calculating A_s as the surface area of the conical frustum undergoing expansion and can be given by (Figure 80) –

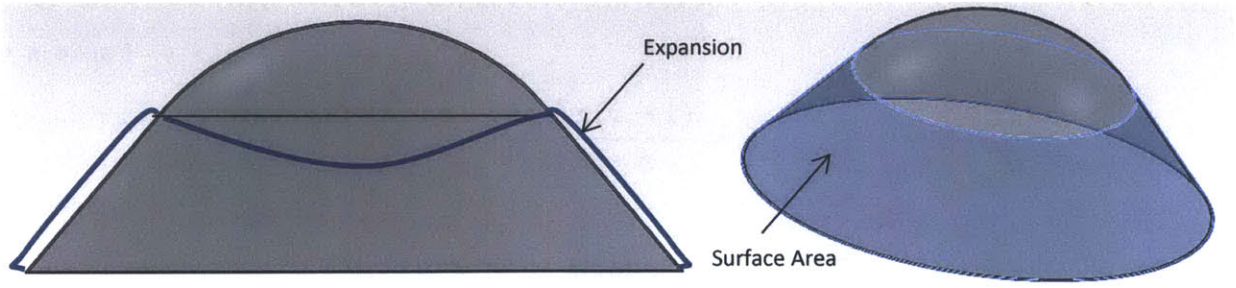

Figure 80: Dome Surface Area Expansion

$$A_s = \pi(R_d + (R_d - (R - h_R)/tan\theta))\sqrt{(R_d - (R_d - (R - h_R)/tan\theta))^2 + (R - h_R)^2}$$

Equation 30

$$\text{Simplified} \Rightarrow A_s = \pi(R - h_R)(2R_d - (R - h_R)cot\theta)cosec\theta$$

Equation 31

The expansion volume can be equated to the lost volume –

$$V_{expansion} = V_{lost}$$

$$\frac{(1-v)}{E}\frac{p_r {r_m}^2}{2t}\pi(R-h_R)(2R_d-(R-h_R)cot\theta)cosec\theta = \frac{\pi x^2\{x^2-4(R+r)x+12Rr\}}{12(R+r-x)}$$

Equation 32

E, v, t, R, R_d. θ, r are all design parameters. r_m, h_R , given earlier, are simply notations to simplify the equation. The above equation allows predicting, the pressure inside the dome as a function of the travel of the plunger into the reservoir dome. This model can also be used to optimize the design parameters to vary rupture pressure with respect to travel.

9.2.2.3 Strain Energy Stored

The maximum amount of energy stored in the dome is calculated by taking into account the stress and the strains generated in the dome wall. The general strain energy density can be given by –

$$U_0 = \frac{1}{2}\left(\sigma_x\varepsilon_x + \sigma_y\varepsilon_y + \sigma_z\varepsilon_z + \tau_{xy}\gamma_{xy} + \tau_{yz}\gamma_{yz} + \tau_{zx}\gamma_{zx}\right)$$

Equation 33

Neglecting shear stresses and strains, the total strain energy stored in the expanding dome material is –

$$U = \int_V U_0\, d\mathbf{V} = \int\left[\int_A U_0\, d\mathbf{A}\right]dt$$

Equation 34

$$U = \frac{1}{2}\left(\sigma_x\varepsilon_x + \sigma_y\varepsilon_y\right)A_s t$$

Equation 35

$$U = \frac{(1-v)}{E}\frac{p_r^2 r_m^2}{4t}A_s$$

Equation 36

The energy stored in the dome appears as excess pressure on the reagent. This pressure contributes to the flow rate when the exits seal opens. The above equation also establishes a relationship between the plunger travel and the rupture pressure and seal strength by extension.

9.2.2.4 Fluid Lumped Parameter Modeling

In a sense, the reagent delivery mechanism can be characterized using lumped parameter modeling of the fluid system. (Figure 81) The plunger can be construed as a piston pressing on a spring. The spring represents the elasticity of the dome film. The energy stored in this spring is equal to the strain energy calculated in the earlier section. The spring pushes on to another piston which pressurizes the reagent inside the reservoir. As long as the exit seal is in place, the reagent, being incompressible supports the lower piston. At a particular pressure, p_r the seal opens, internal pressure drops and the spring pushes the lower piston, driving the reagent out of the reservoir.

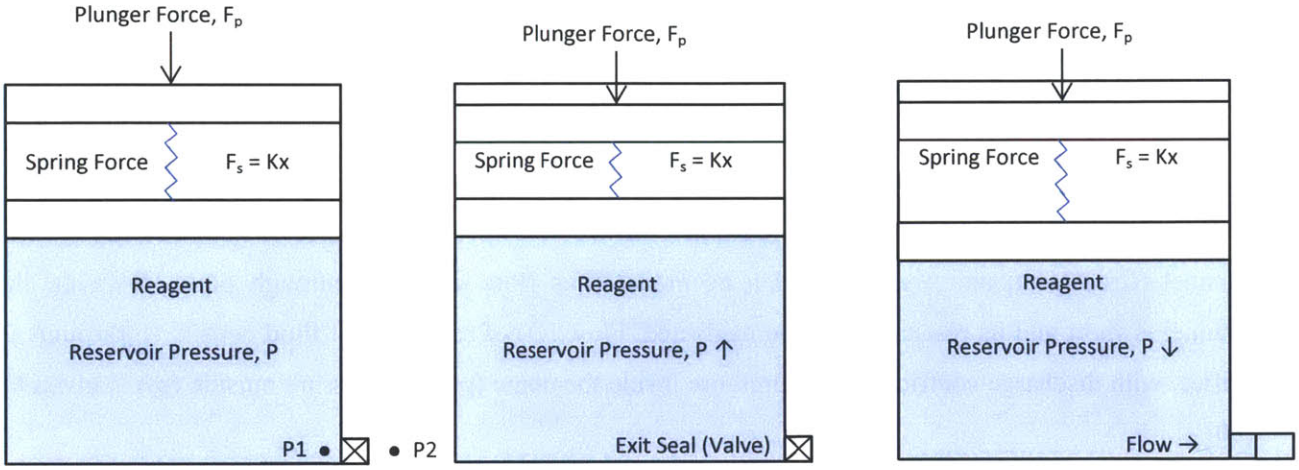

Figure 81: Fluid Modeling

Fluid modeling involves three basic elements – Capacitance (C), Resistance (R) and Inertance (I) which are analogous to the electrical elements of capacitance, resistance and inductance or the mechanical elements of spring, damper and mass. A fluid capacitor has increasing volume with increasing pressure. Examples include – spring pistons, air pistons, open tank. A fluid resistance, relating volumetric flow rate and pressure is often non-linear in real and practical fluid flow systems. Examples of fluid resistance include, flow through pipe, valves, orifices. Inertance arises from momentum of the flowing fluid and provides a relation for the change in pressure required for a change in flow rate. Inertance in often negligible compared to other effects when length of fluid element or mass flow is small. The three elements are given by –

$$C = \frac{V}{P} \qquad R = \frac{P}{V'} \qquad I = \frac{P}{V''}$$

9.2.2.3.1 Capacitance

In the model, the spring, representing the elasticity of the dome film provides the stored capacitance. The model also assumes that the liquid is incompressible (ie. Bulk modulus is high enough to neglect capacitance created by compliance of the fluid). The capacitance due to elasticity can be given as -

$$Energy\ Stored = U = \frac{1}{2} C p_r^2$$

Equation 37

$$C = \frac{(1-v) r_m^2}{2Et} A_s$$

Equation 38

Thus, the capacitance depends on the geometrical and material properties of the dome.

9.2.2.3.2 Resistance

The exit seal geometry is represented by a valve and the resistance through it is calculated treating it as an orifice with an opening ratio (Orifice Area/Exit Channel Area) β. The resistance of flow through the exit channel (Cross-sectional Area = A_e) can be modeled as flow resistance through pipe. However, the channel is short and its resistance can be neglected. Flow (Q) of reagent with fluid density (ρ)through an orifice, with discharge coefficient (C_d) pressure inside the dome (p_1) and pressure outside (p_2) is given by [30] –

$$Q = C_d \beta A_e \sqrt{\frac{2(p_1 - p_2)}{\rho(1-\beta^4)}}$$

Equation 39

Comparing the above equation to the non-linear resistance equation, the fluid resistance (K) can be calculated as follows –

$$Q = K\sqrt{p_{12}}$$

Equation 40

$$K = C_d \beta A_e \sqrt{\frac{2}{\rho(1-\beta^4)}}$$

Equation 41

Discharge Coefficient (C_d) behaves very dramatically at very low Reynolds numbers, characteristic of microfluidic phenomenon. (Figure 82) Research indicates that the discharge coefficient is a product of three coefficients (contraction coefficient, viscosity coefficient and the velocity coefficient). The determination of the coefficient is out of scope for this thesis.

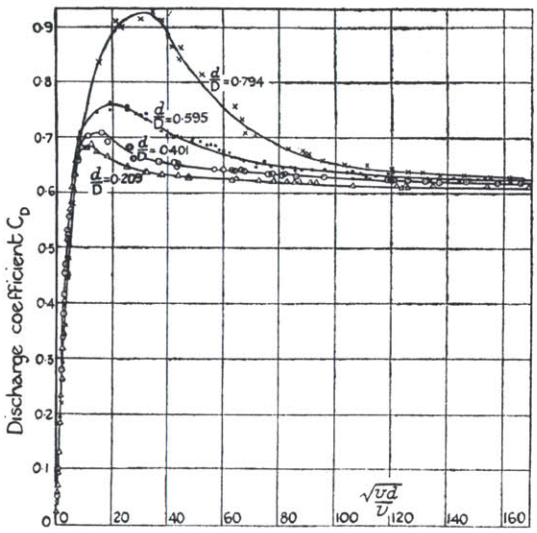

Figure 82: Discharge Coefficient vs. Reynolds Number [31]

9.2.2.3.3 State Variable Model

The capacitor can be described as having a flow (Q_{cap}), when the pressure inside the reservoir dome is p_1 and outside is p_2 (p_2 can be atmospheric pressure, if there is no back pressure at the reservoir via) flow out of the dome is given by Q_{flow} –

$$Q_{cap} = -Q_{flow} = C\frac{d(p_1 - p_2)}{dt}$$

Equation 42

The exit seal is the fluid resistor with resistance K and is given by –

$$Q_{flow} = K\sqrt{(p_1 - p_2)}$$

Equation 43

The whole system can be described in a state variable format –

$$Q_{flow} = -C\frac{d(p_1 - p_2)}{dt} = K\sqrt{(p_1 - p_2)}$$

Equation 44

Or in a more general sense –

$$\frac{dp}{dt} = -\frac{K}{C}\sqrt{p}$$

Equation 45

The fluid capacitance and resistance calculated earlier is now substituted to give a nonlinear relation which is solved using ode45 simulation in Matlab.

$$Q_{flow} = C_d \beta A_e \sqrt{\frac{2p}{\rho(1-\beta^4)}}$$

Equation 46

$$\frac{dp}{dt} = -\frac{2EC_d \beta A_e t}{(1-v) r_m^2 A_s} \sqrt{\frac{2p}{\rho(1-\beta^4)}}$$

Equation 47

The calculations for the ODE, will lead to a relation for the flow after the exit seal opens.

9.2.2.3.3 Pressure and Flow Simulation

The above equation (Equation 47) being a non-linear relationship, an ode45 simulation is carried out for the following values of variables –Young's modulus E (Aluminum) = 69 GPa, C_d =0.15, β = 0.8, A_e = 2E-6 m^2, t = 8E-5 m, v = 0.34, r_m = 7E-3 m, A_s = 9.412E-3 m^2, ρ = 1000 kg/m^3, Pressure (p) = 8000 Pa.

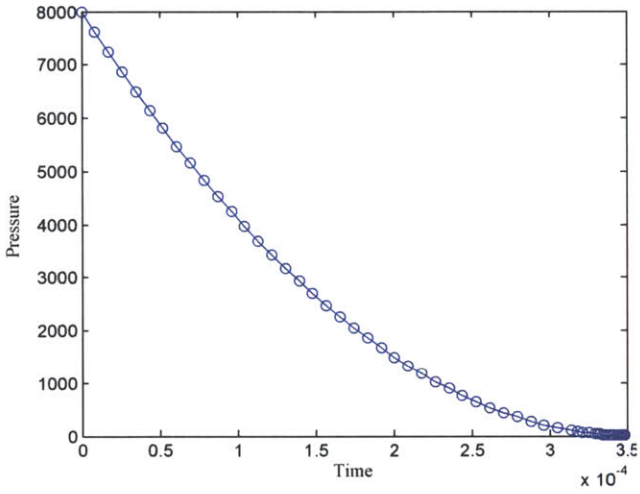

Figure 83: Pressure vs. Time Numerical Solution

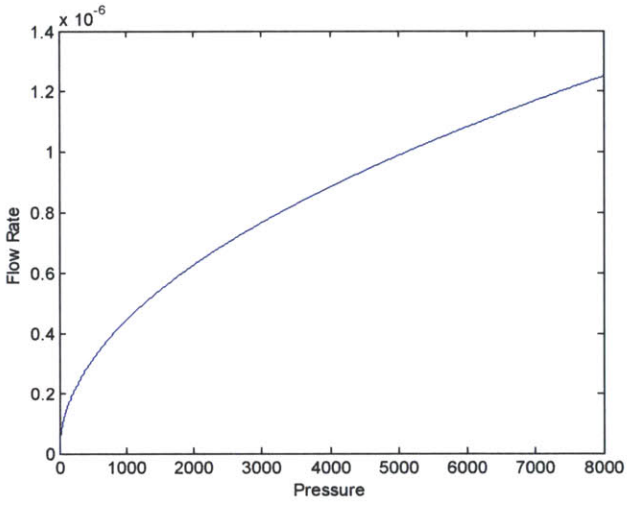

Figure 84: Flow Rate vs. Pressure Numerical Solution

The use of material properties and geometric parameters specific to Daktari yields the above plot of pressure distribution with time. It is important to note here that the time constant is of the order of 0.15 milliseconds. (Figure 83) The energy stored through capacitance gets converted into additional pressure and disappears within this short span of time. The contribution of this stored energy to flow rate is captured in (Figure 84) indicates that once the exit seal opens at 8000 Pa, the contribution of energy storage to excess flow is a maximum of 1.2E-6. This flow rate is only 3-7 % of the designed flow rate. Although, this case is run for a specific case of materials and seal strength, the plot indicates that energy storage may not actually be the dominant contribution to flow anomalies.

The models explored in this chapter are only preliminary exercises in developing an understanding of the dome deformation phenomenon. Understanding the recovery of lost volume during plunder dome interaction, will help understand and even control delamination. The energy storage model may prove helpful when considering changes in material properties and seal strengths.

Chapter 10: Conclusions

This research characterizes the exit seals to understand its influence on phenomenon such as flow anomalies and delamination. The existing exit seal was investigated using microscopy, interferometry, chemical and thermal analysis. The findings from these investigations were combined with patent research on exit seals to develop 4 exit seal plates with a combination of two shapes – Line and Chevron and two profiles – Flat and Hemispherical. A fixture was designed to enable exit seals to be created and tested at Daktari. Following preliminary experiments with different exit seal designs at different parameters, the Line Flat design was selected for a parameter scoping experiment involving four parameters – Temperature, Time, Gap and Distance. A Temperature of 100 units, time = contact, gap of 60 units and distance = 1000 units gave the best flow results. A few replicates were also run at distance = 750 units and led to a sharper rise and drop with no trace of Anomaly 1.

The exit seal is a bond between the aluminum layer on the lid film and heat seal on the dome film. The investigations of the existing exit seal suggest that the heat seal coating on the lid film flows away from the exit seal under the sealing tool pressure, exposing the aluminum layer. On the other hand, the heat seal on the dome film does not flow away, creating the exit seal.

A distance of 1000 units or less results in good flow characteristics with minimal anomalies. Preliminary experiments on exit seal designs indicated that the distance of the exit seal has a strong influence on the delamination around the periphery of the reservoir dome which contributes to flow anomalies.

Preliminary experiments also led to the selection of the Line Flat design for a parameter scoping exercise. The line Hemisphere design provided unpredictable results having no flow anomalies in some cases while showing high Anomaly 1 or Anomaly 2 in other replicates. The chevron shape does not yield good flow patterns and results in large amounts of Anomaly 2. The force plots for rupture of the exit seal indicates a partial rupture which fails to propagate along the arms and open wide. Both flat as well as hemispherical profiles result in large amounts of Anomaly 2.

The temperature of the micro-feature changes after being in contact with the film. A recovery time of 30 to 60 units is usually needed to bring the temperature back up to its original level. The temperature reflected by the thermocouple placed in the platen heater does not accurately represent the temperature at the micro-feature and averages almost 15 units higher than the micro-feature temperature.

The time is not always positively correlated to exit seal strength. The increase in Gap or depression of the tool into the film increases Anomaly 1 but does not have significant impact on exit seal strength.

In general, a weaker seal rupturing below 10 units result in lower Anomaly 2 duration and occurrence. However, the strength of the exit seal must be sufficient to create a hermetic seal for barrier against evaporation or leakage. The line flat exit seal design with a temperature of 100 units, time = contact, gap = 60 units gives fewer flow anomalies.

Finally, the dome deformation phenomenon was studied to understand how the dome reacts on interaction with the plunger. The volume lost is calculated as a function of the travel of the plunger inside the dome. The same equation also helps to develop a relation for flow rate as a function of travel within the spherical region. Two theories for volume recovery are presented – delamination and energy storage. The two phenomena are equally likely to occur under different material properties and seal strengths. Generic mathematical models developed allow for a framework for future reservoir pack and exit seal design optimization.

Chapter 11: Future Work

The following chapter provides a brief snapshot of further work at exploring variations in exit seal and to the more broad based aspects that cover ageing, hermeticity and new manufacturing processes.

Several design variations are left unexplored – Varying the Chevron angle, adding a fillet instead of a sharp corner, a progressively weaker seal along the chevron arms and varying the slope on the flat profile.

The best set of parameters (Temperature of 100 units, time = contact, and a gap of 60 units) from the parameters scoping exercise is only the best from a limited number of parameter combinations. The next step in optimizing parameters for exit seal is varying multiple parameters to study their mutual interaction through a more detailed 3 Factor Design of Experiments. There is also a need to better understand the characteristics of the force plots, especially the influence of reservoir film material properties and flow resistance and their individual contributions to plunger force.

Future work in exit seal selection must ensure hermeticity of the seal through ageing experiments. The hermeticity of the reservoir pack is a necessary condition in point of care diagnostic devices. A weak seal should not break apart leaving reagents exposed to the atmosphere allowing them to leak or evaporate.

The author came across an interesting method of creating exit seal using Radio Frequency Welding [27] methods which allows greater manufacturing tolerances. As a part of manufacturing expansion at Daktari the RF welding process should be looked at as an alternative process in reservoir pack manufacturing. The exit seal is currently manufactured using a hot platen that presses against the film. While this may be an effective manufacturing process, it's still prone to uncontrolled variations.

The models presented in the last chapter must be tested with further virtual simulations as well as physical experiments to validate the accuracy of the mathematical models for delamination and energy storage. Future design optimization, with respect to geometry, material properties can be performed using validated models.

References

[1] M. Bofill et al., "Laboratory control values for CD4 and CD8 T lymphocytes. Implications for HIV-1 diagnosis.," Clinical and experimental immunology, vol. 88, no. 2, pp. 243-52, May 1992.

[2] "CD4 Count," U.S. Department of Health & Human Services AIDS Homepage, 2010. [Online]. Available: http://aids.gov/hiv-aids-basics/just-diagnosed-with-hiv-aids/understand-your-test-results/cd4-count/. [Accessed: 12-Jun-2012].

[3] UNAIDS, UNAIDS Report on the Global AIDS Epidemic. 2010.

[4] UNAIDS, "World AIDS Day Report 2011," 2011.

[5] X. Cheng et al., "A Microchip Approach for Practical Label-Free in Resource-Poor Settings," Cell, vol. 45, no. 3, pp. 257-261, 2007.

[6] "Progress on Global Access to HIV Antiretroviral Therapy," 2006.

[7] V. Linder, "Microfluidics at the crossroad with point-of-care diagnostics," The Analyst, vol. 132, no. 12, p. 1186, 2007.

[8] S. Haeberle and R. Zengerle, "Microfluidic platforms for lab-on-a-chip applications.," Lab on a chip, vol. 7, no. 9, pp. 1094-110, Sep. 2007.

[9] A. M. Dupuy, S. Lehmann, and J. P. Cristol, "Protein biochip systems for the clinical laboratory.," Clinical chemistry and laboratory medicine CCLM FESCC, vol. 43, no. 12, pp. 1291-1302, 2005.

[10] M. Toner and D. Irimia, "Blood-on-a-chip.," Annual review of biomedical engineering, vol. 7, pp. 77-103, Jan. 2005.

[11] P. Yager et al., "Microfluidic diagnostic technologies for global public health.," Nature, vol. 442, no. 7101, pp. 412-8, Jul. 2006.

[12] A. Saber, "Manufacturability of Lab on Chip Devices: Reagent Filled Reservoir Bonding Process and its Effect on Reagents Flow Pattern," Massachusetts Institute of Technology, 2012.

[13] N. Jain, "A Comprehensive Study and Validation of High-Throughput Microscale Electrode Production Using Thermal Transfer Printing Techniques," Massachusetts Institute of Technology, 2012.

[14] B. Judge, "Methods of Heating Microfluidic Components for Assembly," Massachusetts Institute of Technology, 2012.

[15] C.-M. Ho and Y.-C. Tai, "Micro-Electro-Mechanical-Systems (Mems) and Fluid Flows," Annual Review of Fluid Mechanics, vol. 30, no. 1, pp. 579-612, Jan. 1998.

[16] G. M. Whitesides, "The origins and the future of microfluidics.," Nature, vol. 442, no. 7101, pp. 368-73, Jul. 2006.

[17] P. Tabeling, "Introduction to Microfluidics," Angewandte Chemie, vol. 118, no. 47, pp. 8039-8040, 2006.

[18] S. Selvakumar, B. Anthony, T. Supervisor, and D. E. Hardt, "Manufacturing of Lab-on-a-Chip Devices: Variation Analysis of Liquid Delivery using Blister Packs," Massachusetts Institute of Technology, 2010.

[19] L. Donoghue, "Design of a micro-interdigitated electrode for impedance measurement performance in a biochemical assay," MIT Mechanical Engineering Thesis, 2011.

[20] T. V. Oordt, Y. Barb, R. Zengerle, and F. V. Stetten, "Miniature Stick Packaging - An Industrial Technology for pre-storage and release of reagents in Lab-on-a-Chip systems," Strategy, pp. 437-439, 2011.

[21] Yochim, "Compartmented bag and package," U.S. Patent 2756875.

[22] E. Bollmier et al, "Multi-Compartment Package with Internal Breaker Strip," U.S. Patent 2932385.

[23] Yoshida, "Plastic container having an easy-to-peel seal forming compartments," U.S. Patent 4961495.

[24] E. Bollmier et al, "Combination Package," U.S. Patent 3074544.

[25] Hansen, "Rupturable Seal," U.S. Patent 6893696B2.

[26] Roger, "Break seal before access dual chamber bag," U.S. Patent 7618406B2.

[27] E. J. Malek, "Method of forming a burstable pouch," U.S. Patent 4539793.

[28] T. Inamdar, N. Jain, B. Judge, and N. Roche, "Characterizing and Optimizing Blister Foil Thermal Bonding for Pilot Production Line," MIT Mechanical Engineering Academic Paper, vol. 1, no. 1, pp. 1-10, 2012.

[29] P. Kelly, Solid Mechanics Part I: An Introduction to Solid Mechanics. .

[30] D. W. Perry, R.H. and Green, Perry's Chemical Engineers' Handbook, 8th ed. 2007.

[31] A. F. C. Johansen, "Flow through Pipe Orifices at Low Reynolds Numbers," Proceedings of the Royal Society of London, vol. 126, no. 801, pp. 231-245, 1930.

Appendix A: Modeling Nomenclature

1. **r** : Radius of the plunger
2. **R** : Radius of the spherical portion of the dome
3. **R_d or Rd** : Base radius of the dome
4. **d** : Center (plunger) to center (Dome sphere) distance
5. **h_R or hR** : Distance from intersection line to tip of dome sphere
6. **h_r or hr** : Distance from intersection line to tip of plunger
7. **V_R or VR** : Volume (as a spherical cap) lost between intersection line and dome sphere
8. **V_r or Vr** : Volume (as a spherical cap) lost between intersection line and the plunger
9. **x** : Travel of the plunger into the dome
10. **V_p** : Velocity of the plunger
11. **V_{lost}** : Total theoretical volume lost
12. **Q_{flow}** : Theoretical Flow Rate
13. **R_o** : Base radius of delamination
14. **r_d** : Radius of dome at stretch due to delamination
15. **h** : Height of delamination
16. **θ** : Angle of the dome
17. **$V_{recover}$** : Volume created through delamination
18. **$V_{delaminatedfrustum}$** : Frustum volume with R_o as base radius
19. **$V_{frustum}$** : Frustum volume with R_d as base radius
20. **p_r** : Pressure inside the dome just before the exit seal opens
21. **r_i** : Inside radius of the dome (approximated to a sphere)
22. **r_o** : Outside radius of the dome (approximated to a sphere)
23. **t** : Thickness of the dome film
24. **r_m** : Hypothetical mean radius of the dome
25. **σ_t** : Tangential stress
26. **σ_r** : Radial stress
27. **σ_x** : Stress along dome film in x direction
28. **σ_y** : Stress along dome film in y direction
29. **σ_z** : Stress across dome film in z direction
30. **ε_c** : Circumferential or Tangential strain
31. **ε_r** : Radial Strain
32. **ε_x** : Strain along dome film in x direction
33. **ε_y** : Strain along dome film in y direction
34. **ε_z** : Strain across dome film in z direction
35. **p** : Pressure inside the dome
36. **E** : Modulus of elasticity of the film material
37. **v** : Poisson's ratio of the film material
38. **δ_r** : Radial expansion of the dome
39. **$V_{expansion}$** : Maximum expanded volume of the dome
40. **A_s** : Surface area of the conical frustum of the dome
41. **U** : Strain energy stored from expansion
42. **dV** : Volume of the material storing energy
43. **F_p** : Plunger force
44. **F_s** : Spring force modeling elasticity of the film material
45. **K** : Spring stiffness
46. **x** : Spring deformation
47. **C** : Capacitance of the dome
48. **ρ** : Fluid density

49. $\mathbf{C_d}$: Discharge coefficient through partially open exit channel
50. $\boldsymbol{\beta}$: Opening ratio
51. $\mathbf{A_e}$: Cross sectional area of the exit channel
52. $\mathbf{K}$: Resistance at the exit seal
53. $\mathbf{Q_{cap}}$: Flow of modeled capacitance
54. $\mathbf{p_1}$: Pressure inside the dome (here, equal to p_r)
55. $\mathbf{p_2}$: Pressure outside the dome (here, equal to atmospheric pressure)
56. $\mathbf{p}$: Pressure difference across the exit seal